THERMAL, RHEOLOGICAL, AND MECHANICAL PROPERTIES OF A POLYMER
COMPOSITE CURED AT STAGED CURE CYCLES

A Dissertation by

Seyed Rouhallah Alavi Soltani

Master of Business Administration, Sharif University of Technology, 2005

Bachelor of Science, Sharif University of Technology, 2002

Submitted to the Department of Mechanical Engineering
and the faculty of the Graduate School of
Wichita State University
in partial fulfillment of
the requirements for the degree of
Doctor of Philosophy

May 2010

THERMAL, RHEOLOGICAL, AND MECHANICAL PROPERTIES OF A POLYMER
COMPOSITE CURED AT STAGED CURE CYCLES

The following faculty members have examined the final copy of this dissertation for form and content, and recommend that it be accepted in partial fulfillment of the requirement for the degree of Doctor of Philosophy with a major in Mechanical Engineering.

_____
Bob Minaie, Committee Chair

_____
Hamid Lankarani, Committee Member

_____
Ramazan Asmatulu, Committee Member

_____
Klaus Hoffmann, Committee Member

_____
Walter Horn, Committee Member

Accepted for the College of Engineering

_____
Zulma Toro-Ramos, Dean

Accepted for the Graduate School

_____
J. David McDonald, Dean

iii

DEDICATION

To my wife, Zohreh, and my mother who have made numerous sacrifices during these years

ACKNOWLEDGEMENTS

I would like to extend my gratitude to my advisor, Professor Bob Minaie, who encouraged me and gave me the opportunity and technical advice to perform this work. I would also like to thank Dr. Hamid Lankarani, Dr. Ramazan Asmatulu, Dr. Klaus Hoffmann, and Dr. Walter Horn for serving on my dissertation committee and Dr. Melanie Violette for her valuable technical comments.

I am grateful to Seyed Mostafa Sabzevari and Hoda Koushyar, who were my team members in Dr. Minaie's research group, and Alejandro Rodriguez, Behrouz Tavakol, Mauricio Guzman, Pooria Sharif Kashani, Christopher Gernaat, Chee Sern Lim, and Ramin Ranjbar for their friendship and support.

Finally, I am very grateful to my wife, my mother, and my brothers for their impeccable help and support.

ABSTRACT

Thermal, rheological, and mechanical properties of a polymer composite cured at different one-stage and two-stage cure cycles were studied in this dissertation. A commercial carbon-fiber prepreg, Cycom 977-2 UD, was used. This curing-toughened epoxy resin prepreg is formulated for autoclave or press molding. An encapsulated sample rheometer (ESR) was used to obtain its viscoelastic properties, including complex viscosity, gel time, and minimum viscosity time, as well as glass transition temperature (T_g) and pressure window time for one-stage and two-stage cure cycles. A differential scanning calorimeter (DSC) was used to obtain the degree of cure (DOC) for one-stage and two-stage cure cycles. The mechanical properties of interest for specimens cured at one-stage cure cycles were short beam shear (SBS) strength, combined loading compression (CLC) strength, CLC modulus, CLC Poisson's ratio, open-hole compression (OHC) strength, and OHC modulus. The SBS, CLC, and OHC tests were performed at room temperature to obtain the mechanical properties.

For the one-stage cure cycles studied, it was observed that the mechanical properties, except SBS strength, did not vary significantly; therefore, no correlation with the viscoelastic properties or the DOC was found for them. Moreover, the failure mode for OHC specimens cured at different one-stage cure cycles was similar. Likewise, the failure mode for CLC specimens cured at different one-stage cure cycles was the same. However, the failure mode for the least-cured SBS specimens was different from that of other SBS specimens. Also, the SBS strength of the least-cured specimens was significantly less than that of other specimens. The complex viscosity of the specimens cured at one-stage cure cycles in the ESR showed a similar drop-off trend for the least-cured specimens. As such, SBS strength showed a good correlation with the complex viscosity. SBS strength showed a weaker correlation with the T_g and DOC for

the same cure cycles. The T_g had a strong correlation with the DOC for all one-stage cure cycles. No correlation between gel time and other material properties was found. A considerable improvement in SBS strength, final complex viscosity, T_g, and DOC of the least-cured specimens was observed after the dwell time was increased enough to ensure that no further curing occurred.

It was also observed that for the two-stage cure cycles, faster heat-up rates and higher first-stage dwell temperatures resulted in faster curing.

The DOC for the entire cure cycle was modeled using the Springer-Loos cure kinetics model for one-stage and two-stage cure cycles. The complex viscosity up to the gel time was modeled using the Kenny viscosity model for one-stage and two-stage cure cycles. The modeling results agreed well with the experimental data.

The results presented in this dissertation suggest that the ESR can be used as an ex-situ cure-monitoring instrument to mimic autoclave/oven curing and, hence, eliminate the need for multiple measurement instruments. The cure time-temperature data, provided by thermocouples attached to the composite part in the autoclave/oven would be the only input to the rheometer for cure monitoring. The complex viscosity as measured by the ESR was shown to be the best viscoelastic property for monitoring the state of the material during cure for the following reasons: (a) it could be precisely measured throughout the cure and post-cure cycles using the rheometer, (b) it could reveal the important changes in the material state during cure, (c) it could be modeled by sophisticated viscosity models, and (d) it could be correlated to the mechanical properties of the composite material.

Utilizing the ESR as the main ex-situ cure-monitoring instrument makes it possible to offer a new approach to curing composites. In this new approach, called Material State

Management (MSM), the acceptance of cured composite materials is based on the materials' viscoelastic properties as measured by the ESR during cure and post-cure monitoring. Moreover, knowledge of the material's viscoelastic properties during cure can be used to improve the current cure specifications. In the MSM approach, cure process confidence limits can be prescribed based on the viscoelastic properties of the material, thus addressing the shortcomings of the current time-temperature approach to curing.

TABLE OF CONTENTS

TABLE OF CONTENTS (continued)

Chapter   Page

LIST OF TABLES

LIST OF FIGURES

LIST OF FIGURES (continued)

xvi

LIST OF ABBREVIATIONS/NOMENCLATURE

ANOVA	Analysis of Variance
ASTM	American Society for Testing and Materials
CLC	Combined Loading Compression
CV	Coefficient of Variation
DMA	Dynamic Mechanical Analysis
DOC	Degree of Cure
DSC	Differential Scanning Calorimetry/Calorimeter
DTA	Differential Thermal Analysis
EGA	Evolved Gas Analysis
ESR	Encapsulated Sample Rheometer
FTIR	Fourier Transform Infrared
GC	Gas Chromatography
LD	Load Displacement
MRC	Manufacturer Recommended Cure (Cycle)
MSM	Material State Management
OHC	Open-Hole Compression
SACMA	Suppliers of Advanced Composite Materials Association
SBS	Short Beam Shear
TBA	Torsional Braid Analysis
TGA	Thermogravimetric Analysis
TTT	Time Temperature Transformation
UD	Unidirectional
WLF	Williams-Landel-Ferry

LIST OF SYMBOLS

α degree of cure

α_c critical degree of cure

α_{c0} critical degree of cure at $T = 0^{\circ}K$

α_{cT} constant of increase in critical resin degree of cure

α_g degree of cure at gelation

α_n degree of cure at cell n

α_{n+1} degree of cure at cell n+1

γ strain

γ_0 amplitude of sinusoidal strain

γ^* complex strain

δ phase lag of stress response

η viscosity

η_1 viscosity model constant

η_a viscosity model constant

η_0 initial complex viscosity during isothermal cure

η_g viscosity at glass transition temperature

η_∞ final complex viscosity during isothermal cure

η' dynamic viscosity

η'' imaginary part of complex viscosity

η^* complex viscosity

$\ln\eta_n^*$ natural log of complex viscosity at cell n

θ angular rotation

λ	ratio of segmental mobility
π	Pi (=3.14)
σ_s	tensile strength
σ_{T0}	tensile strength at reference temperature
σ_y	yield stress
σ_{yg}	yield stress at glass transition temperature
τ	shear stress
τ_0	amplitude of sinusoidal shear stress
τ^*	complex shear stress
Ψ	torque
ω	angular frequency
A	Kenny model constant
A_0	pre-exponential factor
A_1	first pre-exponential factor
A_2	second pre-exponential factor
A_μ	Kenny model constant
b	yield stress model constant
B	Kenny model constant
B_1	Springer-Loos model constant
C	diffusion constant
c	Gel time model constant
C_1	WLF viscosity model constant

C_2 WLF viscosity model constant

c_r thermal capacitance between reference sensor and furnace

c_s thermal capacitance between sample sensor and furnace

D diameter

E_a activation energy for gel time model

E_k activation energy for viscosity model

E_t activation energy for viscosity model

E_η activation energy for viscosity model

E_μ activation energy for viscosity model

E' tensile storage modulus

E'_{T0} tensile storage modulus at reference temperature

ΔE activation energy

ΔE_1 first activation energy

ΔE_2 second activation energy

f frequency

G shear modulus

G' shear storage modulus

G'' shear loss modulus

G^* complex shear modulus

H thickness

H_{res} residual heat of reaction

H_T total heat of reaction

H_U ultimate heat of reaction

I_p polar moment of inertia

k rate constant

k_1 first-rate constant

k_2 second-rate constant

k' viscosity model constant

k'_∞ viscosity model constant

q heat-flow rate measured by DSC

q_r reference heat-flow rate

q_s sample heat-flow rate

q_{T4} heat flow rate measured by DSC using Tzero technology

t time

m exponential constant

M_W weight average molecular weight

N number of samples

n exponential constant

r radius

R universal gas constant

R_t thermal resistance of the heat-leak disk

R_r thermal resistance between reference sensor and furnace

R_s thermal resistance between sample sensor and furnace

T temperature

t	time
T_0	cell-base sensor temperature
T_c	cure temperature
T_{fr}	temperature of the furnace on reference side
T_{fs}	temperature of the furnace on sample side
T_g	glass transition temperature
t_{gel}	gel time
T_{g0}	initial glass transition temperature
$T_{g\infty}$	ultimate glass transition temperature
$_{gel}T_g$	gelation glass transition temperature
T_n	temperature at cell n
T_r	reference sensor temperature
T_s	sample sensor temperature
ΔT	temperature difference
Δt	time step
ΔT_0	temperature difference between sample sensor and T_0 sensor
$\tan\delta$	tangent of phase lag of stress response
U	activation energy for Dusi model
x_i	individual data value
$\bar{x}$	mean value of data set

CHAPTER 1

INTRODUCTION

1.1.   Curing of Prepreg Composites

Advanced composite materials come in many forms suitable for fabrication. A common form is the so-called prepreg, consisting of fibers covered (preimpregnated) by partially cured resin [1]. The resin system for many aerospace prepregs is a thermosetting polymer resin such as epoxy. Thermosetting resins must be cured for an additional period of time, often in the presence of heat and pressure, to achieve their best mechanical properties. During the irreversible exothermic curing process, polymerization and cross-linking of the polymer molecules occur [2]. Figure 1 shows the curing steps for a thermosetting resin. Curing begins with monomers at the A-stage, then proceeds through concurrent linear growth and branching of monomers to reach the B-stage, just before the gel point of the resin. The linear chains of polymer at this stage are connected by a van der Waal's bond and are not cross-linked. As the cure continues, a gelled network forms with incomplete cross-linking. The cure ends with the fully cured C-stage resin [3]. Cross-linked chains at the C-stage are connected by strong covalent bonds.

$\alpha = 0$
A-Stage

$\alpha = 0.2$
B-Stage

$\alpha = 0.5$
Gelation

$\alpha = 1.0$
C-Stage
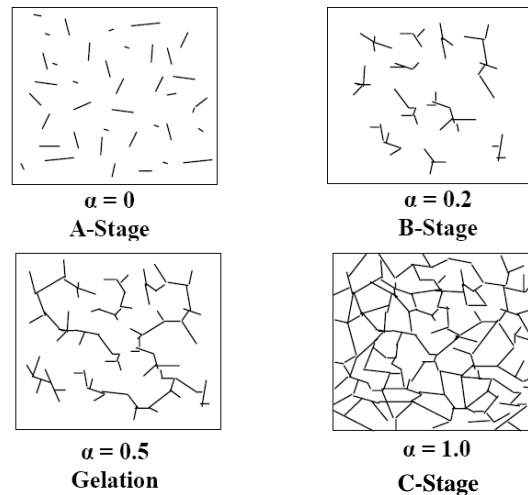
Figure 1. Stages of cure for thermosetting resin [4].

1

As the curing of the thermosetting resin advances, cross-linking density, i.e., the average mass of polymer between cross-links, and molecular weight of the resin increases significantly and results in the formation of a three-dimensional network of highly cross-linked polymers. The state of the material changes from the liquid state of the uncured resin to the solid glassy state of a fully cured resin. The mechanical properties of a thermosetting polymer at its service temperature are directly affected by its molecular weight. The higher the molecular weight, the higher the strength of the polymer [5]. Figure 2 contains a graph that shows the weight-average molecular weight, M_W, as a function of the conversion percent for a thermosetting epoxy resin. The conversion percent, or degree of cure, α, indicates the extent of cure for a thermosetting polymer. For an uncured resin, the degree of cure (DOC) and conversion percent equal zero; whereas, for a fully cured resin, the degree of cure is equal to one and the conversion percent is 100.
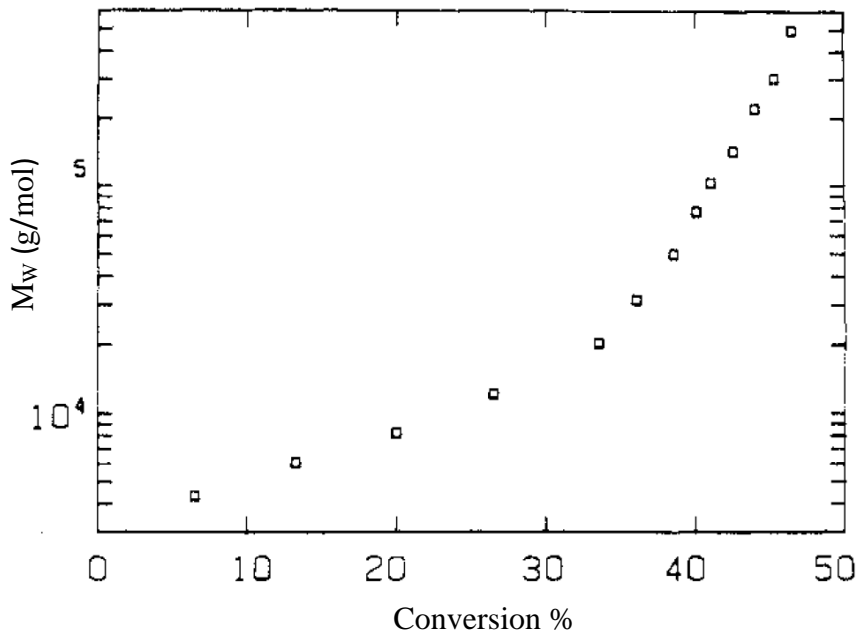
Figure 2. Weight-average molecular weight vs. conversion percent for epoxy resin [6].

The aforementioned material state transitions of a thermosetting resin during cure can be mapped using a time temperature transformation (TTT) diagram, such as the one shown in Figure 3. The vertical and horizontal axes in the TTT diagram are isothermal cure temperature, T_c, and isothermal cure time, respectively. Gelation and vitrification are key material state transitions during curing. Gelation is the point of the cure process at which a network of cross-linked polymer molecules forms a macroscopic molecule [5]. As a result, the resin undergoes a transition from the liquid state to the rubbery state. Vitrification is the point of the cure process at which the resin changes from the rubbery state to the solid glassy state.
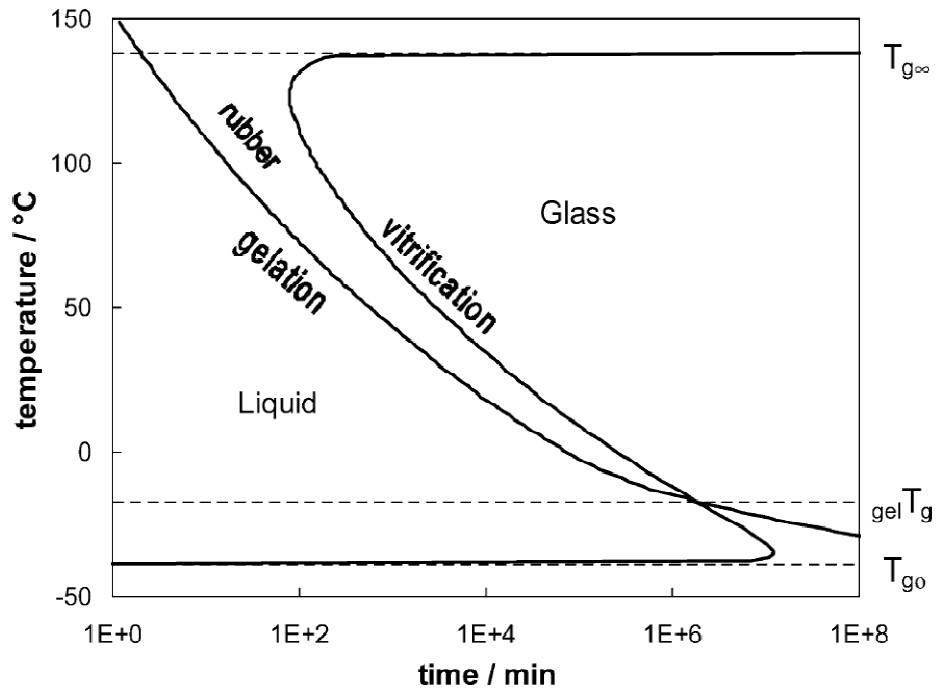
Figure 3. Schematic of time temperature transformation diagram for thermosetting resin [7].

The ultimate glass transition temperature of the fully cured resin and the initial glass transition temperature of the uncured resin have been designated as $T_{g\infty}$ and T_{g0}, respectively. The glass transition temperature (T_g) is the temperature at which the amorphous portion of a

3

polymer softens and the polymer changes from the glassy state to the rubbery state. In polymer science, the glass transition is a second-order transition when compared to first-order transitions, such as crystallization and melting [8]. The temperature at which gelation and vitrification occur together is designated as $_{gel}T_g$. The TTT diagram can be divided into the following four regions [9]:

1. For $T_c < T_{g0}$, the resin is frozen and glassy. No cross-linking and curing happen at this temperature range.

2. For $T_{g0} < T_c < {_{gel}}T_g$, the uncured resin is liquid. As the curing proceeds, the resin vitrifies, i.e., the state of the material directly changes from liquid to glassy.

3. For $_{gel}T_g < T_c < T_{g\infty}$, the uncured resin is liquid. As the curing proceeds, the resin gels, i.e., the state of the material changes from liquid to rubbery. Then the resin vitrifies, i.e., the state of the material changes from rubbery to glassy.

4. For $T_c > T_{g\infty}$, the resin is vitrified and remains in the rubbery state, even after it fully cures.

1.2.   Current Approach to Curing Composites

Thermosetting prepregs are usually cured in an autoclave, which is simply a pressure vessel equipped with temperature control devices. The chemical cross-linking reactions are initiated as the temperature inside the autoclave reaches an elevated temperature that is appropriate for curing the thermosetting resin. The cross-linking reactions at the elevated temperature continue until the resin fully cures and solidifies. Application of pressure to the prepreg helps to remove volatiles and air trapped between the prepreg plies, also known as degasifying, and to consolidate the plies during cure. To assist the degasifying, composite parts are often vacuumed at the early stages of the cure. The prepreg laminates need to be sealed with

4

a vacuum bag before pulling the vacuum. The vacuum bag seals the laminates throughout the cure cycle and protects them from the autoclave gases [10].

It is important to note that neither the autoclave pressure nor the vacuum affects the chemical processes of curing. As such, only the cure temperature, measured by in-situ sensors such as thermocouples, dictates the state of the material during cure. The most important cure-monitoring sensors used in current industry practice are temperature sensors. Nevertheless, other in-situ sensors such as dielectric sensors, Fourier transform infrared (FTIR) spectroscopy sensors, ultrasonic sensors, and fiber optic sensors, which provide useful information about the state of the material during cure, might be used. The cure cycles for prepregs are determined by trial and error. A typical cure specification for an autoclave cure is illustrated in Figure 4. The cure specifications usually come with the upper and lower limits for temperature and pressure, also known as confidence limits.

1. Pull vacuum of at least **X inches Hg**
2. Heat @ **Heat-up Rate 1** to **Intermediate Hold Temperature**
3. Hold at **Intermediate Hold Temperature** for at least **Time 1**
4. Raise autoclave pressure to **Y psi**.
   Vent vacuum when pressure reaches 15 psig.
5. Heat @ **Heat-up Rate 2** to **Final Hold Temperature**.
6. Hold at Final Hold Temperature for **Time 2**.
7. Cool slowly at **Cool-down Rate** to **End Cure Temperature**
8. Release pressure.

Figure 4. Typical specification for autoclave cure [11].

5

The current industry cure practice is based on the assumption that the mechanical properties and other performance criteria of composite parts meet the requirements if they are cured with a controlled time, temperature, and pressure history. As such, extensive coupon testing must be done to statistically assure that the mechanical properties are within the prescribed confidence limits using time and temperature as the specified criteria for cure (Figure 5). Since the extent of cure is based on time and temperature, any deviation from these two variables must be considered a significant difference requiring discrepancy evaluation and potentially additional testing.

The current approach to the cure processing is expensive to support, carries risk, and is difficult to manage [12]. In addition, when using this approach, important changes in the material state during cure are not observable, key variables during cure are not correlated, and an estimation of the actual final mechanical properties during cure is difficult; therefore, many process issues cannot be addressed.
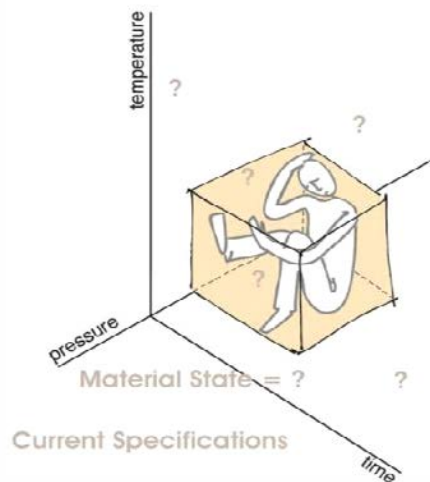
Figure 5. Cure time, temperature, and pressure confidence limits
based on current specifications (courtesy of Thomas Rose, Avpro).

CHAPTER 2

LITERATURE REVIEW

Obtaining the best material properties of composite materials has been of paramount importance for composite manufacturers. From a structural design point of view, these properties are usually mechanical, such as tensile strength, compressive strength, shear strength, and flexural strength. Many factors affect the mechanical properties of composites, one of which is the cure cycle; therefore, it is important to cure the composite materials properly. The proper cure cycle, often provided by the manufacturer of the composite material, is called the manufacturer recommended cure (MRC) cycle [13]. Depending on the desired material features and applications, more than one cure cycle may be developed for a single composite material. The MRC cycle, which is found empirically, should meet certain requirements, such as maximizing the benefit factors by increasing the favorable properties of the cured laminates while minimizing the cost factors by reducing the cure time, temperature, and pressure [10].

During the curing of composites in a production environment, deviations from the MRC cycle happen inevitably. These deviations do not necessarily alter the material properties drastically [14], and if the material properties are being monitored during cure, any deviation from the MRC cycle that can possibly change the material properties significantly may be avoided through corrective actions, such as proper change of cure temperature or pressure.

2.1.   Cure Monitoring

The cure of thermosetting composites is an irreversible process during which properties (chemical, physical, and mechanical) of the composite material change permanently. Figure 6 illustrates the viscosity of Hercules 3501-6 resin vs. cure time for different isothermal cure temperatures.
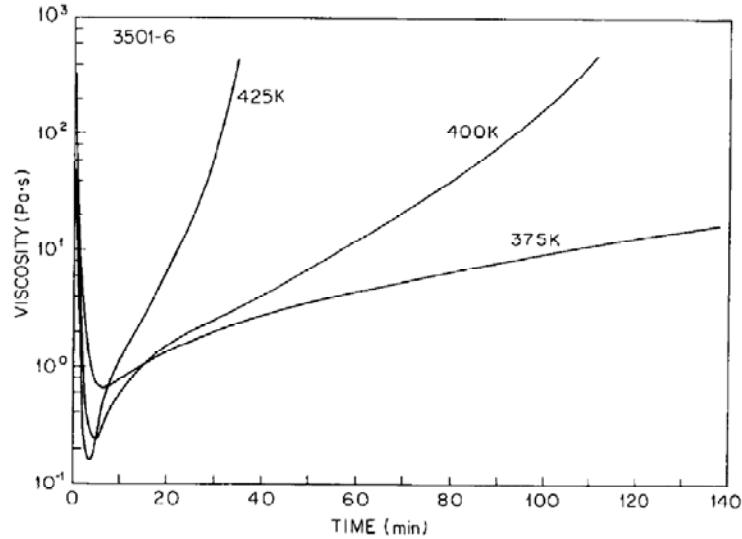
Figure 6. Viscosity of a thermosetting resin during cure at different isothermal cure temperatures [15].

It is possible to monitor the cure of composites once the evolution of any of these properties during cure is known. The cure-monitoring sensors that have been developed fall into two main categories: in-situ and ex-situ. In-situ sensors are embedded within the composite part and measure the change in properties as the composite material undergoes the curing process in the autoclave or oven. On the other hand, ex-situ cure monitoring instruments are not embedded within the composite part. Rather, a small sample of the material is placed inside the instrument to measure the desired properties. As such, the ability of simulating a real cure environment, especially the cure temperature, is key to using these instruments as cure-monitoring sensors.

Table 1 shows in-situ sensors that have been developed for cure monitoring using different measurement techniques. The temperature sensors, i.e., thermocouples, are by far the most popular in-situ cure-monitoring sensors in industry since they are inexpensive, reliable, and easy to use [16]. However, temperature sensors do not directly measure the state of the material or the extent of cure. As such, the temperature data provided by thermocouples should be analyzed using additional cure data and models to determine the state of the material during cure.

8

Other in-situ sensors are not recommended for cure monitoring on an industrial scale since they are expensive, difficult to use, and less reliable because they are sensitive to the method of application, susceptible to damage, and prone to failure during cure.

TABLE 1

IN-SITU CURE MONITORING SENSORS [17]

Sensor Type	Measured Property
Thermocouple [18]	Temperature
Ultrasound [19, 20]	Ultrasonic Velocity
Acoustic [21, 22]	Acoustic Wavelength
Fiber Optic [23]	Strain
Piezoelectric [24, 25]	Strain/Deformation
Dielectric [26, 27]	Ionic Conductivity/Viscosity
Fourier Transform Infrared (FTIR) Spectroscopy [28]	Degree of Cure
Raman Spectroscopy [29, 30]	Degree of Cure
Fluorescence [31, 32]	Degree of Cure

To overcome the issues associated with using the in-situ sensors, the ex-situ cure monitoring instruments are used. The most important ex-situ instruments for cure monitoring are listed in Table 2. Robustness of the measurement is a big advantage of the ex-situ instruments over the in-situ sensors. Moreover, the ex-situ instruments are usually able to directly provide the cure state during cure.

TABLE 2

EX-SITU CURE-MONITORING INSTRUMENTS

Instrument Type	Measured Property
Differential Scanning Calorimeter (DSC) [34]	Heat Flow/Degree of Cure
Differential Thermal Analyzer (DTA) [35]	Heat Flow/Degree of Cure
Thermogravimetric Analyzer (TGA) [36]	Thermal Stability
Torsional Braid Analyzer (TBA) [37]	Viscoelastic Properties
Dynamic Mechanical Analyzer (DMA) [38]	Viscoelastic Properties
Gas Chromatograph (GC) [39]	Chemical Composition
Evolved Gas Analyzer (EGA) [40]	Chemical Composition

The degree of cure and viscosity monitoring are far more popular in determining the state of the material during cure, although some efforts have been made by investigators over the years to use in-situ sensors such as ultrasound sensors to measure the mechanical properties of composites like elastic moduli during cure [33]. Establishing a strong correlation between the state of the material, as measured by the sensors, and the mechanical properties can address the process engineers' need for knowledge of material properties during cure.

The viscosity/viscoelastic monitoring of the material makes it possible to track important material-state transitions. The equations that relate the viscoelastic properties of the thermosetting composites to their mechanical properties make the viscoelastic properties more viable for cure monitoring. For example, the Bosze equation states the relation between tensile strength of a cured unidirectional epoxy composite and its storage modulus measured by DMA for temperatures ranging from $50^{\circ}C$ to $250^{\circ}C$ as follows [41]:

$$\sigma_s(\mathrm{T}) = \sigma_{\mathrm{T}_0}\left(\frac{E'(T)}{E'_{\mathrm{T}_0}}\right) \tag{1}$$

where $\sigma_s(\mathrm{T})$ is the tensile strength at temperature T, E'(T) is the storage modulus at temperature T, σ_{T0} is the tensile strength at reference (room) temperature, and E'$_{\mathrm{T0}}$ is the storage modulus at reference (room) temperature.

2.2.   Monitoring Degree of Cure

It is possible to measure the degree of cure using Fourier transform infrared (FTIR) spectroscopy, Raman spectroscopy, the fluorescence technique, and differential scanning calorimetry (DSC). DSC is the most popular technique among the aforementioned techniques. It measures the difference in heat flow rate between a sample and an inert reference material as a function of time and temperature [42] and has long been used to study the cure kinetics of

10

different resin systems and composites. The equations for calculating the thermal degree of cure are defined based on the heat released from the sample during cure measured by DSC.

Figure 7 Figure 7 shows the cross section of a DSC heat flux cell. As it can be seen, two thermocouples are used that measure the reference and sample temperatures. The equivalent thermal circuit for this type of DSC is illustrated in Figure 8. Equations (2) to (5) describe the heat balance in the heat flux DSC [42]:

$$q_s = \frac{T_{fs} - T_s}{R_s} \tag{2}$$

$$q_r = \frac{T_{fr} - T_r}{R_r} \tag{3}$$

$$q = q_s - q_r \tag{4}$$

$$q = \frac{T_r - T_s}{R_t} = \frac{\Delta T}{R_t} \tag{5}$$

where q_s is the sample heat flow rate, q_r is the reference heat flow rate, q is the heat flow rate measured by DSC, T_s is the sample sensor temperature, T_r is the reference sensor temperature, T_{fs} is the temperature of the furnace on the sample side, T_{fr} is the temperature of the furnace on the reference side, ΔT is the temperature difference between sample and reference sensors, R_s is the thermal resistance between the sample sensor and furnace, R_r is the thermal resistance between the reference sensor and furnace, and R_t is the thermal resistance of the heat leak disk.

The governing equations of the conventional heat flux DSC are obtained assuming that the DSC cell is symmetric. That is, the thermal resistances of the sample and reference, and also the temperatures of the furnace on the sample side and on the reference side, are assumed to be equal. Moreover, the governing equations of the conventional heat flux DSC do not incorporate

11

other known heat flows that take place in the DSC cell. It is important to note that in the real

world, none of the DSC designs satisfy the required precision for a symmetric cell.
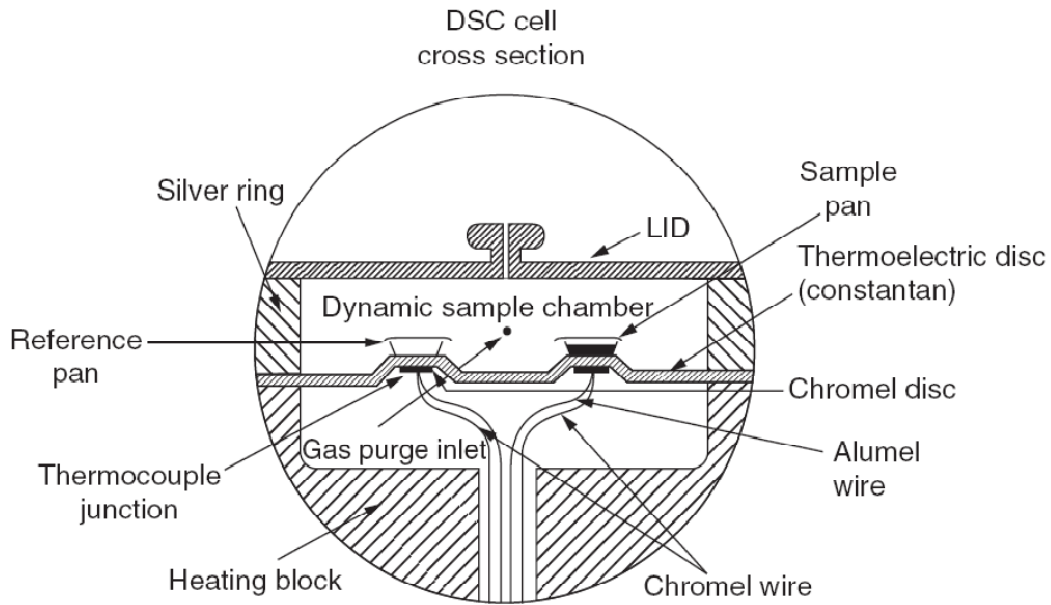
Figure 7. Cross section of a DSC heat flux cell [3].
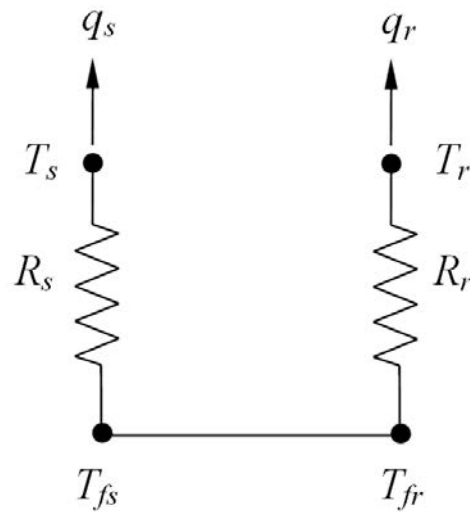
Figure 8. Equivalent thermal circuit of a conventional DSC heat flux cell [42].

To address the shortcommings of the conventional heat flux DSC, TA Instruments has developed a new technolgy called Tzero. This technology utilizes three thermocouples. As Figure 9 shows, two area thermocouples placed undeneath the sample and reference platforms measure the sample and reference temperatures, respectively. The third thermocouple (Tzero or T_0), which is placed in between the reference and sample platforms, measures the temperature of the cell base. For heat flow calculations in this thechnology, two ΔTs are used. The first ΔT is the temperature difference between the sample and the reference sensors, and the second ΔT (ΔT_0) is the temperature difference between the sample and T_0 sensors.
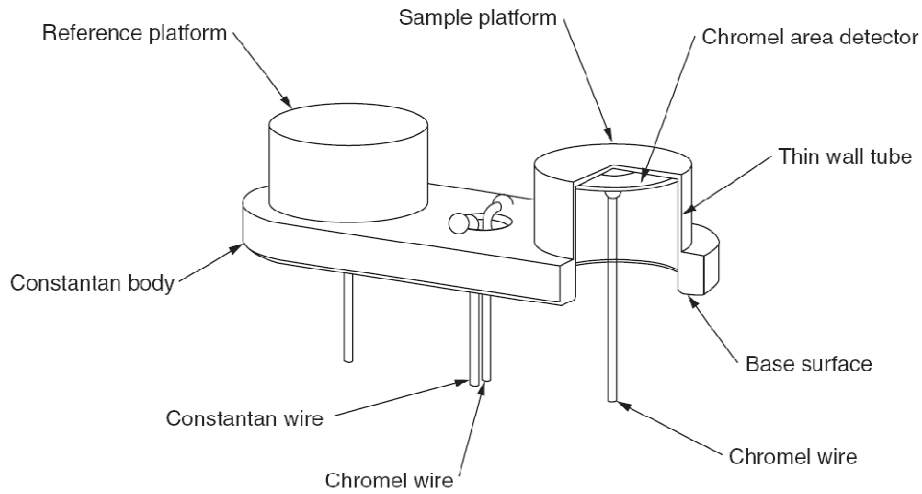
Figure 9. DSC cell design using Tzero technology [3].

The equivalent thermal circuit for a DSC cell with Tzero technology is illustrated in Figure 10. Equations (6) to (11) describe the heat balance in the Tzero DSC [42]:

$$\Delta T = T_s - T_r \tag{6}$$

$$\Delta T_0 = T_0 - T_s \tag{7}$$

$$q_s = \frac{\Delta T_0}{R_s} - c_s \frac{dT_s}{dt} \tag{8}$$

$$q_r = \frac{\Delta T_0 + \Delta T}{R_r} - c_r \frac{dT_r}{dt} \tag{9}$$

$$q_{T4} = q_s - q_r \tag{10}$$

$$q_{T4} = -\frac{\Delta T}{R_r} + \Delta T_0 \left(\frac{1}{R_s} - \frac{1}{R_r} \right) + (c_r - c_s) \frac{dT_s}{dt} - c_r \frac{d\Delta T}{dt} \tag{11}$$

where T_s is the sample sensor temperature, T_r is the reference sensor temperature, T_0 is the cell base sensor temperature, ΔT is the temperature difference between sample and reference sensors, ΔT_0 is the temperature difference between sample and T_0 sensors, dT_s/dt is the sample heating rate, $d\Delta T/dt$ is the time rate of change of ΔT, q_s is the sample heat flow rate, q_r is the reference heat flow rate, q_{T4} is the heat flow rate measured by DSC, c_s is the thermal capacitance between sample sensor and furnace, c_r is the thermal capacitance between reference sensor and furnace, R_s is the thermal resistance between sample sensor and furnace, and R_r is the thermal resistance between reference sensor and furnace.
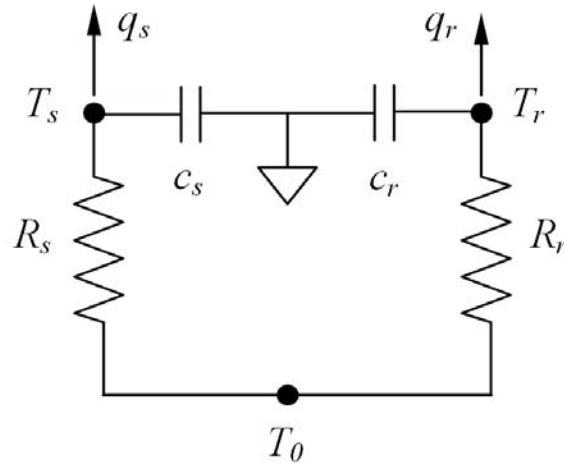
Figure 10. Equivalent thermal circuit for a DSC cell with Tzero technology [42].

The first term on the right hand side of equation (11) is equal to the heat flow measured by conventional DSC (equation (5)). The second and third terms account for the thermal

14

resistance and capacitance imbalances between the sample and reference, respectively. The fourth term accounts for the heating rate imbalance between the sample and reference. The second, third, and fourth terms in equation (11) make it possible to measure the heat flow accurately without assuming that the DSC cell is symmetric.

The measured heat flow from the thermosetting prepreg sample during cure can be used to calculate its degree of cure with the following equation:

$$\alpha(t) = \frac{\int_0^t q\,dt}{H_U} \tag{12}$$

where $\alpha(t)$ is the degree of cure, q is the heat released from the sample from time 0 to time t during cure measured by DSC, and H_U is the ultimate heat of reaction obtained by the experiment.

2.2.1. Cure Kinetic Models

Cure kinetic models are used to find the degree of cure at any arbitrary time-temperature during cure. To date, several models have been developed to characterize the curing process of different resin systems [43]. Those models with more than one rate constant have proven to be more appropriate for resin systems with complicated cure reactions. The addition of a diffusion term to the cure kinetics models helps improve their accuracy when the cure process approaches completion and the reactions become diffusion controlled rather than kinetics controlled. Cure kinetics models without the diffusion term are more appropriate when the curing process rate is controlled by kinetics of bond formation [44].

2.2.1.1. Barrett Model

The Barrett model, also known as the Borchardt and Daniels model, or the nth-order model, has one rate constant and can be defined as [45]

$$\frac{d\alpha}{dt} = k(1-\alpha)^n \qquad (13)$$

where n is the exponential constant, and k is the rate constant, which depends on the temperature in an exponential manner and is defined as:

$$k = A_0 \exp(-\frac{\Delta E}{RT}) \qquad (14)$$

where A_0 is the pre-exponential factor, ΔE is the activation energy, R is the universal gas constant, and T is the absolute temperature. A_0, ΔE, and n are the parameters of the model found by fitting curve to the $d\alpha/dt$ vs. α and T data.

2.2.1.2. Kamal Model

The Kamal model, also known as the autocatalytic model, can be defined as [46]

$$\frac{d\alpha}{dt} = (k_1 + k_2\alpha^m)(1-\alpha)^n \qquad (15)$$

where α is the degree of cure, $d\alpha/dt$ is the time rate of the degree of cure, m and n are the first and second exponential constants, respectively, and k_1 and k_2 are the rate constants, which depend on the temperature in an exponential manner and are defined by equations (16) and (17):

$$k_1 = A_1 \exp(-\frac{\Delta E_1}{RT}) \qquad (16)$$

$$k_2 = A_2 \exp(-\frac{\Delta E_2}{RT}) \qquad (17)$$

where A_1 and A_2 are the pre-exponential factors, ΔE_1 and ΔE_2 are the activation energies, R is the universal gas constant, and T is the absolute temperature. A_1, A_2, ΔE_1, ΔE_2, m, and n are the parameters of the model found by fitting the curve to the $d\alpha/dt$ vs. α and T data.

2.2.1.3. Kamal-with-Diffusion Model

The Kamal-with-diffusion model is simply the Kamal model with an extra diffusion term. It can be defined as [47, 48]

$$\frac{d\alpha}{dt} = \frac{1}{1 + \exp(C(\alpha - \alpha_c))}(k_1 + k_2\alpha^m)(1-\alpha)^n \tag{18}$$

where m, n, k_1, and k_2 are the same as those of the Kamal model. The term $1/(1+\exp(C(\alpha-\alpha_c)))$ is the diffusion factor that includes two constants: C, the diffusion constant, and α_c, the critical degree of cure. A_1, A_2, ΔE_1, ΔE_2, C, m, and n are the parameters of the model found by fitting the curve to the $d\alpha/dt$ vs. α and T data.

2.2.1.4. Springer-Loos Model

The Springer-Loos model is defined as [15]

$$\frac{d\alpha}{dt} = (k_1 + k_2\alpha)(1-\alpha)(B_1 - \alpha) \tag{19}$$

where B_1 is a constant, and k_1 and k_2 are the rate constants, which depend on the temperature in an exponential manner and are defined by equations (16) and (17). A_1, A_2, ΔE_1, ΔE_2, and B_1 are the parameters of the model found by fitting the curve to the $d\alpha/dt$ vs. α and T data.

2.2.1.5. Cole-with-Diffusion Model

The Cole-with-diffusion model can be defined as [49, 50]

$$\frac{d\alpha}{dt} = \frac{1}{1 + \exp\left(C(\alpha - (\alpha_{c0} + \alpha_{cT}T))\right)}(k\alpha^m)(1-\alpha)^n \tag{20}$$

where m and n are the first and second exponential constants, respectively, and k is the rate constant, which depends on the temperature in an exponential manner and is defined as

$$k = A\exp(-\frac{\Delta E}{RT}) \tag{21}$$

where A is the pre-exponential factor, $\varDelta E$ is the activation energy, R is the universal gas constant, and T is the absolute temperature. The term $1/(1+\exp(C(\alpha-(\alpha_{c0}+\alpha_{cT}T))))$ is the diffusion factor that includes three constants: C, the diffusion constant; α_{c0}, the critical degree of cure at $T= 0^{\circ}K$; and α_{cT}, a constant that accounts for increase in the critical resin degree of cure with temperature. A, $\varDelta E$, C, α_{c0}, and α_{cT} are the parameters of the model found by fitting the curve to the $d\alpha/dt$ vs. α and T data.

2.3.   Monitoring Viscoelastic Properties

Viscoelastic properties of the resins and composites are usually measured by a dynamic mechanical analyzer (DMA). The DMA applies steady-state oscillation or vibration to a sample of the viscoelastic material and measures the state of stress in the sample during its vibration [51]. Several methods are used to apply oscillatory force to the sample: tensile, compression, torsion, or bending [52]. Storage modulus (G'), loss modulus (G"), tanδ, and complex viscosity are different viscoelastic properties that can be measured using the DMA [53]. Gel time and glass transition temperature are other material properties that can be obtained using the DMA; however, these properties are not directly measured and should be derived from other viscoelastic properties. The viscoelastic properties of the thermosetting resins and composites change as they are being cured. If these changes are measured continuously, the state of the material and cure will be known throughout the cure cycle.

A parallel-plate encapsulated sample rheometer (ESR) equipped with a DMA has proven to be a good choice for monitoring the state of material during cure, since it can measure its viscoelastic properties from the low viscosity region to the solid glassy region [12].

Figure 11 depicts the torsion of a cylinder under torque Ψ. As can be seen, for a cylinder with unit thickness ($H = 1$) [54],

18

$$\gamma = r\theta \tag{22}$$

where γ is the strain, r is the radius of the cylinder, and θ is the angular rotation. For linear elastic torsion, shear stress is proportional to the distortion as

$$\tau = G\gamma = Gr\theta \tag{23}$$

where τ is the shear stress, and G is the shear modulus. In order to find the torque for a cylinder with unit thickness, the stresses acting on the circular cross should be integrated as

$$d\Psi = (\tau 2\pi r dr)r = G\gamma 2\pi r^2 dr = G\theta 2\pi r^3 dr \tag{24}$$

$$\Psi = 2G\theta\pi \int_0^R r^3 dr = G\theta I_p \tag{25}$$

where Ψ is the torque, I_p ($= \dfrac{\pi D^4}{32}$) is the polar moment of inertia of the cylindrical sample's cross section with respect to its center, D is the diameter of the cylinder, and GI_p is the torsional stiffness of the cylinder. For a cylinder with thickness H, torque is

$$\Psi = \frac{I_p G\theta}{H} \tag{26}$$

where θ is the angular rotation, Ψ is the torque, I_p is the polar moment of inertia of the cylindrical sample's cross section with respect to the center, GI_p is the torsional stiffness of the cylinder, and H is the thickness of the cylinder.
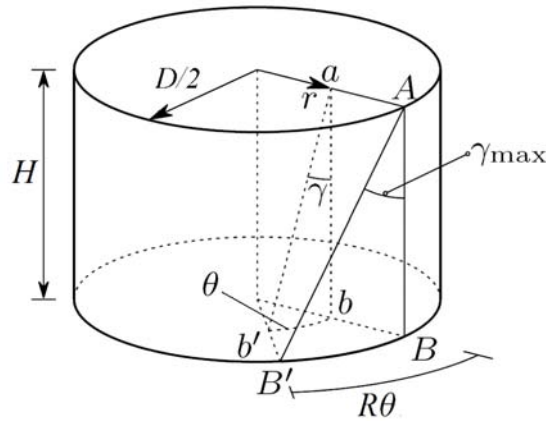
Figure 11. Torsion of cylinder under torque [54].

19

The parallel-plate strain-controlled rheometer applies a sinusoidal strain to a cylindrical sample and measures the torque in order to obtain viscoelastic properties of the sample during cure (Figure 12). The complex shear modulus of the sample is then obtained using

$$\left|G^*\right| = \frac{\Psi H}{I_p \theta} \tag{27}$$

where G^* is the complex shear modulus of the sample, θ is the angular rotation, Ψ is the measured torque, I_p is the polar moment of inertia of the cylindrical sample's cross section with respect to the center, and H is the thickness of the sample. Then, the complex viscosity of the sample is calculated using

$$\left|\eta^*\right| = \frac{\left|G^*\right|}{\omega} \tag{28}$$

where η^* is the complex viscosity, G^* is the complex shear modulus, and ω is the angular frequency of the sinusoidal strain.
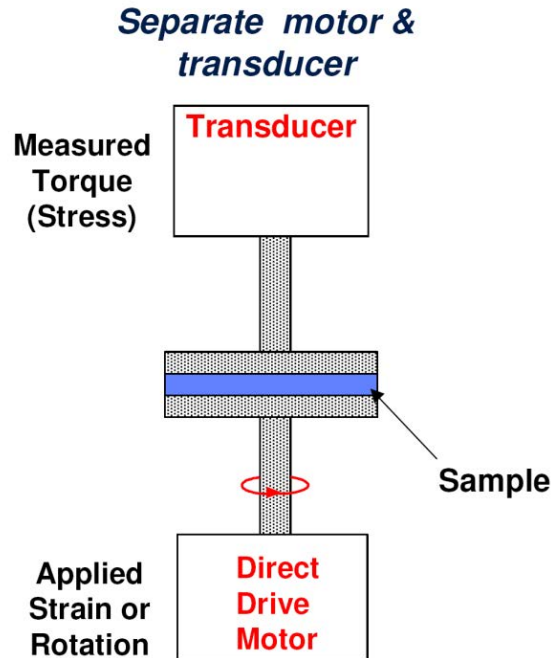
Figure 12. Schematic of strain-controlled parallel-plate rheometer [55].

20

2.3.1. Complex Viscosity Models

Viscosity of the thermosetting resins changes drastically during cure. The resin viscosity depends on the cure temperature and degree of cure. As such, advanced viscosity models should include these two variables. Viscosity models are often fitted to the complex viscosity data obtained during cure of the thermosetting resins and composites using the rheometer.

2.3.1.1. Ampudia Model

The Ampudia viscosity model relates the complex viscosity of the thermosetting resin with its isothermal cure time and is defined as [56]

$$\eta^* = \eta_1 \exp(k't) \tag{29}$$

where η^* is the complex viscosity, t is the isothermal cure time, and η_1 and k' are defined by the following equations:

$$\eta_1 = \eta_a \exp(\frac{E_\eta}{RT}) \tag{30}$$

$$k' = k'_\infty \exp(-\frac{E_k}{RT}) \tag{31}$$

where η_a and k'_∞ are constants, E_η and E_k are the activation energies, R is the universal gas constant, and T is the absolute isothermal cure temperature. Parameters η_a, k'_∞, E_η, and E_k of the model are found by fitting the curve to the η^* vs. t data.

2.3.1.2. Dusi Model

The Dusi viscosity model, which has found the most application in complex viscosity modeling for thermosetting resins is defined as [34]

$$\eta^* = \eta_a \exp(k'\alpha) \exp(\frac{U}{RT}) \tag{32}$$

where η^* is the complex viscosity, η_a is a constant, α is the degree of cure, U is the activation energy for viscosity assumed to be independent of the degree of cure, k' is a constant assumed to be independent of temperature, R is the universal gas constant, and T is the absolute temperature. Parameters η_a, k', and U of the model are found by fitting the curve to the η^* vs. α and T data. To make the curve fitting easier, one can take the natural log of both sides of the above equation to obtain the following:

$$\ln\eta^* = \ln\eta_a + k'\alpha + \frac{U}{RT} \tag{33}$$

2.3.1.3. Kenny Model

The Kenny viscosity model is defined as [57]

$$\eta^* = A_\mu \exp(\frac{E_\mu}{RT})\left[\frac{\alpha_g}{\alpha_g - \alpha}\right]^{A+B\alpha} \tag{34}$$

where η^* is the complex viscosity, α is the degree of cure, α_g is the degree of cure at gelation, R is the universal gas constant, T is the absolute temperature, E_μ is the activation energy, and A_μ, A, and B are constants. Parameters A_μ, A, B, and E_μ of the model are found by fitting the curve to the η^* vs. α and T data. To make the cure fitting easier, equation (34) is rewritten in the natural log form as

$$\ln\eta^* = \ln A_\mu + \frac{E_\mu}{RT} + (A+B\alpha)\ln\left(\frac{\alpha_g}{\alpha_g - \alpha}\right) \tag{35}$$

2.3.1.4. Williams–Landel–Ferry Model

The Williams-Landel-Ferry (WLF) viscosity model states the viscosity of thermosetting resins in terms of the degree of cure and cure temperature and is defined as [57]

$$\eta^* = \eta_g \left(\frac{-C_1(T-T_{g0})}{C_2+T-T_{g0}} \right) \left[\frac{\alpha_g}{\alpha_g - \alpha} \right]^n \qquad (36)$$

where η^* is the complex viscosity, η_g is the viscosity at glass transition temperature, α is the degree of cure, α_g is the degree of cure at gelation, T is the absolute temperature, T_{g0} is the glass transition temperature of the uncured resin, and C_1 and C_2 are WLF constants equal to 17.44 and 56.1, respectively. The exponential constant n is found by fitting the curve to the η^* vs. α and T data.

2.3.1.5. Sun Model

The Sun viscosity model is developed for the isothermal cure of epoxy prepregs and is defined as [48]

$$\eta^* = \frac{\eta_0 - \eta_\infty}{1 + \exp(k'(t - t_c))} + \eta_\infty \qquad (37)$$

where η^* is the complex viscosity, η_0 and η_∞ are the initial and final complex viscosities during isothermal cure, respectively, t is the isothermal cure time, k' is a rate constant, and t_c is the critical time defined by

$$t_c = A_t \exp\left(\frac{E_t}{RT}\right) \qquad (38)$$

where A_t is a constant, E_t is the activation energy, R is the universal gas constant, and T is the absolute temperature. Parameters η_0 and η_∞ are directly found from the complex viscosity data. Parameters A_t, and E_t of the model are found by fitting the curve to the η^* vs. t data.

2.3.2. Glass Transition Temperature and Gel Time Models

The glass transition temperature of polymers and polymer composites has been studied by many investigators [58, 59]. Above the T_g, large-scale molecular motions (molecular mobility) occur in thermosetting resins. While the uncross-linked polymers become liquid as a

result of such an increase in molecular mobility, the cross-linked thermosetting resins become rubber-like above the T_g, due to the covalent cross-links that serve as constraints for the mobility of the chain segments [60]. In the aerospace industry, the glass transition temperature is a design parameter since the service temperature of composite parts should be well below the T_g of the cured composite material [61]. The T_g is correlated to the degree of cure by equation (39), known as the DiBenedetto equation [62]:

$$T_g = \frac{(1-\alpha)T_{g0} + \lambda\alpha T_{g\infty}}{(1-\alpha) + \lambda\alpha} \tag{39}$$

where α is the degree of cure; $T_{g\infty}$ and T_{g0} are the ultimate glass transition temperature of the fully cured resin and the initial glass transition temperature of the uncured resin, respectively; and λ, the ratio of segmental mobility, is an adjustable structure-dependent parameter ($0 \leq \lambda \leq 1$) that can be found by fitting the cure to the T_g vs. α data.

Gel time is more important than the T_g from a processing point of view and, therefore, has been the focus of attention by investigators interested in processing composite materials [63]. After the gelation polymer loses its fluidity, it is not possible to force out the air and volatiles trapped between the layers of the composite laminate by applying pressure. Equation (40) relates the natural log of the gel time with the reciprocal of the isothermal cure temperature [48]:

$$t_{gel} = c\exp(\frac{E_a}{RT}) \tag{40}$$

where t_{gel} is the gel time, R is the universal gas constant, T is the absolute temperature, E_a is the activation energy, and c is a constant. Parameters E_a and c are found by fitting the curve to the t_{gel} vs. $1/T$ data.

2.4. Mechanical Properties

The effect of the cure cycle on the mechanical properties of thermosetting resins has been studied previously. The results of these studies suggest the following:

- Mechanical properties of the cured composite laminate depend on its state of cure [64].

- If the composite laminate is not cured enough, its mechanical properties drop [65].

The extent of cure affects the resin-dominated mechanical properties of composites, such as compression strength and interlaminar shear strength, more than the fiber-dominated mechanical properties of composites, such as tensile strength. This is because the yield stress of thermosetting resins is influenced by the cross-link density: the distance between the covalent cross-links that serve as the topological constraints in thermosetting resins is of a length scale relevant for yielding/plastic deformation.

The yield stress of thermosetting resins at temperatures below T_g can related to the T_g using the following equation [60]:

$$\sigma_y = \sigma_{yg} + b(T_g - T) \tag{41}$$

where σ_y is the yield stress, σ_{yg} is the yield stress at T_g, T is the temperature, T_g is the glass transition temperature, and b is a positive constant.

On the other hand, the elastic modulus of the thermosetting resins at temperatures below T_g is mainly dominated by the inter-chain interactions on a local-length scale and, therefore, is not strongly affected by the cross-link density.

2.5. Staged Cure Cycles

Viscosity evolution and cure kinetics of several polymer composites during isothermal and ramp cure cycles have been studied extensively [43]; however, the staged cure cycles that include both ramp and isothermal steps have been studied less. Figure 13 illustrates the different

types of cure cycles that might be appropriate for thermosetting polymer composites. Staged cure cycles are commonly used in industry for autoclave curing. Much effort has been devoted in recent years to studying two-stage cure cycles for epoxy polymer composites. For example, some researchers have tried to reduce thermal residual stresses in composites [66, 67] using the staged cure cycles, while others have tried to eliminate voids and improve mechanical properties of the composites [68-71] using the staged cure cycles. Although calculating the degree of cure for either the isothermal or ramp cure cycles is straightforward, obtaining this parameter for the staged cure cycles is challenging because the heat-flow baseline for the ramp stage is different than for the isothermal stage.
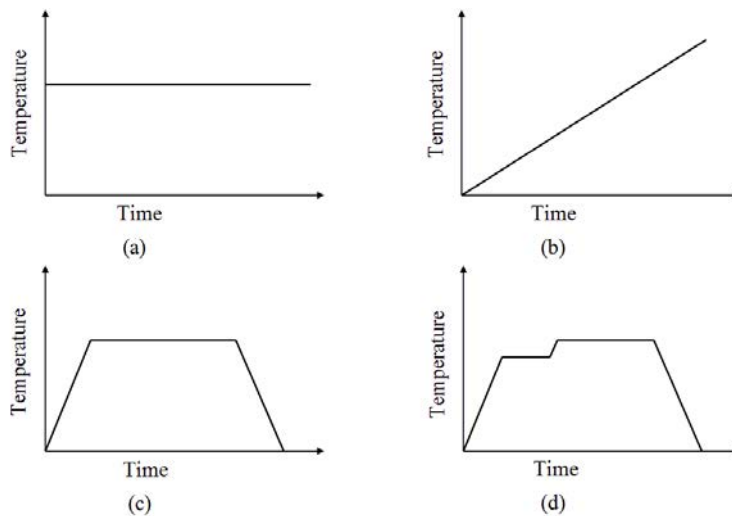
Figure 13. Schematic of different cure cycles for thermosetting polymer composites: (a) isothermal, (b) ramp, (c) one-stage, and (d) two-stage.

This dissertation addresses the baseline issue for DSC heat flow for the staged cure cycles. When the heat flow baseline is determined, the degree of cure can be obtained for any staged cure cycle. Then, it can be modeled and the model used to predict the viscosity of the polymer composite materials at any time during the cure cycle. The degree of cure and viscosity models can be used as a tool to provide a direct estimation of the material state during curing.

CHAPTER 3

TECHNICAL APPROACH

3.1. Proposed Approach to Curing of Composites

Recent development of a parallel-plate encapsulated sample rheometer equipped with a dynamic mechanical analyzer has enabled complete and repeatable measurement of the viscoelastic properties of a composite material during cure from a low-viscosity region to a high-viscosity region [12]. The rheometer can be used as an ex-situ cure monitoring instrument, simulating the real curing processes such as autoclaving and hence eliminating the need for multiple measurement instruments. The measured viscoelastic properties can be used to determine the material state throughout the curing process. The cure time-temperature data as provided by thermocouples attached to the composite part is the only input to the rheometer for cure simulation.

Utilizing the rheometer as the main ex-situ cure monitoring instrument makes it possible to offer a new approach to curing composites. In the new approach, called Material State Management (MSM), the acceptance of the cured composite parts is based on the viscoelastic properties of the material as measured by the rheometer during cure and post-cure simulation (Figure 14). MSM is based on the assumption that the viscoelastic properties are indicative of other important material properties, such as mechanical properties, and therefore can be used for acceptance or rejection of composite materials.

Moreover, the knowledge of the viscoelastic properties of the material during cure can bring the possibility of modifying the current time-temperature-based specifications [72]. Confidence limits of the new cure process in the new specifications will be defined based on the viscoelastic properties of the material. The existence of a massive material state database and

model makes it feasible to design the new specifications based on the viscoelastic properties. Although the rheometer can provide the viscoelastic properties data during cure, developing the material state models requires DOC data as well, since many sophisticated viscoelastic properties models need both DOC and cure temperature data to predict the stat of the material during cure. As such, the DSC should be coupled with the rheometer to provide the required data for material state models.
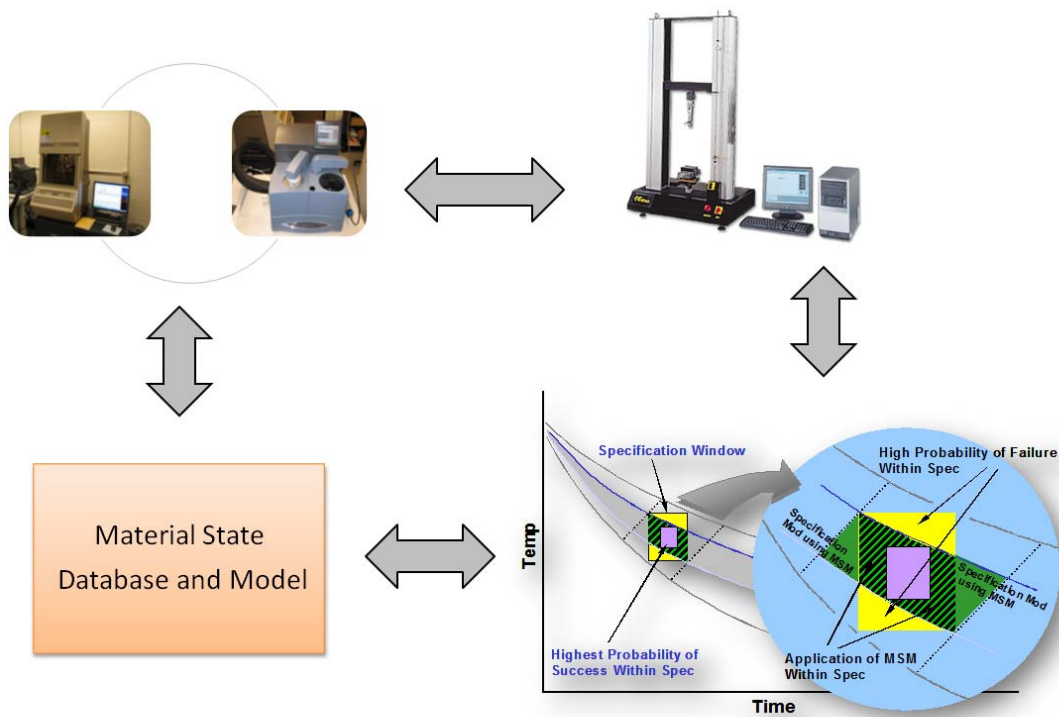
(Graph courtesy of Mike Frena, OO-ALC)

Figure 14. Proposed approach to curing composites.

The new approach to curing addresses shortcomings of the current approach. For example, the new approach lowers the risk of curing by offering larger cure confidence limits and eliminates the need for extensive coupon testing to certify the cured parts [12]. Moreover, important changes in the material state during cure will be observable, and the actual final mechanical properties of the material will be predictable once the viscoelastic properties of the

28

material are known. Also, with the new approach, it is possible to correlate the key variables during cure.

In this dissertation, complex viscosity is the viscoelastic property of choice for monitoring the state of the material during cure. The reasons for selecting the complex viscosity for material-state monitoring are as follows:

- Complex viscosity can be precisely measured throughout the cure and post-cure cycles using the rheometer.

- Complex viscosity can be used for monitoring the state of the material during cure; as explained in sections 3.3.1.1 and 3.4.1.1.

- Important changes in the material state during cure, such as minimum viscosity, gelation, and vitrification, can be found using the complex viscosity graph. As such, complex viscosity can provide the information required for designing the proper cure cycle, as explained in sections 3.3.1.5 and 3.4.1.5.

- Complex viscosity can be adequately modeled by existing viscosity models, as explained in section 3.5.2.

- Complex viscosity can be correlated to the mechanical properties, as explained in section 3.5.3.

3.1.1. Thermal Analysis

3.1.1.1. Degree of Cure Equations

Equation (42) states the heat released from the sample during cure in terms of the material properties [73]:

$$\frac{dQ}{dt} = C_p \frac{dT}{dt} + f(T,t) \tag{42}$$

where dQ/dt is the sample heat flow measured by DSC, C_p is the sample heat capacity (sample specific heat × sample weight), dT/dt is the heating rate, and $f(T,t)$ is the kinetic heat flow, which is a function of time at an absolute temperature. Note that for an isotehrmal DSC run, the first term on the right-hand side of equation (42) is equal to zero since dT/dt is zero. Figure 15 shows the heat flow of a thermosetting resin during cure measured by DSC using dynamic scanning (i.e., being heated at a constant heating rate) and isothermal scanning (i.e., being held at a constant temperature).
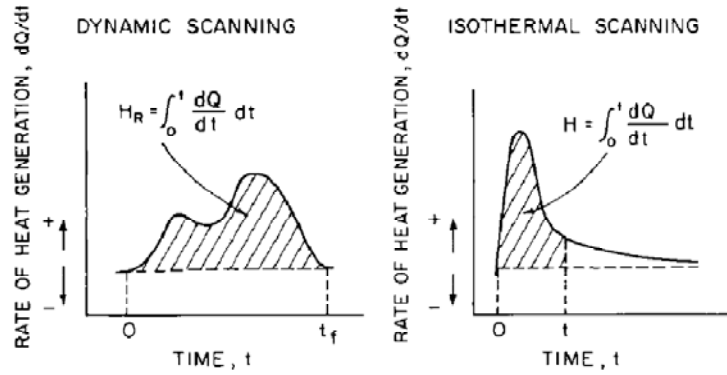
Figure 15. Heat flow of thermosetting resin during cure measured by DSC using dynamic scanning and isothermal scanning [15].

During the cure cycle, the degree of cure at time t is given by [74]

$$\alpha(t) = \frac{H(t)}{H_U} \tag{43}$$

where $\alpha(t)$ is the degree of cure, and $H(t)$ is the total amount of heat released from the sample from time 0 to time t during cure (Figure 16) and is defined as

$$H(t) = \int_0^t \left(\frac{dQ}{dt}\right) dt \tag{44}$$

H_U, the ultimate heat of reaction, is defined as

$$H_U = H_T + H_{res} \tag{45}$$

where H_T is the total heat released during cure, and H_{res}, the area under the heat flow curve in dynamic scanning performed immediately after the end of the cure cycle in order to release the residual heat of the sample, is defined as

$$H_{res} = \int_{t_s}^{t_e} \left(\frac{dQ}{dt} \right) dt \tag{46}$$

where t_s and t_e represent the start and end times, respectively, of the exothermic reactions during dynamic scanning.
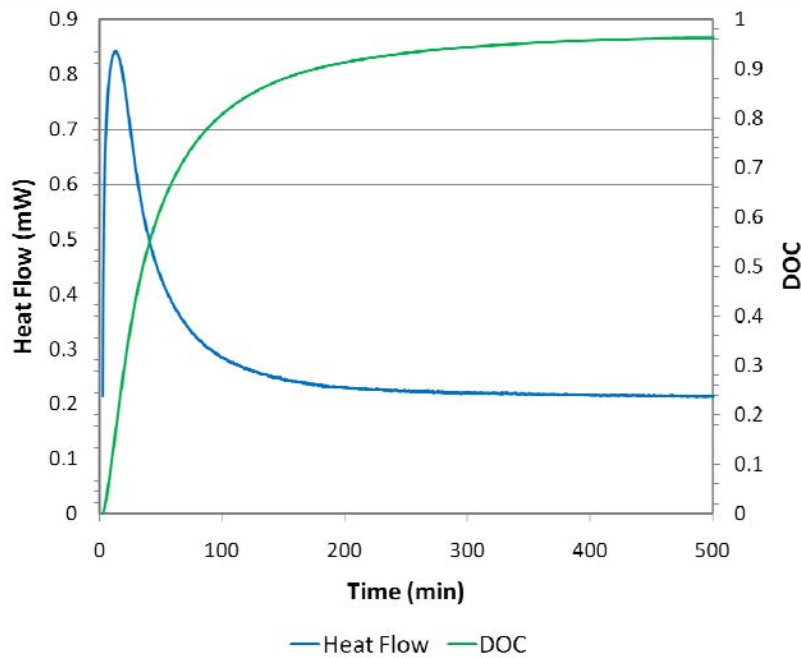
Figure 16. Heat flow and degree of cure for a 977-2 UD sample cured at 177°C.

After substituting equation (43) into equation (45), the degree of cure will be

$$\alpha(t) = \frac{H(t)}{H_T + H_{res}} \tag{47}$$

Subsequently, the rate of the degree of cure is

$$\frac{d\alpha(t)}{dt} = \frac{dH(t)/dt}{H_T + H_{res}} \tag{48}$$

31

Since H_U is used in DOC calculations, it is important to obtain its accurate value. While some scholars assume that H_U is a material property and independent of the cure cycle it undergoes [48], others assume that H_U depends on the cure cycle [74]. The latter assumption was used in this study, as it described the behavior of the subject prepreg properly. It is important to note that for a fully cured resin, the DOC is equal to one, whereas for an uncured resin, the DOC is equal to zero. The prepreg resin is partially cured. This means that the DOC for the resin of the prepreg is greater than zero; however, since the exact DOC of the fresh prepreg is usually unknown for its users, it is usually assumed that the DOC for the prepreg is equal to zero [15, 74]. That is why some researchers refer to the prepreg DOC as the relative conversion or relative DOC [75]. The measured results shown in Figure 16 illustrate the relation between the heat flow and degree of cure for a 977-2 UD sample cured at 177°C.

The baseline in DSC terminology has three definitions [3]:

1. The instrument baseline, also called the zeroline [76]. This baseline is the DSC residual heat-flow signal when it runs empty [77]. It is desirable to keep this baseline as close as possible to zero.

2. The extrapolated portion of the DSC curve in exothermic or endothermic transitions over which the heat flow peak should be integrated.

3. The premelting and postmelting baselines.

In this dissertation, the second definition of the baseline, which affects calculation of thermal properties measured by DSC, is referred to as the baseline.

Figure 17 shows the zeroline, baseline, peak, and characteristic temperatures for an arbitrary heat-flow curve. A peak in the DSC heat-flow curve, such as the one shown in Figure 17, appears when the DSC sample generates heat. Parameter t_i marks the time (temperature) at

which the heat-flow curve deviates from its original direction and moves toward the peak.

Parameter t_f is the time (temperature) at which the heat flow curve merges back into the baseline.

The heat-flow peak occurs at time (temperature) t_p. The interpolated baseline (dashed line under

the peak) connects t_i to t_f. It is obtained assuming that the sample have not released heat from

time t_i to time t_f. The baselines for the isothermal and dynamic scanning using DSC have been

studied previously [76, 78-80]. Höhne et al. developed a method for finding the baseline for DSC

heat-flow curves [76]. Table 3 shows different heat-flow baseline constructions for calculating

the enthalpy of ice melting. The suggested heat-flow baselines can also be used for degree-of-

cure calculations.
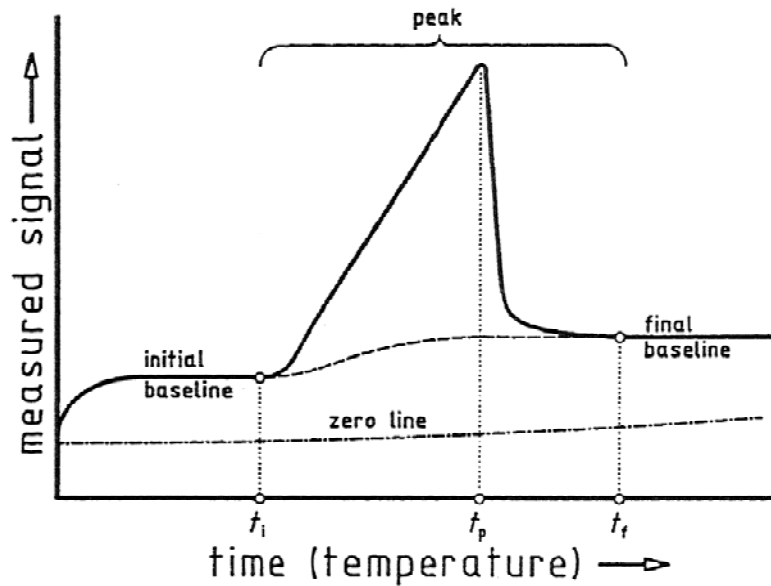
Figure 17. Zeroline, baseline, and peak for arbitrary heat flow curve [79].

33

TABLE 3

DIFFERENT BASELINE CONSTRUCTIONS FOR CALCULATING THE ENTHALPY OF ICE MELTING [79]

Baseline Number	Method	Representation
1	e-function (true baseline)	
2	straight line	
3	step	
4	polygon	
5	intersection	
6	intersection + triangle	
7	parabola	
8	thermodynamic	
9	proportional to degree of conversion	
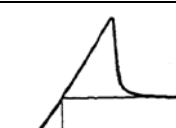
3.1.2. Rheological Analysis

In order to obtain viscoelastic properties of the sample during cure, the rheometer applies

a sinusoidal shear strain with frequency f to a cylindrical sample (Figure 18). The applied shear

strain is then [81]

$$\gamma = \gamma_0 \sin(\omega t) \qquad (49)$$

where γ is the sinusoidal strain, ω (=$2\pi f$) is the angular frequency of the strain, and γ_0 is the

amplitude of the strain.
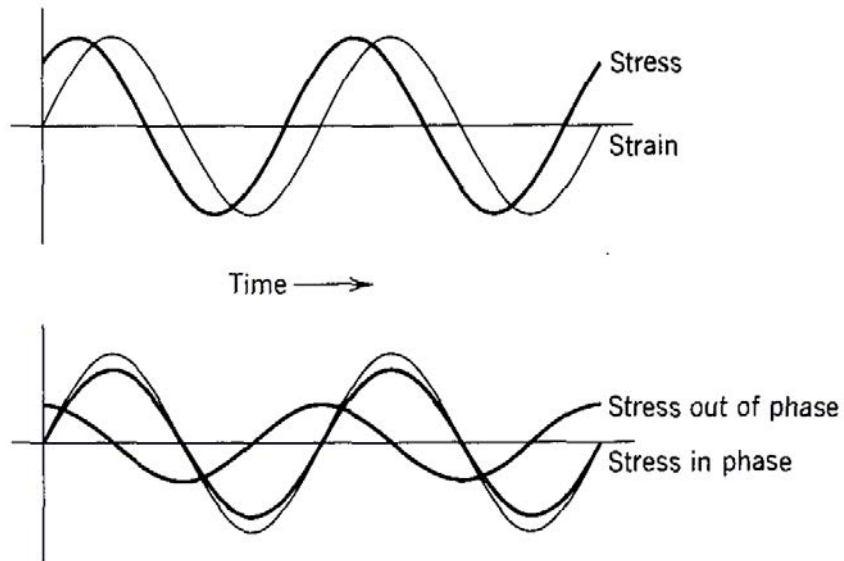
Figure 18. Viscoelastic material's stress response to sinusoidal strain [82].

If the shear strain amplitude is small enough, the relation between the shear strain and

stress will be linear [51]. The stress response τ of the viscoelastic sample, therefore, will be

sinusoidal with a phase lag δ and amplitude τ_0 (Figure 18):

$$\tau = \tau_0 \sin(\omega t + \delta) \qquad (50)$$

where τ is the stress response of the viscoelastic sample, τ_0 is the amplitude of the stress, and δ is

the phase lag of the stress response. It is noticeable that for a pure elastic material, $\delta = 90^\circ$,

35

whereas for a pure viscous material, $\delta = 0^o$, and for a viscoelastic material, $0^o < \delta < 90^o$. The stress response equation can be rewritten as

$$\tau = (\tau_0 \cos\delta)\sin(\omega t) + (\tau_0 \sin\delta)\cos(\omega t) \tag{51}$$

To express the response of the viscoelastic material in terms of shear modulus, both sides of the above equation should be divided by strain amplitude γ_0:

$$\frac{\tau}{\gamma_0} = \frac{\tau_0 \cos\delta}{\gamma_0}\sin(\omega t) + \frac{\tau_0 \sin\delta}{\gamma_0}\cos(\omega t) \tag{52}$$

$$G = G'(\omega)\sin(\omega t) + G''(\omega)\cos(\omega t) \tag{53}$$

where G is the shear relaxation modulus, G' $(=\tau_0 \cos\delta/\gamma_0)$ is the storage modulus representing the energy storage or the elastic portion of the viscoelastic material's behavior, and G" $(=\tau_0 \sin\delta/\gamma_0)$ is the loss modulus representing the energy loss. The tangent of the phase lag, tanδ, is equal to the ratio of the loss modulus to the storage modulus, G"/G'. The parameter tanδ is a measure of energy dissipation. Parameters G', G", and tanδ are viscoelastic properties of the material.

Sometimes viscoelastic properties of the material are expressed in terms of imaginary variables. The imaginary complex shear modulus is defined as [82]

$$\tau * / \gamma * = G* = G' + iG'' \tag{54}$$

and

$$|G*| = \tau_0 / \gamma_0 = \sqrt{G'^2 + G''^2} \tag{55}$$

3.1.2.1. Complex Viscosity

Another viscoelastic property is complex viscosity, $\eta*$, which is defined as [83]

$$\eta* = \eta' - i\eta'' = \frac{G*}{i\omega} = \frac{G''}{\omega} - i\frac{G'}{\omega} \tag{56}$$

where η', the dynamic viscosity, is defined as [84]

$$\eta' = \frac{G''}{\omega} \tag{57}$$

and the elastic part of the complex viscosity is [84]

$$\eta'' = \frac{G'}{\omega} \tag{58}$$

Complex viscosity, which is a viscoelastic property, is related to steady shear viscosity by the Cox-Mertz equation [85, 86]:

$$\eta(\dot{\gamma}) = |\eta^*|(\omega) \quad at \quad \dot{\gamma} = \omega \tag{59}$$

Equation (59) states that when the apparent frequency equals the shear rate, the magnitude of the complex viscosity is equal to the magnitude of the shear viscosity.

The complex viscosity, degree of cure, and cure temperature during cure for 977-2 UD samples cured at $177^{\circ}C$ for 180 minutes is shown in Figure 19. As the figure shows, at the start of the cure cycle (the first 50 minutes of the cure cycle), the effect of cure temperature is dominant. At this stage, the degree of cure is almost zero, indicating occurrence of little or no chemical cross-linking reactions. At the temperature-dominated region, the viscosity of resin, as with most fluids, decreases with an increase in the cure temperature. Nevertheless, as the cure proceeds, the effect of cross-linking becomes more dominant. At this stage, cross-linking reactions occur at an increasingly fast rate, thus causing the degree of cure curve to climb rapidly. As a result, the viscosity rises significantly since the mobility of the resin becomes progressively restricted due to intermolecular cross-linking [87]. The degree of cure approaches its plateau value after 200 minutes, which means completion of the cross-linking reactions.

Figure 20 shows a typical two-stage cure cycle for composites. As can be seen, the dwell temperature and time at the first stage are usually less than at the second stage. The effect of the cure temperature is dominant in the first stage. During this stage, the resin flows and consolidates the composite part. In addition, unwanted gasses trapped in the composite part, such as air, water vapor, and volatiles, escape. The effect of cross-linking is dominant in the second stage. The

resin cures in this stage, and as a result, the mechanical properties of the composite are developed [11].
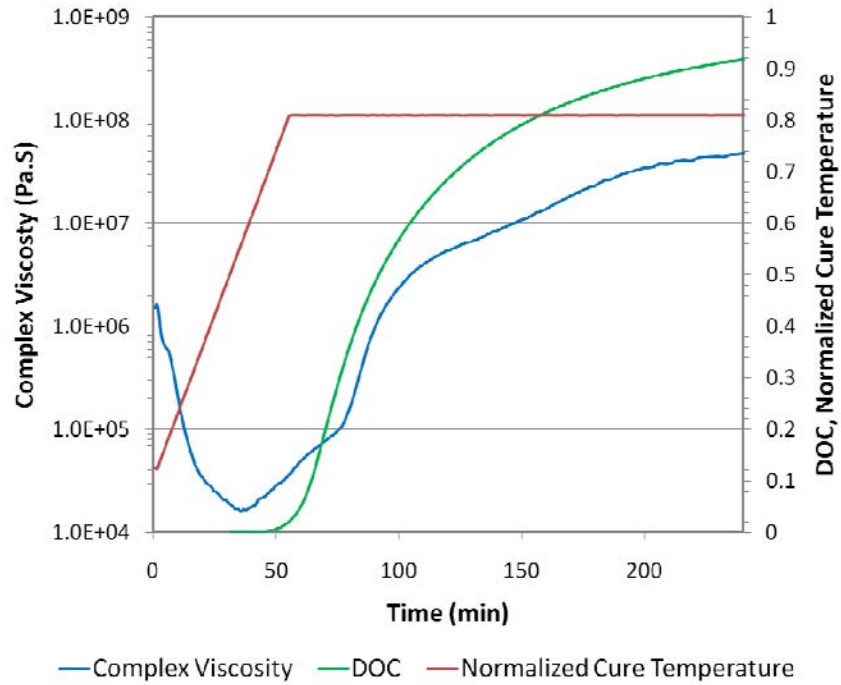
Figure 19. Complex viscosity, degree of cure, and cure temperature during cure for 977-2 UD.
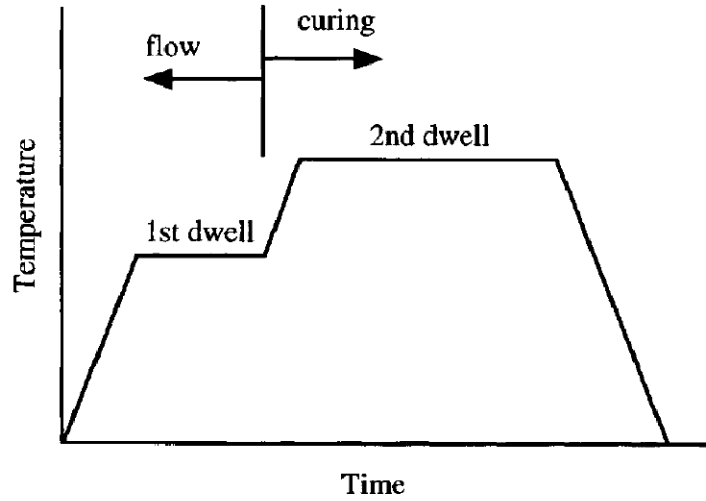
Figure 20. Typical two-stage cure cycle for composites [11].

3.1.3. Mechanical Properties

Combined loading compression (CLC) tests, open-hole compression tests (OHC), and short beam shear (SBS) tests are commonly used to obtain the mechanical properties of aerospace composite materials [61]. CLC tests provide compressive modulus, strength, and Poisson's ratio. OHC tests provide OHC strength and modulus. SBS tests provide only SBS strength.

Although the SBS test is extensively used in industry to assess the interlaminar (short beam) shear of composite materials, SBS strength is not related to any material property, due to the diversity of failure modes that may happen in SBS specimens and the complexity of internal stresses caused by the SBS test [88].

The CLC test is widely accepted in industry since its test coupon preparation is simple and inexpensive [89]. Moreover, the unique CLC test fixture helps reduce unacceptable end-crushing failures compared to other compression tests such as ASTM D 695 [90] and, therefore, makes this test very reliable.

The OHC test is usually performed to obtain notched compressive strength data. It is used primarily to measure structural design allowables, material specifications, and quality assurance parameters [91].

3.1.3.1. Statistical Analysis

One-way analysis of variance (ANOVA) was the statistical analysis method used to investigate the difference between mechanical properties for different sets of specimens and to determine if different sets of data are members of the same population and, therefore, show no statistically significant difference. Minitab$_{TM}$ was the statistical software package used. Table 4 contains a sample of the Minitab$_{TM}$ ANOVA output.

TABLE 4

SAMPLE OF MINITAB ANOVA ANALYSIS

```
               Individual 95% CIs For Mean Based on Pooled StDev
Level            -+---------+---------+---
182C 180min                            (---*-|    Overlapping
177C 180min                          (---*---)   Confidence
171C 180min                          --*---      Intervals
160C 180min                            (----*---)
149C 180min      (---*---)
160C 400min                          (---*---)
149C 400min                              (---*---)
               -+---------+---------+---------+--------
               80.0      85.0      90.0      95.0
```
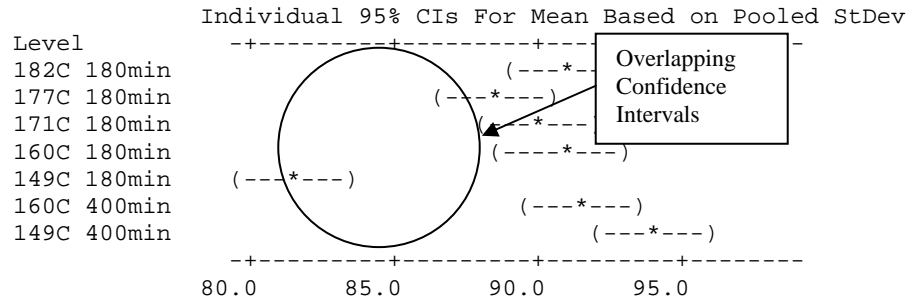
If the data shows an overlap in the confidence intervals, then there is no statistically significant difference between the data sets for the given parameter. This is true if there is more than a 5 percent chance that two samples achieve the same mean value.

Standard deviation and coefficient of variation are two statistical terms utilized in this dissertation to show the variation in mechanical testing data. The standard deviation is a common statistical measure of the dispersion of the data set around the average value of the data set and can be defined as

$$SD = \sqrt{\frac{1}{N}\sum_{i=1}^{N}(x_i - \bar{x})^2} \tag{60}$$

where SD is the standard deviation, N is the number of samples, x_i is the individual data value, and $\bar{x}$ is the mean value of the data set.

The coefficient of variation shows the variation around the average value of the data set as a percentage of the mean value and can be defined as

$$CV = \frac{SD}{\bar{x}} \times 100 \tag{61}$$

where CV is the coefficient of variation, $\bar{x}$ is the mean value of the data set, and SD is the standard deviation.

40

3.2.   Experimental Studies

3.2.1.   Material

A commercial prepreg manufactured by Cytec, Cycom 977-2 UD, was used in the experimental studies. This prepreg is a 177°C curing toughened epoxy resin reinforced by unidirectional (UD) carbon fiber and designed for autoclaving or press-mold curing. It is mainly used for aircraft primary and secondary structures, space applications, ballistics, cryogenic tanks, or any application where impact resistance and light weight are required. The Cytec-recommended cure cycle for this prepreg is 180 minutes, held at 177°C isothermal temperature. Table 5 shows the selected mechanical properties for 977-2 UD published by Cytec [92].

TABLE 5

SELECTED MECHANICAL PROPERTIES FOR 977-2 UD
PUBLISHED BY CYTEC

Mechanical Property	Value Obtained at Room Temperature
0° Tensile Strength	2,690 MPa
0° Tensile Modulus	165 GPa
0° Compressive Strength	1,580 MPa
0° Compressive Modulus	152 GPa
Quasi Open-Hole Tensile Strength	448 MPa
Quasi Open-Hole Compression Strength	310 MPa

3.2.2.   One-Stage Cure Cycles

The thermal, rheological, and mechanical properties of 977-2 UD for different one-stage cure cycles were measured. Figure 21 and Table 6 show the temperature profiles for the one-stage cure-cycle study. Cure cycles were designed to study the effect of dwell temperature variations on the properties of the prepreg for dwell temperatures both above and below the manufacturer's recommended cure temperature (177°C), while the dwell time was kept constant at 180 minutes, the manufacturer's recommended cure time. Since the specimens cured at 160°C and 149°C for 180 minutes were not fully cured, and since their properties, therefore, were

expected to drop, it was important to know if increasing the dwell time could help improve the material properties for these dwell temperatures. As such, new specimens were cured at 160°C and 149°C, with long enough dwell times to ensure that no further curing could occur at these dwell temperatures. Since the DOC for both dwell temperatures reached a plateau value after 400 minutes, the new dwell time was selected to be 400 minutes.
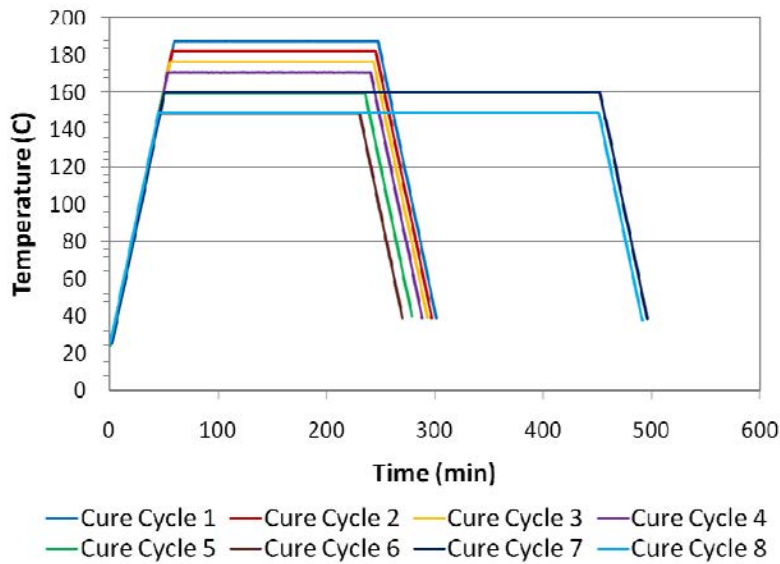
Figure 21. One-stage cure cycles.

TABLE 6

ONE-STAGE CURE CYCLES

Cure Cycle Number	Ramp-Up (°C/min)	Dwell Temperature (°C)	Dwell Time (min)	Ramp-Down (°C/min)
1	2.8	188	180	2.8
2	2.8	182	180	2.8
3	2.8	177	180	2.8
4	2.8	171	180	2.8
5	2.8	160	180	2.8
6	2.8	149	180	2.8
7	2.8	160	400	2.8
8	2.8	149	400	2.8

42

3.2.2.1. Shear Rheometery Testing

Rheometer samples were cured using the temperature profiles shown in Table 6 to obtain viscoelastic properties of 977-2 UD contained in Table 7. Each cure profile was followed by the T_g test recommended by the Suppliers of Advanced Composite Materials Association (SACMA) [93]. Rheology experiments were carried out using the ATD CSS 2000 rheometer with 41.3 mm diameter parallel plates, shown in Figure 22. The rheometer's plates were designed with grooves to prevent slippage of the sample at high torque. Each side of the sample had a total of 20 ridges, each 0.25 mm high, and equally spaced and arranged in a radial fashion. The width of the ridges was 1.5 mm, and the length was 15 mm. The thickness of samples used in this study was 2.5 mm. The quality of the rheometer samples was similar to that of the parts manufactured in the autoclave due to the high pressure (2000–4000 KPa) that the ATD rheometer applied on the samples and also encapsulation of samples using the rubber o-rings.

The rheometer experiments were conducted at 1 Hz frequency to obtain the rheological properties. A constant rotation angle of 0.05 degrees was used. Samples of the prepreg, which weighed about 6.5 g, were prepared using 28 plies in 0/90/0/90 sequence. Since the ATD CSS 2000 rheometer data for curing the prepregs is highly repeatable, only one rheometer sample was cured for each cure cycle shown in Table 6.

TABLE 7

MEASURED VISCOELASTIC PROPERTIES

Viscoelastic Property	Unit
Complex Viscosity	Pa.S
Gel Time	min
Glass Transition Temperature (T_g)	C
Minimum Viscosity Time	min
Pressure Window Time	min

Figure 22. ATD CSS 2000 rheometer.

3.2.2.2. Differential Scanning Calorimetry Testing

The cure kinetics of 977-2 UD was studied using a DSC. The prepreg samples, weighing between 10 and 15 mg, were encapsulated in Tzero aluminum pans. Then, the heat of reaction and the degree of cure of the samples were measured with a TA Instruments Q2000 DSC (Figure 23). The temperature profiles for the DSC tests are shown in Table 6.

Figure 23. TA Instruments Q2000 differential scanning calorimeter.

3.2.2.3. Mechanical Testing

The OHC, CLC, and SBS tests were performed on five specimens from seven panels and cured in an autoclave using one-stage cure cycles 2 to 8, as shown in Table 6. Table 8 shows the measured mechanical and physical properties. In order to obtain balanced symmetric laminates, the panel lay-up was 32 plies of unidirectional tape placed in 0/90/90/0 order. The cure pressure for all panels was 586 KPag. The cured panels were cut into coupons and tested according to the ASTM standards listed in Table 8.

TABLE 8

MEASURED MECHANICAL AND PHYSICAL PROPERTIES
FOR ONE-STAGE CURE CYCLES

Measured Property	Test Method	Standard
Interlaminar Shear Strength	Short Beam Shear	ASTM D2344
Compressive Strength	Combined Loading Compression	ASTM D6641
Compressive Modulus	Combined Loading Compression	ASTM D6641
Compressive Poisson's Ratio	Combined Loading Compression	ASTM D6641
Open-Hole Ultimate Compression Strength	Open-Hole Compression	ASTM D6484
Open-Hole Compression Percent Bending	Open-Hole Compression	ASTM D6484
Void Content	Acid Digestion	ASTM D3171

3.2.3. Two-Stage Cure Cycles

Thermal and rheological properties of 977-2 UD during four combined ramp and isothermal cure cycles were measured using the DSC and rheometer. Figure 24 and Table 9 show the temperature profiles for the two-stage cure-cycle study. Cure cycles were designed to study the effect of ramp-up rate and the first dwell temperature on the properties of the prepreg. While the selected ramp-up rate for cure cycles 1 and 2 was 2.8^{o}C/min, which is a common heat-up rate for curing 977-2 UD in the autoclave, the designed ramp-up rate for cure cycles 3 and 4 was 8.3^{o}C/min, which is almost the fastest possible heat-up rate in many autoclaves. The first dwell temperature for the two-stage cure cycles for the 977-2 resin system is usually between 120°C

and 165°C. As such, the first dwell temperature for all studied cure cycles was either 149°C or

163°C. The first dwell time for two-stage cure cycles for the 977-2 resin system is usually

between 60 and 100 minutes. Therefore, the first dwell time for all cure cycles was either 80 or

100 minutes. The first dwell time for cure cycles with a lower first dwell temperature (cure

cycles 2 and 4) was longer, in order to give the material more time to cure. The second dwell

temperature for all studied cure cycles was set at 177°C to ensure that the samples were fully

cured.

TABLE 9

TWO-STAGE CURE CYCLES

Cure Cycle Number	First Ramp-Up (°C/min)	First Dwell Temperature (°C)	First Dwell Time (min)	Second Ramp-Up (°C/min)	Second Dwell Temperature (°C)	Second Dwell Time (min)	Ramp-Down (°C/min)
1	2.8	163	80	2.8	177	300	2.8
2	2.8	149	100	2.8	177	350	2.8
3	8.3	163	80	8.3	177	300	2.8
4	8.3	149	100	8.3	177	350	2.8
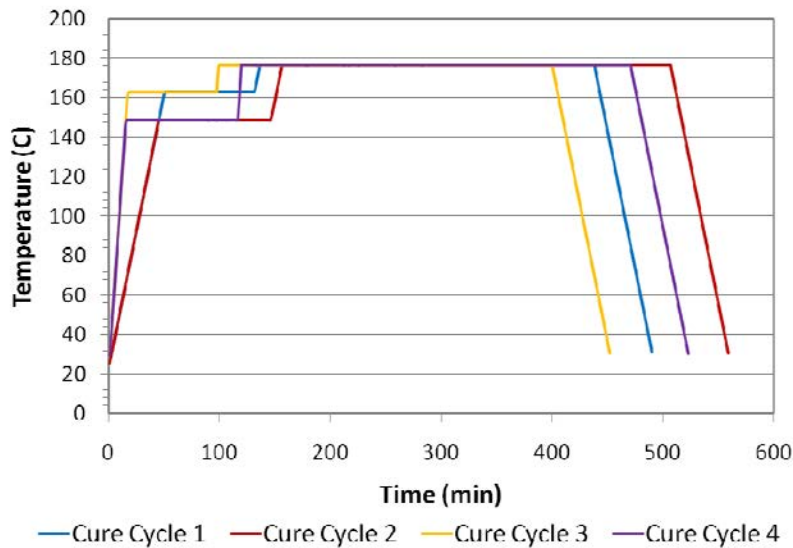
Figure 24. Two-stage cure cycles.

3.2.3.1. Shear Rheometry Testing

Rheometer samples were cured using the temperature profiles shown in Figure 24 to obtain the viscoelastic properties of 977-2 UD contained in Table 7. Similar to one-stage cure cycle tests, each cure profile was followed by the T_g test recommended by SACMA [93]. Rheology experiments were carried out using the ATD CSS 2000 rheometer. Test conditions were the same as those used for one-stage cure-cycle tests. The two-stage cure-cycle samples, weighing about 6.2 g, were prepared using 27 plies in 0/90 sequence.

3.2.3.2. Differential Scanning Calorimetry Testing

Similar to one-stage cure cycle tests, the prepreg samples, weighing between 10 and 15 mg, were encapsulated in Tzero aluminum pans. Then, the heat of reaction and the degree of cure of the samples were measured with a TA instruments Q2000 differential scanning calorimeter. Temperature profiles of the DSC tests were the same as those used for the two-stage rheometry tests.

CHAPTER 4

RESULTS AND DISCUSSION

In this chapter, first the experimental results obtained for the specimens cured at one-stage and two-stage cure cycles are presented and discussed. Then, the degree of cure and complex viscosity modeling results for the one-stage and the two-stage cure cycles are reported. Finally, the correlation between different material properties obtained from the experimental results for the one-stage cure cycles is studied.

For the one-stage cure cycles, the experimental results include the viscoelastic properties obtained with the rheometer, the degree of cure obtained with the differential scanning calorimeter, the mechanical properties obtained with the OHC, CLC, and SBS tests and the void content obtained with the acid digestion test. For the two-stage cure cycles, the experimental results include viscoelastic properties obtained with the rheometer and the degree of cure obtained with the differential scanning calorimeter.

4.1.   One-Stage Cure Cycles

As can be seen in Table 5, cure cycles 2 to 6 had different dwell temperatures. As such, the testing results for these cure cycles showed the effect of dwell temperature on the material properties. Also, cure cycles 5 and 7 and cure cycles 6 and 8 had different dwell times. Therefore, the testing results for these cure cycles showed the effect of the dwell time in the material properties.

4.1.1.   Rheometry Results

Viscoelastic properties of the prepreg, including G', G", tanδ, and complex viscosity, were measured for different one-stage cure cycles using the parallel-plate shear rheometer. Since complex viscosity was the main viscoelastic property used for describing the state of the material

48

in this dissertation, only the graph for the complex viscosity during the cure and post-cure T_g test was used.

4.1.1.1. Complex Viscosity

Figure 25 shows complex viscosity during cure and post-cure T_g tests for different one-stage cure cycles. As shown, the complex viscosity graph indicates the state of the material throughout the cure cycle and post-cure cycle. In addition, important material-state transitions during cure, such as gelation and vitrification, are visible in the complex viscosity graph. Also, other crucial material-state regions, such as the low-viscosity region and pressure-window region, can be found using the complex viscosity data. As such, complex viscosity seems to be an appropriate option for monitoring the state of the material during cure.
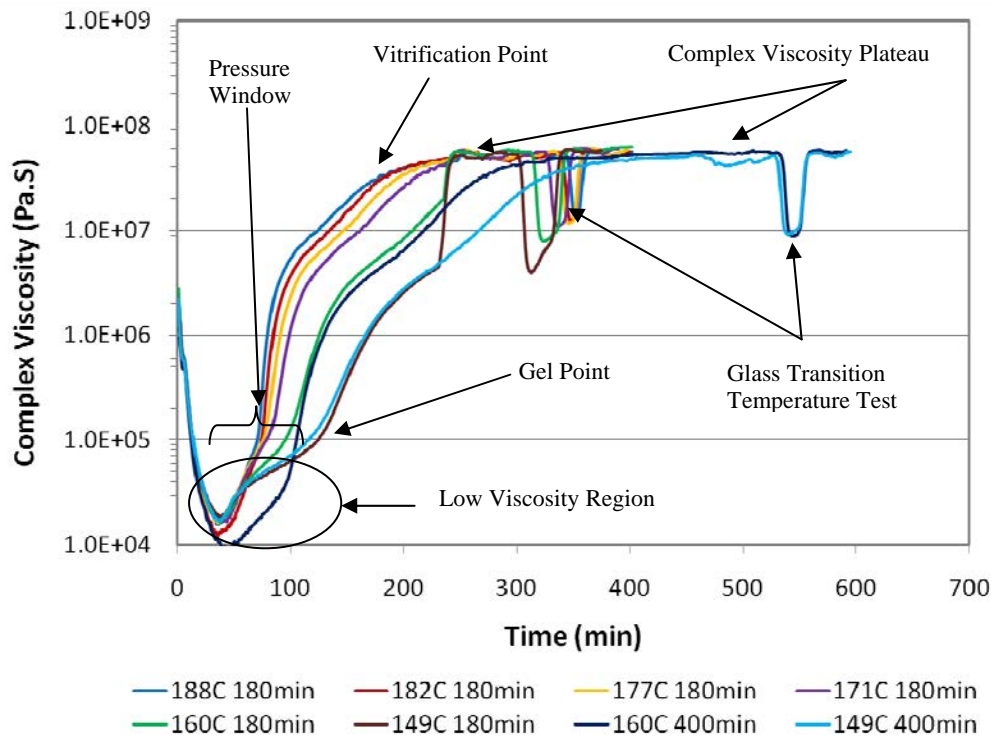
Figure 25. Complex viscosity during cure and post-cure T_g tests for one-stage cure cycles.

As Figure 25 shows, the complex viscosity plateau value indicating completion of the cure was not achieved for samples cured at 160°C and 149°C for 180 minutes. Nevertheless, the complex viscosity plateau was achieved during cure after the dwell time for these two cycles was increased to 400 minutes. The final complex viscosity for different one-stage cure cycles is shown in Figure 26. These values were obtained after the cured samples were cooled down to the room temperature. For all cure cycles except cure cycle 8, the cured samples reached a stable final complex viscosity at room temperature. In the case of cure cycle 8, the sample reached a stable complex viscosity plateau after being cooled down right before the data became unstable, due to slippage of the sample between the parallel plates. Since the unstable data did not provide an acceptable final complex viscosity, only the portion of the complex viscosity graph that was stable in the cool-down region was used to determine the final complex viscosity
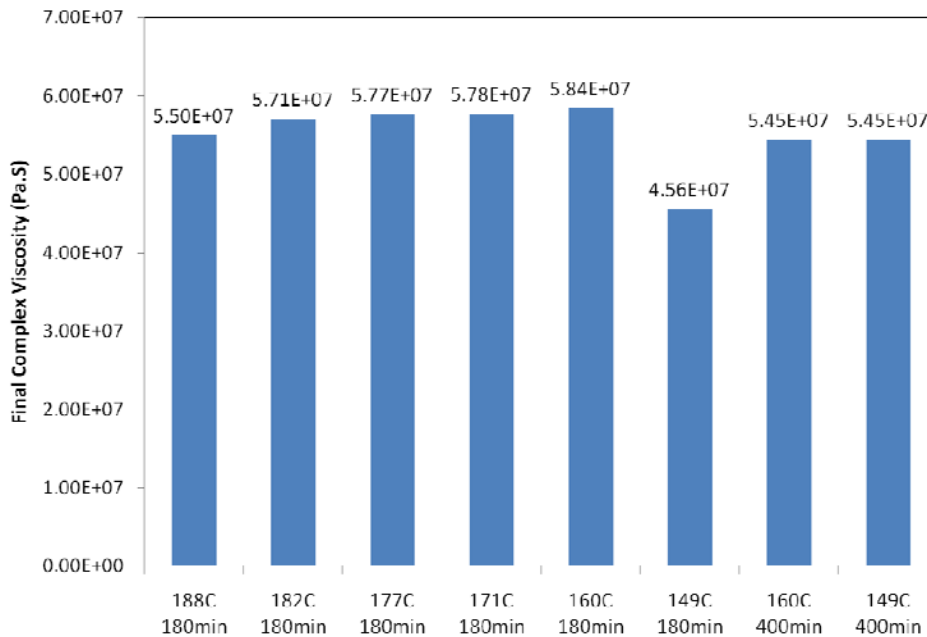
Figure 26. Final complex viscosity for one-stage cure cycles.

Figure 26 shows that only the sample cured at 149°C for 180 minutes had a significant drop in the final complex viscosity. This drop is similar to the drop observed in the average short

50

beam shear strength obtained for specimens cured at the same cure cycle. As such, complex viscosity seems to be a good candidate for correlation to the mechanical properties of the material.

4.1.1.2. Gel Time

Gel time was defined as the time at which the tangent of the slope of the complex viscosity graph tends to infinity. For the studied one-stage cure cycles, gelation occurred at the beginning of the isothermal stage and coincided with the complex viscosity value equal to 10^5 Pa.S. Several factors may affect the magnitude of the complex viscosity at gel point, such as properties of the material, thickness of the sample, and orientation of the sample plies. As will be shown later, varying the rheometer sample thickness by using a different number of plies and changing the orientation of the sample's plies alter the complex viscosity value at gel point. As Figure 27 illustrates, the gel time for different one-stage cure cycles increased as the dwell temperature decreased. The relation between the gel time and dwell time for different one-stage cure cycles for 977-2 UD can best be described by equation (40). The change in the dwell temperature for samples cured at 160^oC and 149^oC did not significantly affect gel time.

4.1.1.3. Glass Transition Temperature (T_g)

Figure 28 shows glass transition temperatures for different one-stage cure cycles. As can be seen, T_g gradually increases in value as the dwell temperature increases. T_g for the sample cured at 188^oC for 180 minutes was 186^oC, which is the ultimate glass transition temperature for 977-2 UD obtained using the parallel-plate rheometer. For samples cured at 171^oC to 188^oC for 180 minutes, T_g was very close to the isothermal cure temperature; however, for samples cured at 160^oC and 149^oC for 180 minutes, T_g was considerably less than the isothermal cure temperature. The drop in T_g was related to incomplete cure of the samples. As such, increasing

51

the dwell time to 400 minutes for the samples cured at 160°C and 149°C improved the degree of cure and hence the glass transition temperature. T_g for all specimens was determined using G' data according to SACMA SRM18R-94.
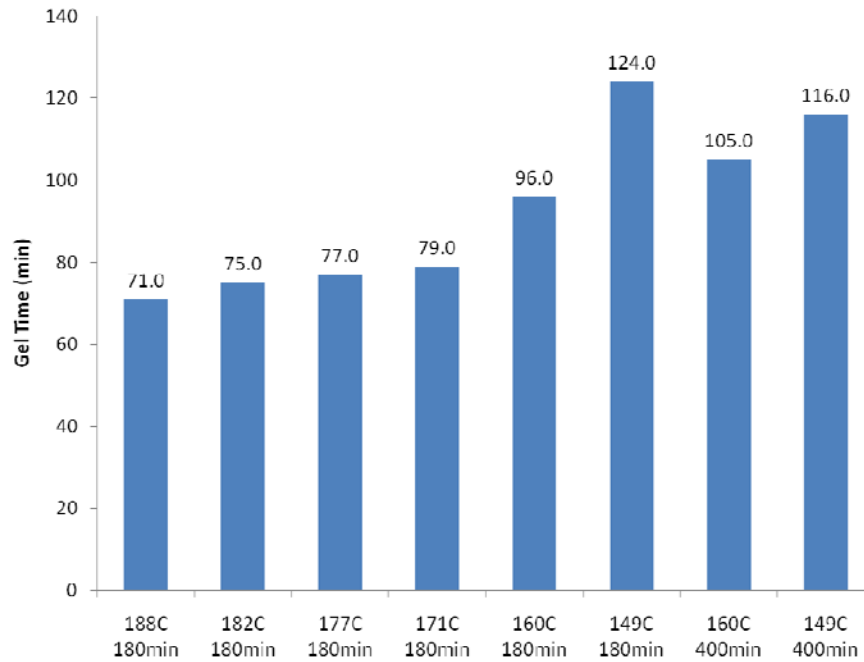
Figure 27. Gel times for one-stage cure cycles.

4.1.1.4.   Minimum Complex Viscosity Time

The time at which the complex viscosity of the prepreg sample reached its minimum value for different one-stage cure cycles is shown in Figure 29. The minimum complex viscosity for all cure cycles occurred during the ramp-up stage around 36 minutes after the start of the cure cycles. Minimum complex viscosity time was used to obtain the pressure window.

4.1.1.5.   Pressure Window Time

Figure 30 shows pressure window times for different one-stage cure cycles. Pressure window time signifies the time span during which the pressurization has a considerable effect on the composite laminates cured in the autoclave and is defined as the gel time minus the minimum

52

complex viscosity time [11]. The timing of pressure application during cure could affect the final mechanical properties of the composite materials. If the cure pressure is applied too early and the composite part is not surrounded by a resin dam, too much resin may be squeezed out, and therefore, the resin content of the cured laminate may become too low. On the other hand, even if the prepreg panel is surrounded by a resin dam, early application of the cure pressure may result in formation of a resin-rich region in the laminates [94]. This may also cause higher void content and lower mechanical strength. If the cure pressure is applied after the gel time, volatiles and air trapped in the composite part will not be forced out.

Since the minimum complex viscosity time for all one-stage cure cycles was about 36 minutes, gel time was the only dominant factor in determining the pressure window time, and as such, the trend of pressure window time for different cure cycles is the same as that of gel time.
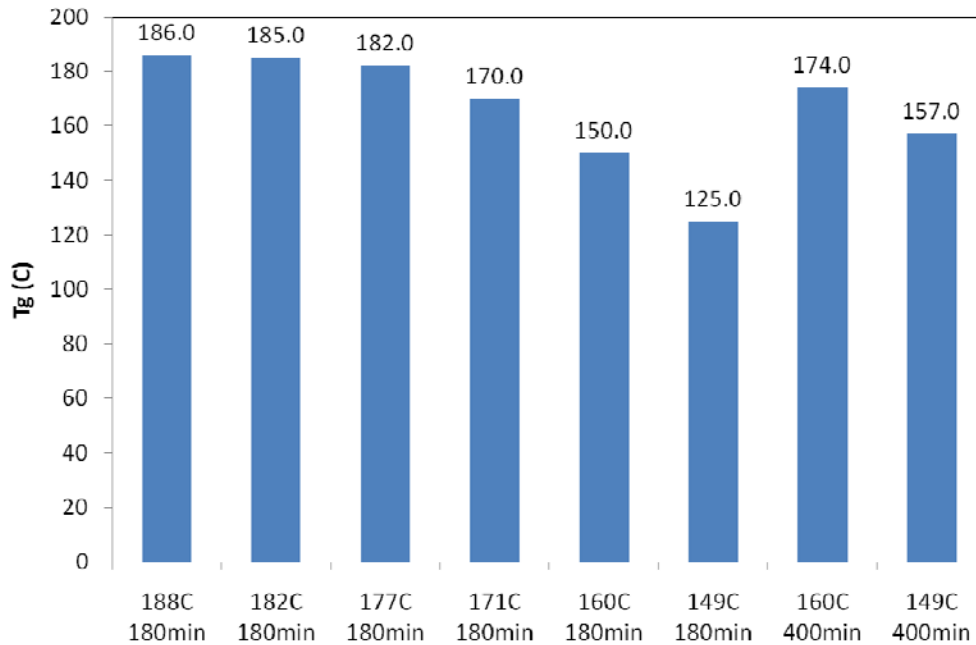
Figure 28. Glass transition temperatures for one-stage cure cycles.
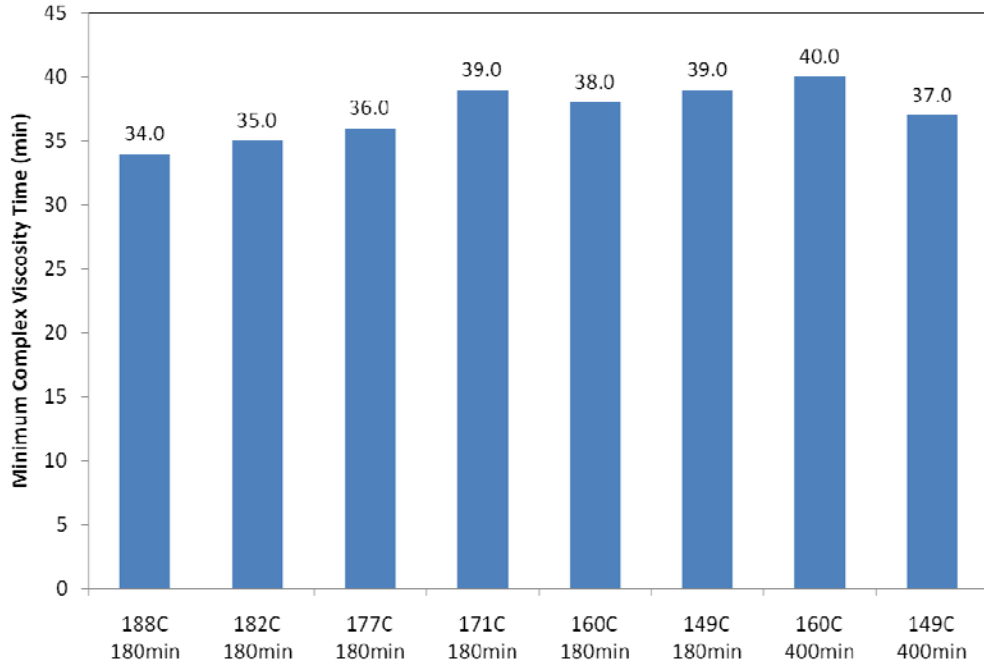
Figure 29. Minimum complex viscosity times for one-stage cure cycles.
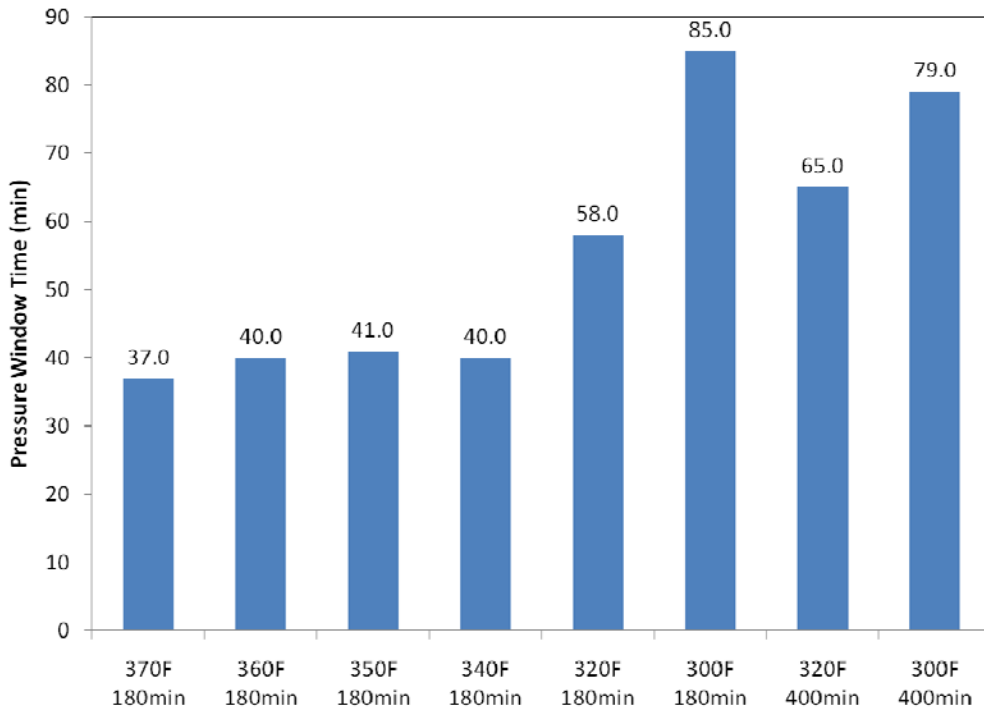
Figure 30. Pressure window times for one-stage cure cycles.

4.1.2.   Differential Scanning Calorimetry Results

The heat flow of the prepreg samples during cure was measured for different one-stage cure cycles using the DSC. The measured heat flow was then used to obtain the degree of cure for each cure cycle after the heat flow baselines for the ram–up, and isothermal heat flows were defined properly.

4.1.2.1. Degree of Cure

Degree of cure during cure for different one-stage cure cycles is shown in Figure 31. The DOC increased rapidly at the beginning of each cure cycle before it slowed down to approach the plateau value. The rapid increase in the DOC means a high cross-linking reaction rate. As such, the curing reactions were kinetics-controlled in this region. As the DOC approached its plateau value, the cross-linking reaction rate became significantly slow. The curing reactions in this region were diffusion-controlled. Figure 32 shows the time rate of DOC vs. DOC for different one-stage cure cycles. As can be seen, when the DOC is greater than 0.8, the time rate of the DOC is almost zero. This means a very slow increase in the degree of cure with cure time. The final DOC for different one-stage cure cycles is shown in Figure 33. As can be seen, for samples cured for 180 minutes, the DOC decreased as the dwell temperature decreased. Increasing the dwell time to 400 minutes for samples cured at 160°C and 149°C improved the DOC. Table 10 contains different heats of reaction and the final DOC for one-stage cure cycles. For samples cured for 180 minutes, the residual heat increased with decreasing isothermal cure temperature. An increase in the residual heat indicates lower degree of cure. As such, for the samples cured at 160°C and 149°C, the residual heat decreased with increasing dwell time from 180 to 400 minutes. It is important to note that the ultimate heat of reaction, H_U, for different one-stage cure cycles was not the same. Fluctuation in H_U could be related to the variation in the prepreg

sample's weight and also variation in the fiber and resin volume fraction. Since the heats of reaction are weight-normalized and only the thermosetting resin portion of the prepreg sample generates heat, a higher fiber-volume fraction results in a lower heat of reaction since the carbon fiber does not contribute to the heat of reaction. It is important to note that it is not possible to use the DOC measured by DSC for real-time monitoring of the cure process since the ultimate heat of reaction needed for DOC calculations is obtained only after the end of the cure cycle.

4.1.2.1.1. Heat-Flow Baseline

The one-stage cure cycles consisted of one ramp-up step and one isothermal step. To find the total heat of reaction, the heat flow integration for each of these steps had to be done separately using the appropriate heat-flow baseline. To obtain the ramp-up heat flow baseline, a dynamic scanning was performed on a 977-2 UD sample. The baseline of the dynamic scanning was a straight line (baseline number 2 in Table 3), as shown in Figure 34. The starting point of the baseline was where the heat flow curve started to rise, and its ending point was where the heat flow cure reached its minimum. This baseline was used to calculate DOC for the dynamic scanning. To find the baseline for the isothermal step, the sample was kept at the isothermal cure temperature until the heat flow approached the plateau value, as shown in Figure 35. The heat flow plateau obtained was then used as the baseline for the isothermal step.

4.1.3. Material Characterization Results

Test coupons for mechanical and void content testing were cut from panels cured at one-stage cure cycles. The size of the panels was 17 inches by 17 inches. Figure 36 compares the cross section for panels cured at cure cycles 6 and 8. As shown, the layup for the panel cured at cure cycle 8 was missing one ply in the 90° direction. The layup for all other panels was correct.

Since only one ply in the 90° direction missing out of 32 plies total was not a huge difference, as observed in the test data, the mechanical test results for this panel were also reported.
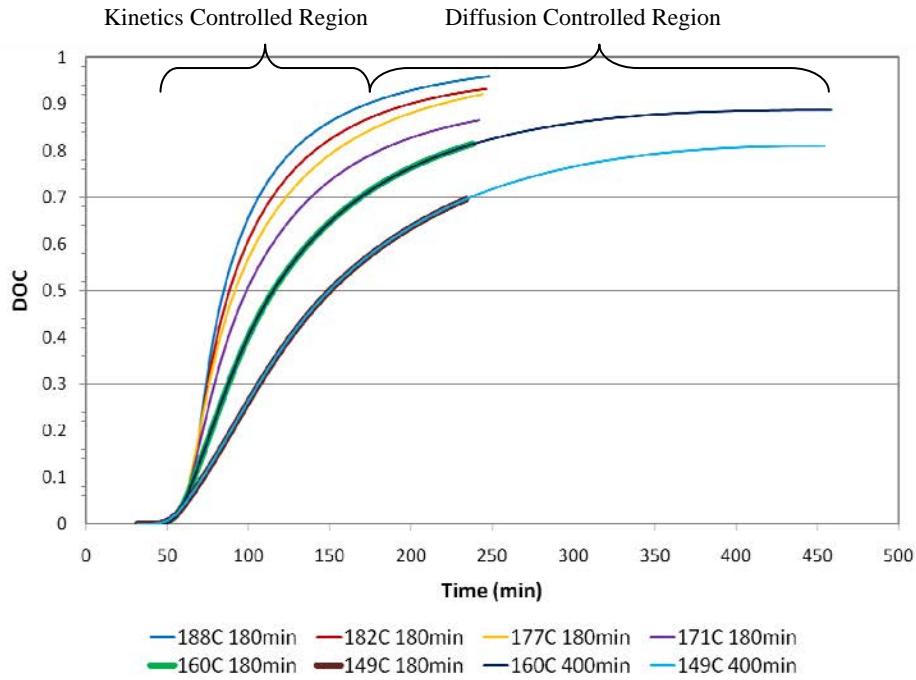
Figure 31. Degree of cure during cure for one-stage cure cycles.
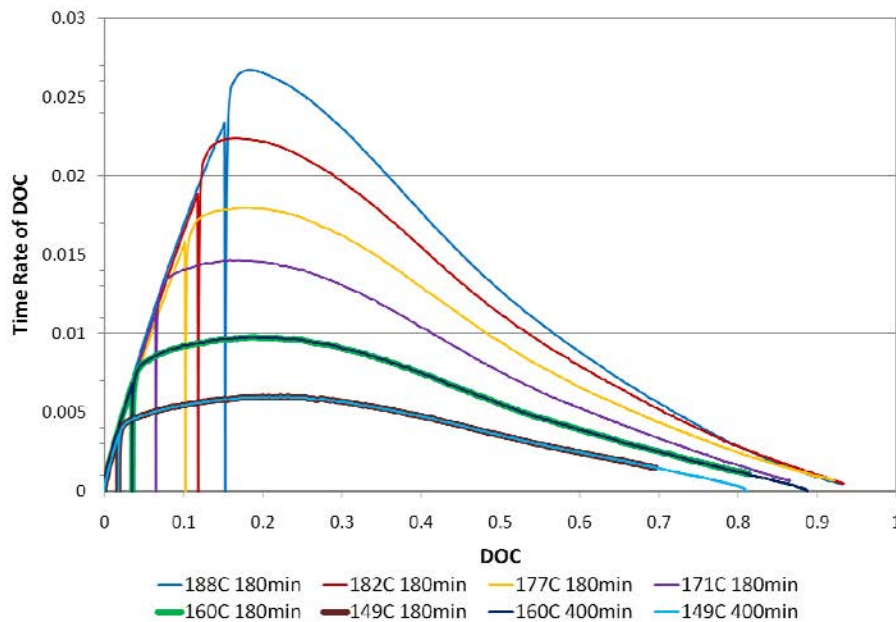
Figure 32. Time rate of degree of cure vs. degree of cure for one-stage cure cycles.
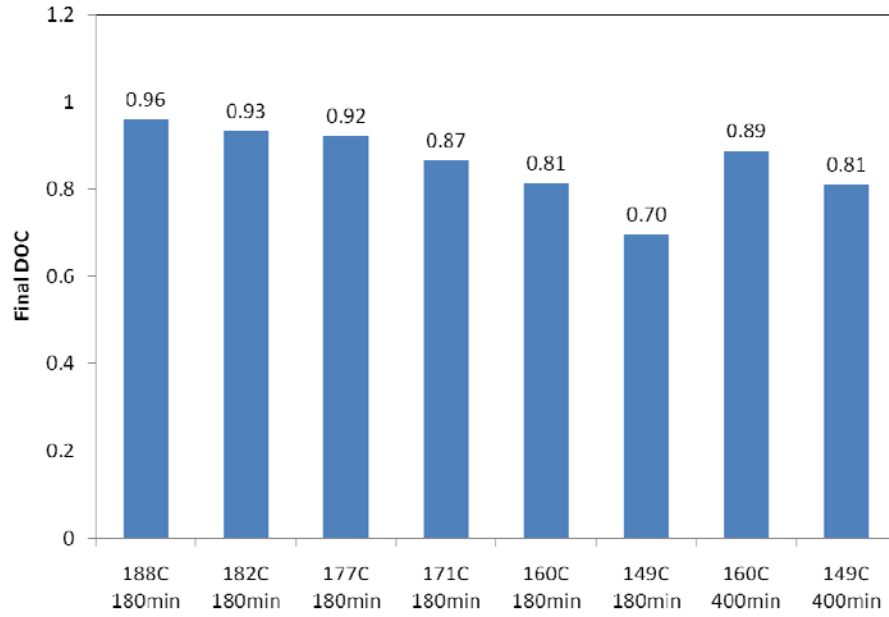
Figure 33. Final degree of cure for one-stage cure cycles.
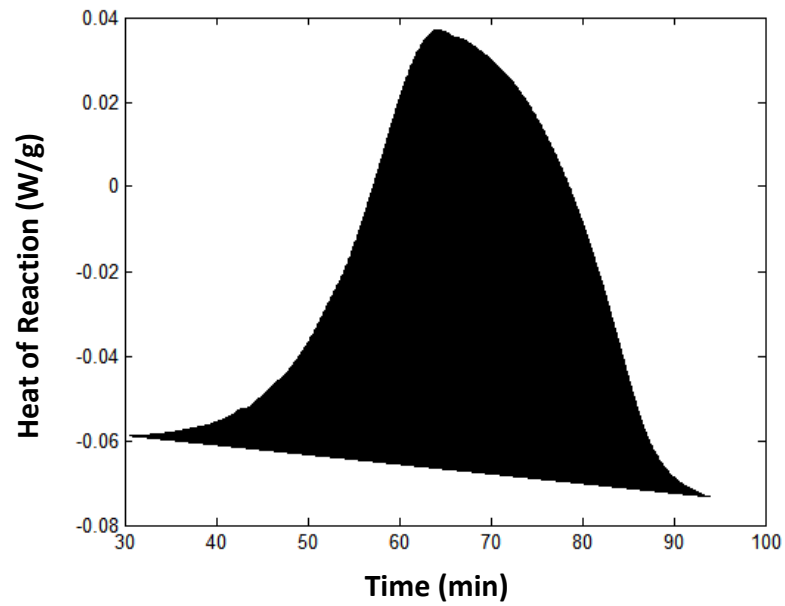
Figure 34. Heat-flow baseline for dynamic scanning with heat-up rate of 2.8°C/min.
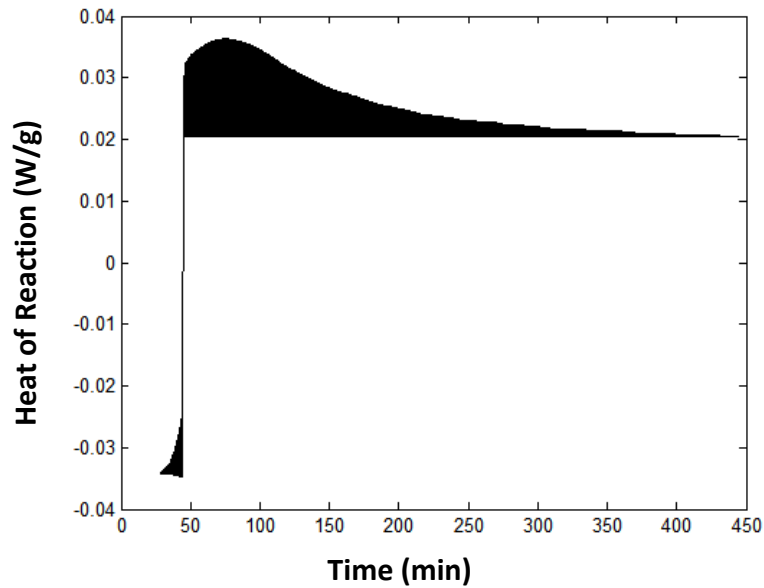
Figure 35. Heat-flow baseline for one-stage cure cycle.

TABLE 10

HEAT OF REACTION AND FINAL DEGREE OF CURE FOR
ONE-STAGE CURE CYCLES

Cure Cycle	H_T (J/g)	H_{res} (J/g)	H_U (J/g)	α_{max}
188°C 180 min	121.90	4.51	126.42	0.96
182°C 180 min	111.95	8.01	119.96	0.93
177°C 180 min	128.45	10.94	139.39	0.92
171°C 180 min	105.14	16.39	121.53	0.87
160°C 180 min	121.74	27.78	149.52	0.81
149°C 180 min	119.48	52.22	171.70	0.70
160°C 400 min	118.71	15.00	133.71	0.89
149°C 400 min	116.44	27.34	143.78	0.81

4.1.3.1.   Short Beam Shear (SBS) Properties

Figure 37 and Table 11 show average SBS strength and standard deviation for different

one-stage cure cycles. Statistical analysis (Table 12) showed that the average SBS strength of the

specimens cured at 149°C for 180 minutes was significantly less than the other specimens. In

addition to the average SBS strength, the failure mode for the specimens cured at 149°C for 180

minutes was different from that of other specimens.
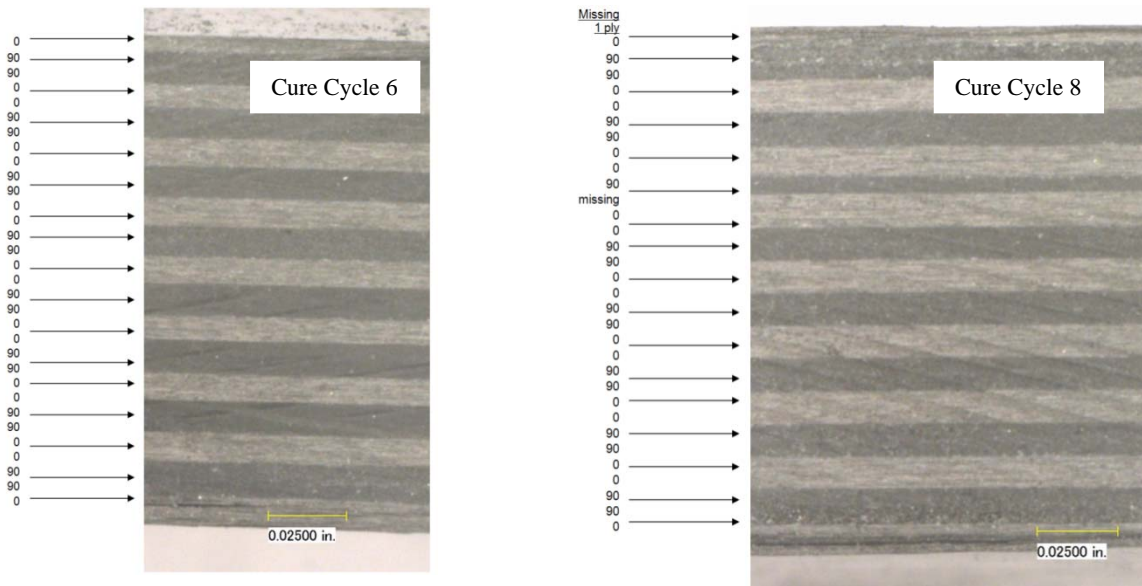
Figure 36. Cross section of panels cured at one-stage cure cycles 6 and 8.
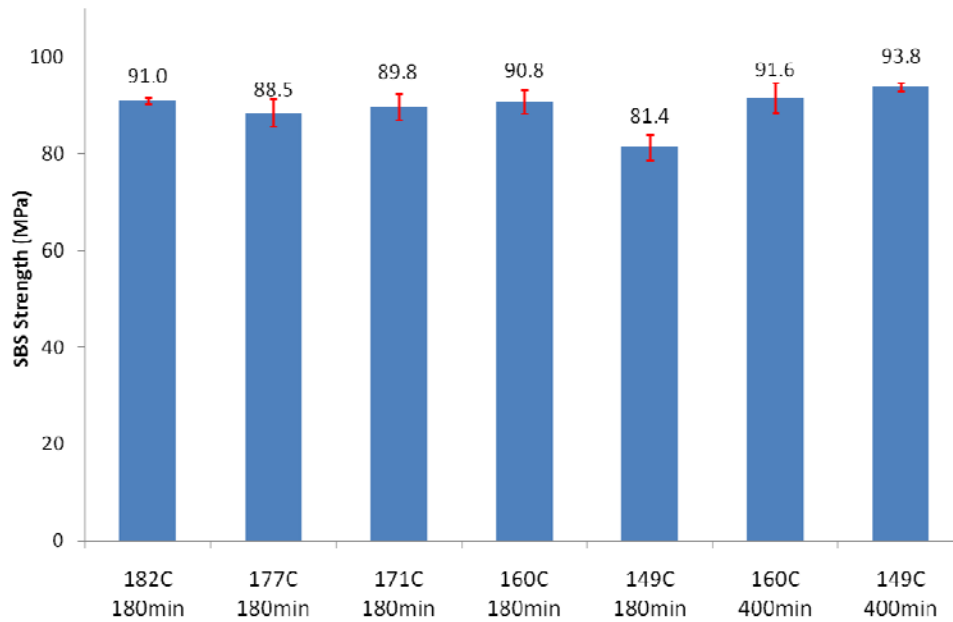
Figure 37. Average SBS strength for one-stage cure cycles.

TABLE 11

AVERAGE SBS STRENGTH FOR ONE-STAGE CURE CYCLES

Cure Cycle	SBS Strength (MPa)	Standard Deviation (MPa)	Coefficient of Variation (CV)
182°C 180 min	91.0	0.72	0.79
177°C 180 min	88.5	2.88	3.25
171°C 180 min	89.8	2.70	3.00
160°C 180 min	90.8	2.39	2.63
149°C 180 min	81.4	2.55	3.14
160°C 400 min	91.6	3.10	3.39
149°C 400 min	93.8	0.88	0.94

TABLE 12

MINITAB ANOVA ANALYSIS OF SBS STRENGTH VARIANCE
FOR ONE-STAGE CURE CYCLES

```
Level          N     Mean   StDev
182C 180min    5   90.979   0.715
177C 180min    5   88.512   2.880
171C 180min    5   89.822   2.696
160C 180min    5   90.752   2.388
149C 180min    5   81.353   2.552
160C 400min    5   91.607   3.101
149C 400min    5   93.821   0.882
               Individual 95% CIs For Mean Based on Pooled StDev
Level           -+---------+---------+---------+--------
182C 180min                      (---*---)
177C 180min                  (---*---)
171C 180min                   (---*---)
160C 180min                    (----*---)
149C 180min        (---*---)
160C 400min                     (---*---)
149C 400min                         (---*---)
                -+---------+---------+---------+--------
               80.0      85.0      90.0      95.0
```
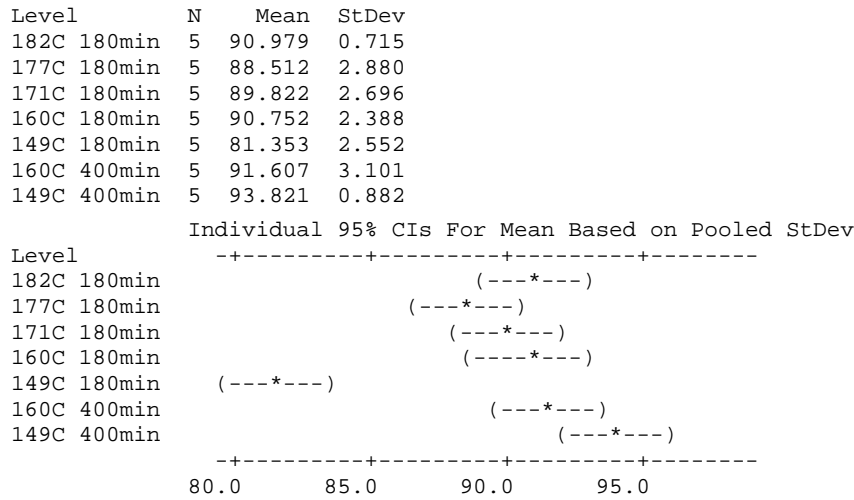
The cross section of a failed SBS specimen is shown in Figure 38. To further investigate the failure mode for different cure cycles, SBS specimens were observed under the microscope. It was found that the SBS failure mode for all cure cycles, except cure cycle 6, was compression-interlaminar shear. The failure mode for cure cycle 6 was interlaminar shear. The compressive failure mode indicates a strong fiber-resin adhesion since the resin can transfer the load to the fibers, and hence the fibers fracture at the upper surface of the specimen. The interlaminar shear failure mode indicates lack of strong bond between prepreg layers to prevent slippage of the cured layers on top of each other. The change in the failure mode for the least cured specimens

61

(cure cycle 6 specimens) was expectable since insufficient cure causes inadequate bonding between prepreg layers.
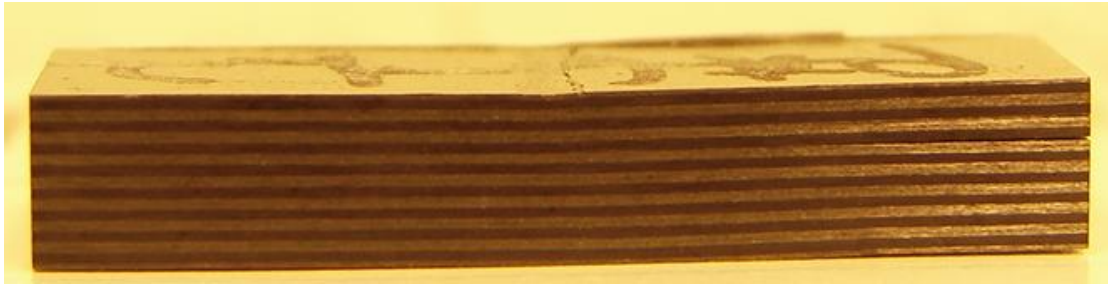
Figure 38. Failure mode for SBS specimens.

Figures 39 to 41 show the magnified cross section of the failed SBS specimens around the load region. The compression failure for all cure cycles, except cure cycle 6, started under the load region, and the resulting crack propagated into different layers of the specimen, thus causing delamination (Figures 39 and 40). However, this type of crack propagation was not observed for cure cycle 6 specimens. These specimens failed due to interlaminar shear at multiple locations (Figure 41).
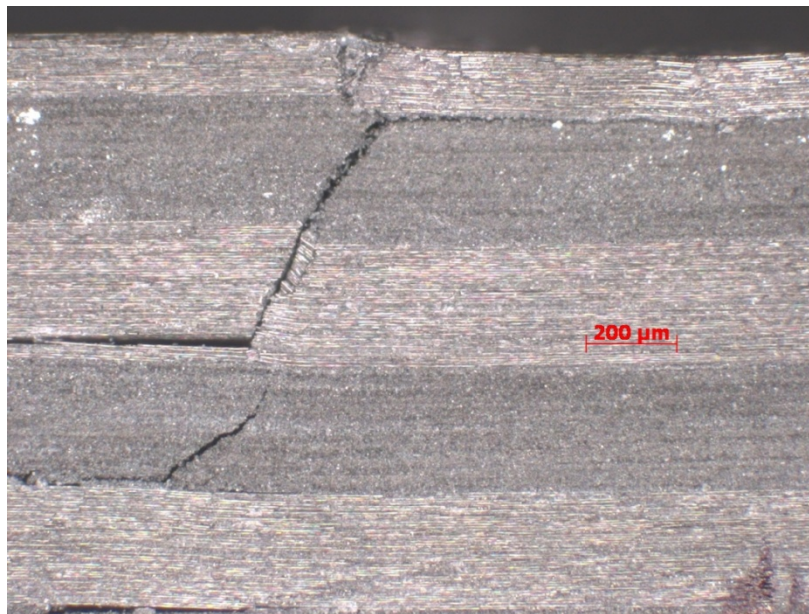
Figure 39. Magnified cross section of SBS specimen cured at 177°C for 180 min.
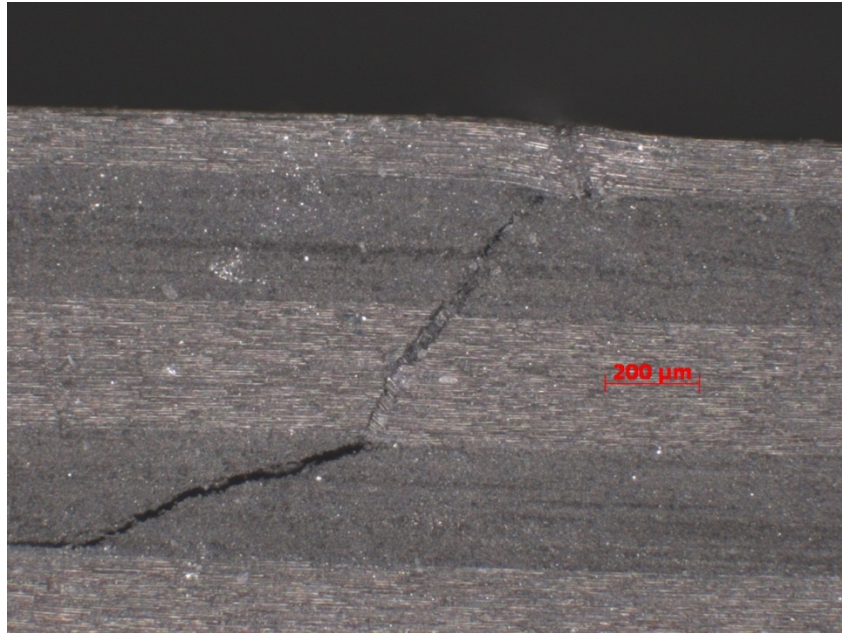
Figure 40. Magnified cross section of SBS specimen cured at 149°C for 400 min.
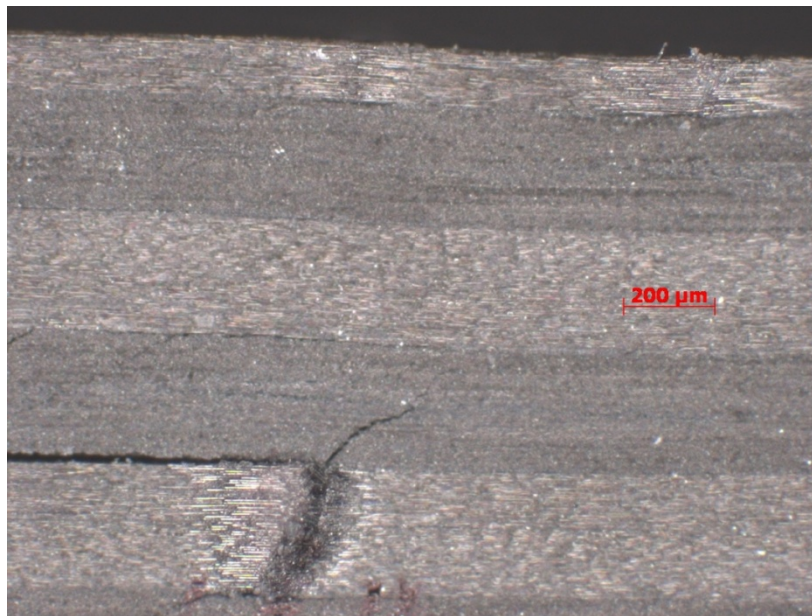
Figure 41. Magnified cross section of SBS specimen cured at 149°C for 180 min.

The SBS load displacement (LD) curves for all cure cycles, except cure cycle 6, followed the same pattern. The LD curves for these cure cycles had a huge drop right after the peak load (Figures 42 to 43). This drop signified compression failure of the SBS specimens. The LD curves for cure cycle 6 (Figure 44) had a slight drop before reaching the maximum load and a huge drop after the peak load. The huge drop in LD curves for this cure cycle could be due to the failure at multiple locations. The slight drop before reaching the maximum load could be the result of early delamination of one of the plies. It is important to note that the failure mode and LD curve pattern for cure cycle 8 was similar to those of the other cure cycles, except cure cycle 6. This clearly shows that the SBS properties for cure cycle 8 were mainly affected by the state of the cure, and missing one ply in the layup did not significantly affect the properties of the corresponding panel. The failure modes for all SBS specimens were acceptable according to ASTM D2344 (Figure 45). This means that the SBS test results for all specimens were valid.
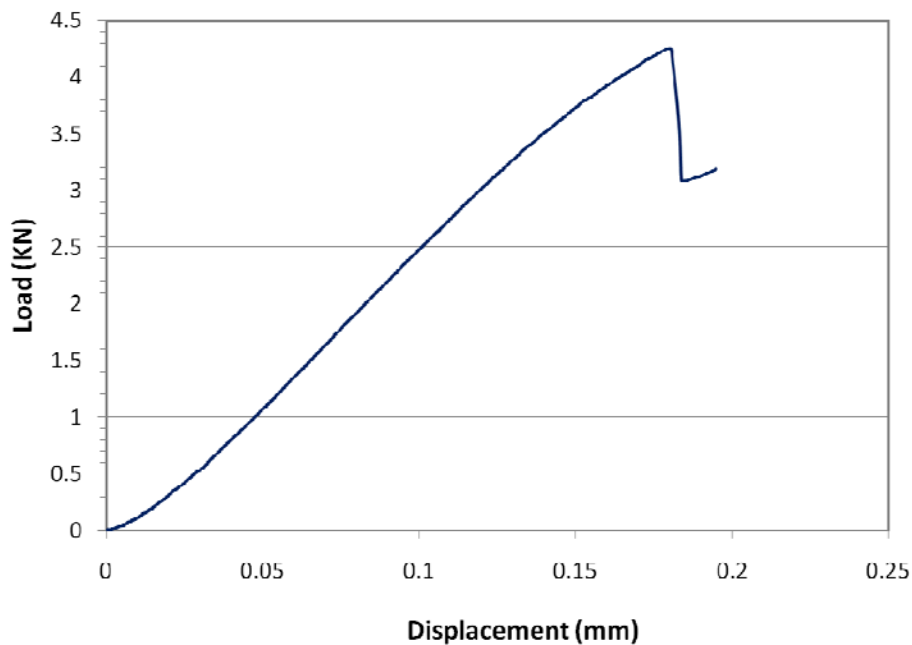
Figure 42. Load displacement curve for SBS specimen cured at 177°C for 180 min.
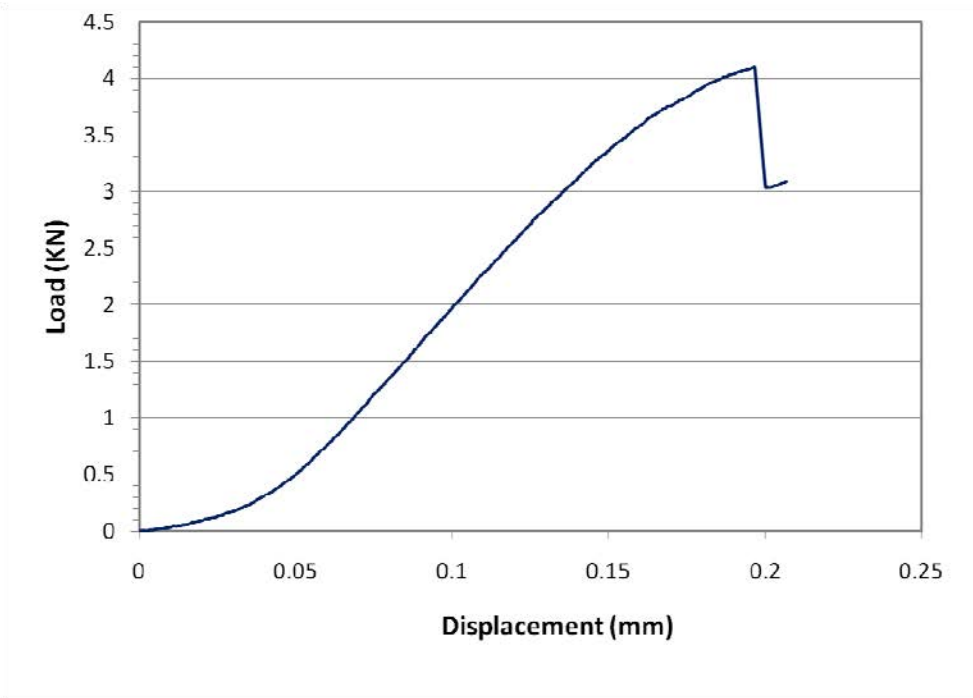
Figure 43. Load displacement curve for SBS specimen cured at 149°C for 400 min.
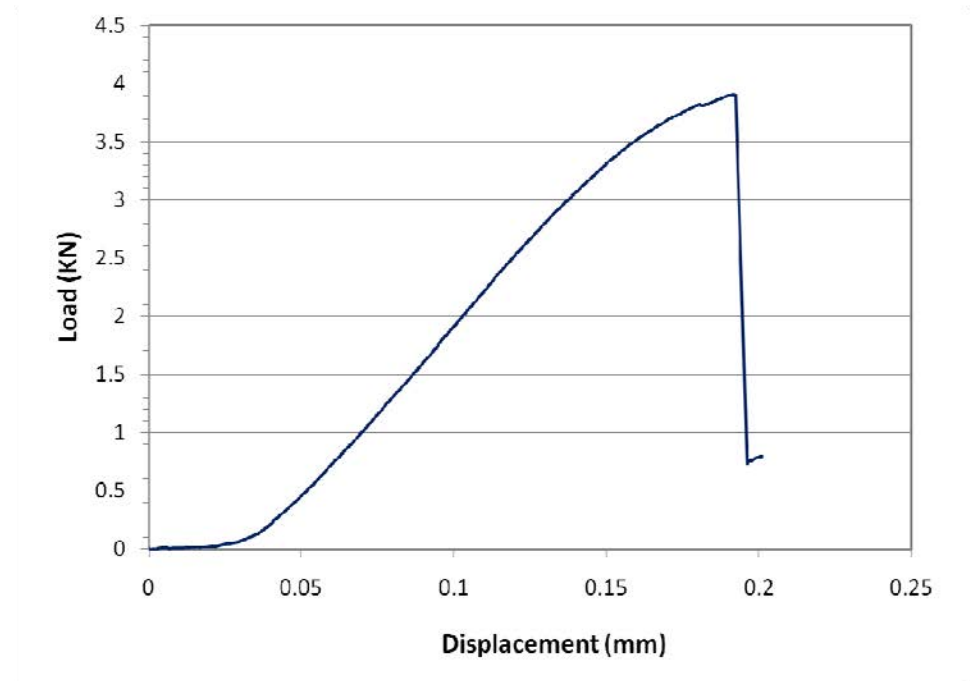
Figure 44. Load displacement curve for SBS specimen cured at 149°C for 180 min.
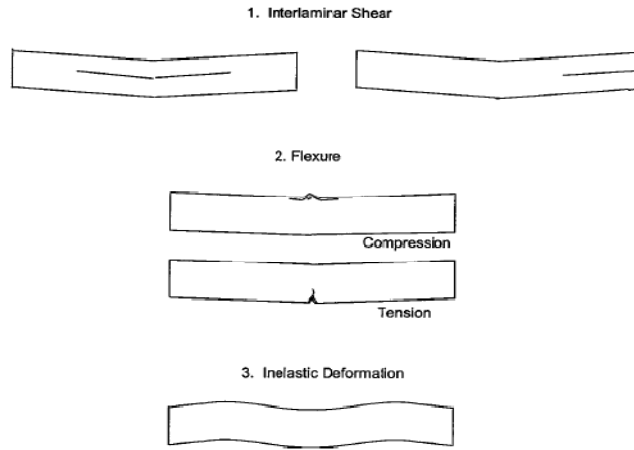
Figure 45. Typical failure modes in the short beam shear test
according to ASTM D2344 [88].

4.1.3.2. Combined Loading Compression Properties

Tables 13 and 14 and Figure 46 show average compressive strength and standard deviation for different one-stage cure cycles. Average compressive modulus for different one-stage cure cycles is shown in Tables 15 and 16 and Figure 47. The average compressive modulus was obtained using the slope of the linear portion of the stress strain curve for each specimen. Poisson's ratio for specimens cured at one-stage cure cycles is summarized in Table 17 and Figure 48. The values for CLC strength, CLC modulus, and Poisson's ratio did not vary significantly for different cure cycles. However, the average CLC strength decreased with decreasing dwell temperature for the samples cured for 180 minutes. This could be due to the fact that the yield stress of thermosetting resins at temperatures below T_g is influenced by the degree of cure: the less the degree of cure the less the compressive yield stress. On the other hand, the compressive modulus showed no decreasing trend with decreasing dwell temperature. As mentioned previously, the elastic modulus of thermosetting resins at temperatures below T_g is not strongly affected by the degree of cure.

66

TABLE 13

AVERAGE CLC STRENGTH FOR ONE-STAGE CURE CYCLES

Cure Cycle	CLC Strength (MPa)	Standard Deviation (MPa)	Coefficient of Variation (CV)
182°C 180 min	803.0	33.03	4.11
177°C 180 min	813.2	25.61	3.15
171°C 180 min	823.3	16.56	2.01
160°C 180 min	794.2	19.87	2.50
149°C 180 min	782.9	35.03	4.47
160°C 400 min	809.2	32.39	4.00
149°C 400 min	790.0	39.77	5.03

TABLE 14

MINITAB ANOVA ANALYSIS OF CLC STRENGTH VARIANCE
FOR ONE-STAGE CURE CYCLES

```
                                Individual 95% CIs For Mean Based on
                                Pooled StDev
Level           N    Mean   StDev   --------+---------+---------+---------+-
182C 180min     5   803.04  33.03          (---------*--------)
177C 180min     5   813.18  25.61             (--------*--------)
171C 180min     5   823.30  16.56                (--------*---------)
160C 180min     5   794.21  19.87         (--------*--------)
149C 180min     5   782.90  35.03     (--------*--------)
160C 400min     5   809.21  32.39             (--------*--------)
149C 400min     5   789.99  39.77       (--------*---------)
                                        --------+---------+---------+---------+-
                                         780       810       840       870
```
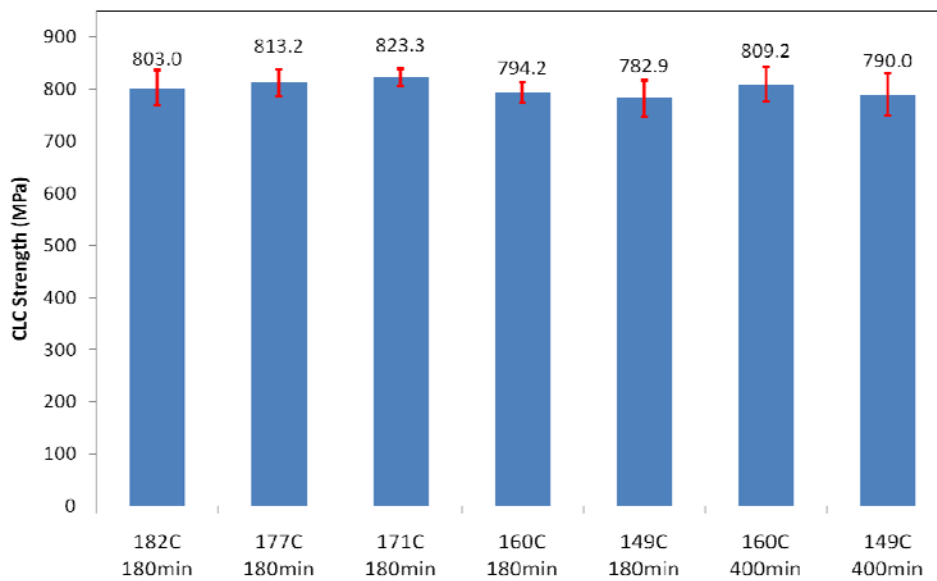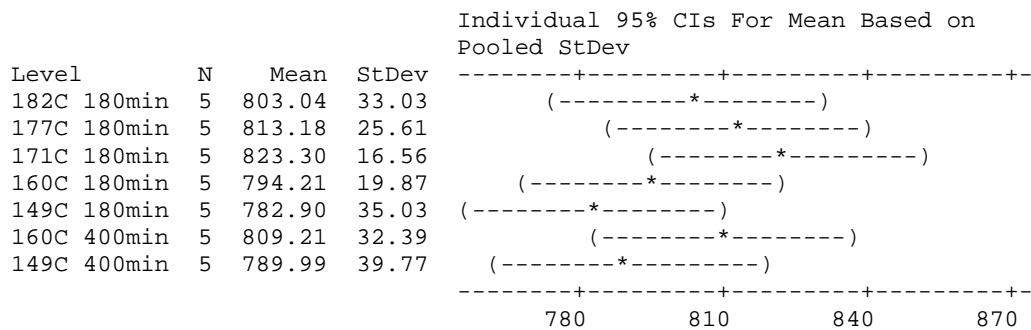

Figure 46. Average CLC strength for one-stage cure cycles.

67

TABLE 15

AVERAGE CLC MODULUS FOR ONE-STAGE CURE CYCLES

Cure Cycle	CLC Modulus (GPa)	Standard Deviation (GPa)	Coefficient of Variation (CV)
182°C 180 min	73.8	2.39	3.24
177°C 180 min	74.4	1.50	2.02
171°C 180 min	74.1	0.98	1.33
160°C 180 min	74.7	0.83	1.11
149°C 180 min	75.5	1.21	1.60
160°C 400 min	75.8	2.82	3.72
149°C 400 min	76.2	2.52	3.31

TABLE 16

MINITAB ANOVA ANALYSIS OF CLC MODULUS VARIANCE
FOR ONE-STAGE CURE CYCLES

```
Level          N    Mean   StDev
182C 180min    5  73.813  2.393
177C 180min    5  74.406  1.503
171C 180min    5  74.105  0.984
160C 180min    5  74.739  0.827
149C 180min    5  75.508  1.205
160C 400min    5  75.792  2.823
149C 400min    5  76.163  2.521
                    Individual 95% CIs For Mean Based on Pooled StDev
Level             +---------+---------+---------+---------
182C 180min       (-----*-----)
177C 180min         (-----*-----)
171C 180min        (-----*-----)
160C 180min          (-----*-----)
149C 180min              (-----*-----)
160C 400min              (-----*-----)
149C 400min                (-----*-----)
                  +---------+---------+---------+---------
                 72.0      75.0      78.0      81.0
```
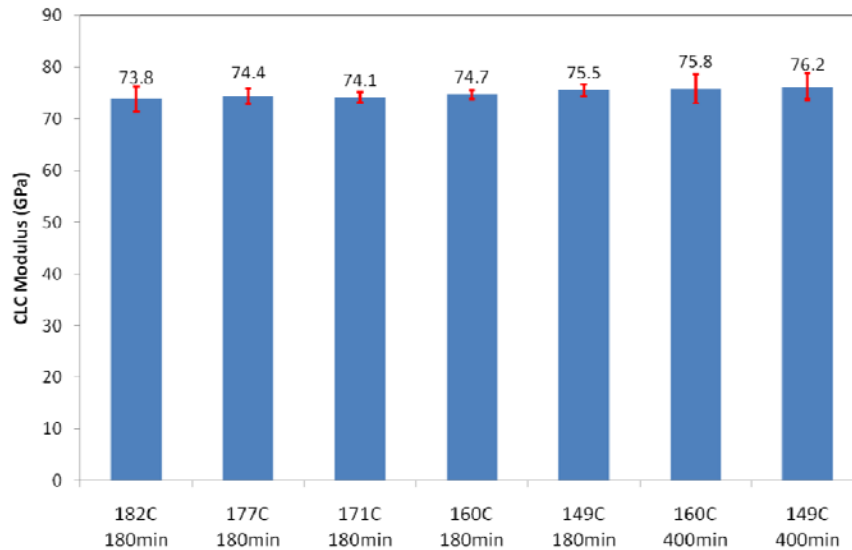

Figure 47. Average CLC modulus for one-stage cure cycles.

68

TABLE 17

AVERAGE CLC POISSON'S RATIO FOR ONE-STAGE CURE CYCLES

Cure Cycle	CLC Poisson's Ratio	Standard Deviation	Coefficient of Variation (CV)
182°C 180 min	0.038	0.0015	3.90
177°C 180 min	0.039	0.0010	2.61
171°C 180 min	0.041	0.0052	12.76
160°C 180 min	0.039	0.0023	5.99
149°C 180 min	0.043	0.0048	11.18
160°C 400 min	0.039	0.0016	4.03
149°C 400 min	0.038	0.0023	6.13
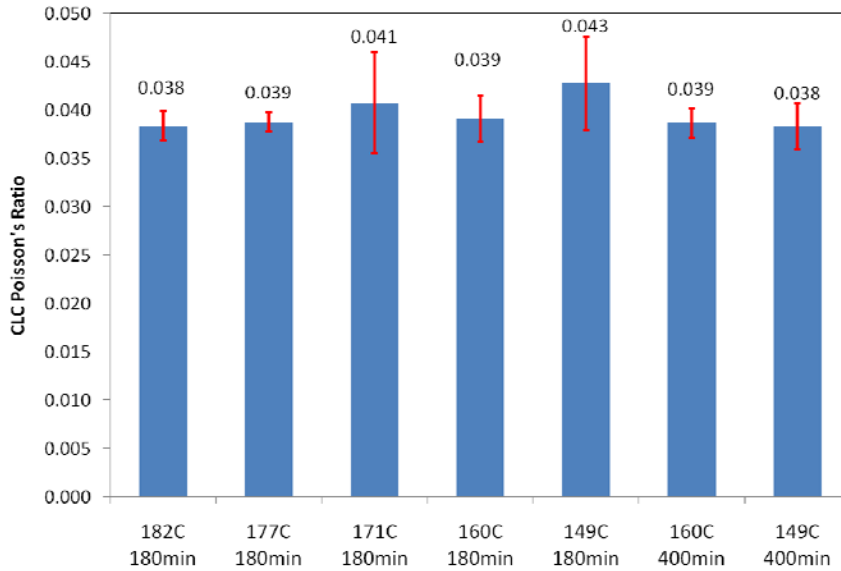
Figure 48. Average CLC Poisson's ratio for one-stage cure cycles.

The failure mode for CLC specimens was similar for different cure cycles. As Figures 49 to 55 show, the failure mode for all specimens was brooming in the middle of the gage section (BGM). Brooming usually occurs in untabbed compression specimens tightened inside the CLC test fixture with high clamping torque (90 lb.in. for the tested CLC specimens). It indicates a strong fiber-resin adhesion, since the resin could transfer the load to the fibers that in turn caused the fibers to fracture explosively at the gage section. BGM is an acceptable failure mode according to ASTM D3410 (Figure 56) as referenced by ASTM D6641. The percent bending for all specimens was less than 5 percent, which means that the specimens did not buckle during the

test. While the failure mode for SBS specimens cured at 149°C for 180 minutes was different than that of the other specimens, the failure mode for CLC specimens cured at 149°C for 180 minutes was not different than that of the other specimens. This could be related to the difference in the method of load application between SBS and CLC tests. While the load in the SBS test is applied on top of the specimen and not on the sides of the specimens, thus allowing the sample layers to slide with respect to each other during testing, the load in the CLC test is applied on both ends of the specimen, thus eliminating the possibility of movement of the layers with respect to one another during testing [65].

Figure 49. Compressive failure mode for CLC specimens cured at 182°C for 180 min.

Figure 50. Compressive failure mode for CLC specimens cured at 177°C for 180 min.

Figure 51. Compressive failure mode for CLC specimens cured at 171°C for 180 min.

Figure 52. Compressive failure mode for CLC specimens cured at 160°C for 180 min.

Figure 53. Compressive failure mode for CLC specimens cured at 149°C for 180 min.

71

Figure 54. Compressive failure mode for CLC specimens cured at 160°C for 400 min.

Figure 55. Compressive failure mode for CLC specimens cured at 149°C for 400 min.
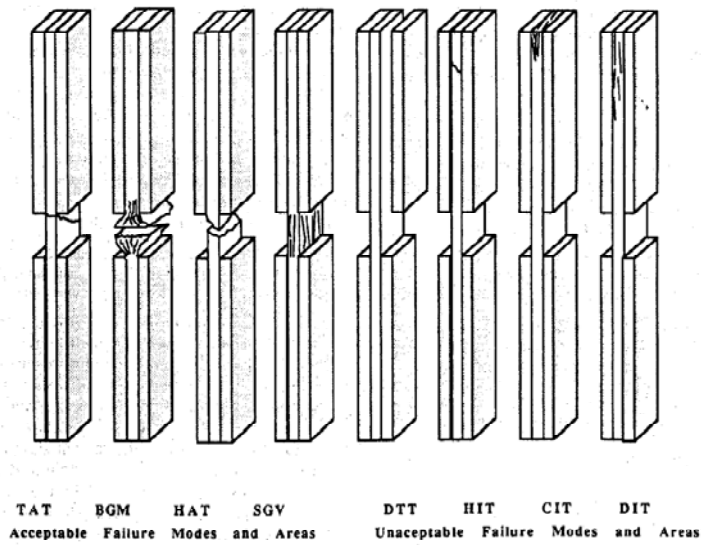
Figure 56. Typical failure modes in compression test according to ASTM D3410 [95].

4.1.3.3.   Open-Hole Compression Properties

Average OHC strength and standard deviation for different one-stage cure cycles is shown in Tables 18 and 19 and Figure 57. Average OHC modulus for different cure cycles is shown in Tables 20 and 21 and Figure 58. The average OHC modulus was obtained using the slope of the linear portion of the stress-strain curve for each specimen. The values for OHC strength and modulus did not vary significantly and showed no particular trend for different cure cycles. The maximum percent bending at 2,000 microstrains for specimens cured at each one-stage cure cycle is shown in Table 22 and Figure 59.

As with CLC specimens, OHC specimens showed no change in the failure mode for different cure cycles. Figures 60 to 66 show the typical failure mode for each one-stage cure cycle. The observed failure mode was laminate compressive failure laterally across the center of the hole, with 0°-dominated ply kinking (LGM). Fiber kinking in OHC specimens indicates a strong fiber-resin adhesion, since the modulus of the resin controls the ability of the fibers to kink [96]. LGM is an acceptable failure mode according to ASTM D6484 (Figure 67).

TABLE 18

AVERAGE OHC STRENGTH FOR ONE-STAGE CURE CYCLES

Cure Cycle	OHC Strength (MPa)	Standard Deviation (MPa)	Coefficient of Variation (CV)
182°C 180 min	319.4	5.25	1.64
177°C 180 min	313.3	7.03	2.24
171°C 180 min	321.1	11.89	3.70
160°C 180 min	318.7	9.88	3.10
149°C 180 min	338.0	14.35	4.25
160°C 400 min	341.5	10.75	3.15
149°C 400 min	327.3	3.51	1.07

TABLE 19

MINITAB ANOVA ANALYSIS OF OHC STRENGTH VARIANCE
FOR ONE-STAGE CURE CYCLES

```
                             Individual 95% CIs For Mean Based on
                             Pooled StDev
Level          N    Mean   StDev  --------+---------+---------+---------+
182C 180min    5  319.35    5.25     (-----*----)
177C 180min    5  313.32    7.03  (-----*----)
171C 180min    5  321.11   11.89     (-----*----)
160C 180min    5  318.74    9.88     (----*-----)
149C 180min    5  338.05   14.35           (-----*-----)
160C 400min    5  341.46   10.75             (-----*----)
149C 400min    5  327.33    3.51        (-----*----)
                                    --------+---------+---------+---------+
                                          320       340       360       380
```
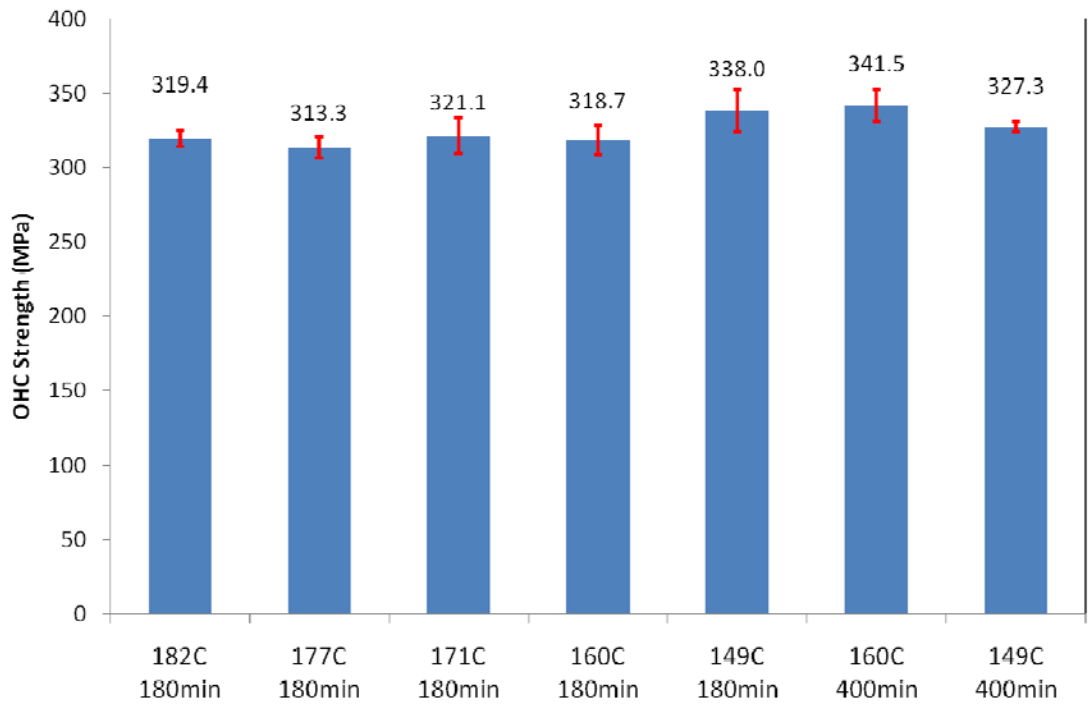

Figure 57. Average OHC strength for one-stage cure cycles.

TABLE 20

AVERAGE OHC MODULUS FOR ONE-STAGE CURE CYCLES

Cure Cycle	OHC Modulus (GPa)	Standard Deviation (GPa)	Coefficient of Variation (CV)
182°C 180 min	69.9	2.93	4.19
177°C 180 min	69.2	5.71	8.26
171°C 180 min	77.2	4.77	6.17
160°C 180 min	72.0	5.59	7.77
149°C 180 min	74.2	6.43	8.66
160°C 400 min	74.0	4.89	6.60
149°C 400 min	75.5	4.61	6.11

TABLE 21

MINITAB ANOVA ANALYSIS OF OHC MODULUS
VARIANCE FOR ONE-STAGE CURE CYCLES

```
Level         N    Mean   StDev
182C 180min   5  69.850  2.929
177C 180min   5  69.161  5.710
171C 180min   5  77.205  4.766
160C 180min   5  72.029  5.594
149C 180min   5  74.188  6.428
160C 400min   5  74.033  4.888
149C 400min   5  75.482  4.613
                 Individual 95% CIs For Mean Based on Pooled StDev
Level         -+---------+---------+---------+--------
182C 180min      (--------*--------)
177C 180min    (--------*--------)
171C 180min                  (--------*---------)
160C 180min          (--------*--------)
149C 180min            (--------*---------)
160C 400min            (--------*--------)
149C 400min               (--------*--------)
              -+---------+---------+---------+--------
              65.0      70.0      75.0      80.0
```
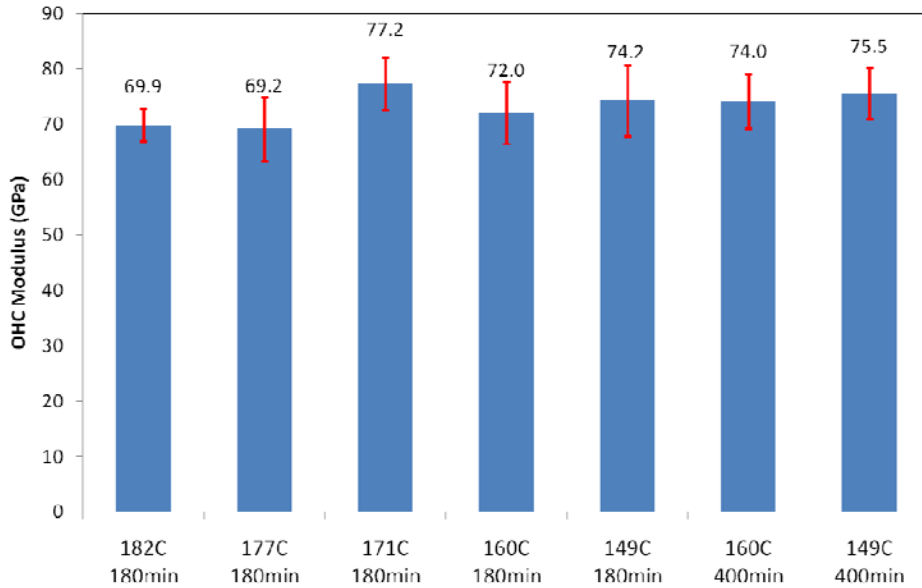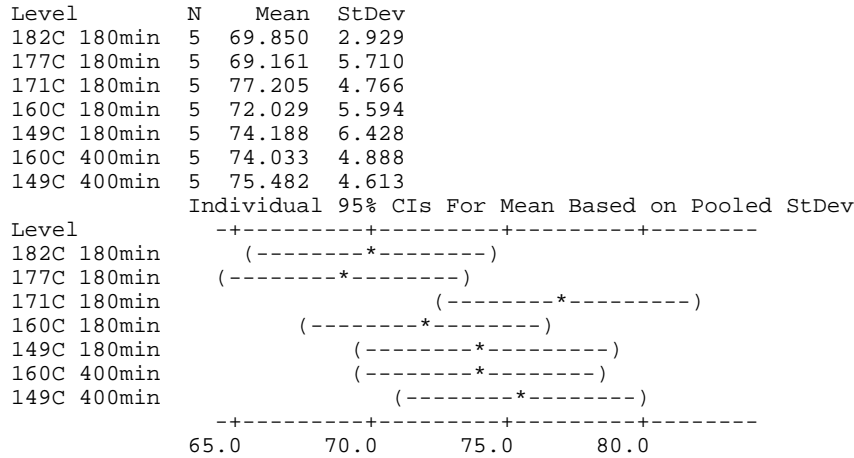

Figure 58. Average OHC modulus for one-stage cure cycles.

75

TABLE 22

OHC MAXIMUM PERCENT BENDING FOR ONE-STAGE CURE CYCLES

Cure Cycle	Maximum Percent Bending
182°C 180 min	12.90
177°C 180 min	16.58
171°C 180 min	17.27
160°C 180 min	8.72
149°C 180 min	10.16
160°C 400 min	8.94
149°C 400 min	9.99
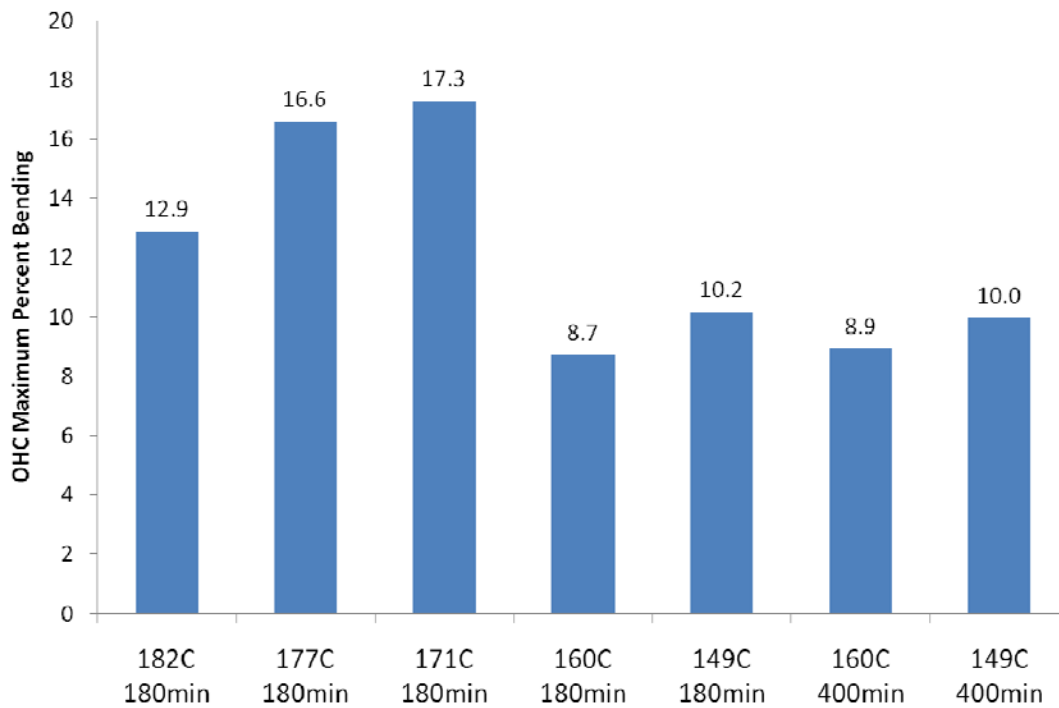
Figure 59. OHC maximum percent bending for one-stage cure cycles.
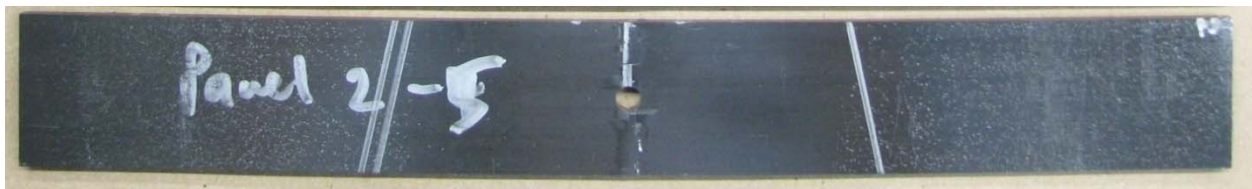
Figure 60. Compressive failure mode for OHC specimen cured at 182°C for 180 min.

Figure 61. Compressive failure mode for OHC specimen cured at 177°C for 180 min.

Figure 62. Compressive failure mode for OHC specimen cured at 171°C for 180 min.

Figure 63. Compressive failure mode for OHC specimen cured at 160°C for 180 min.
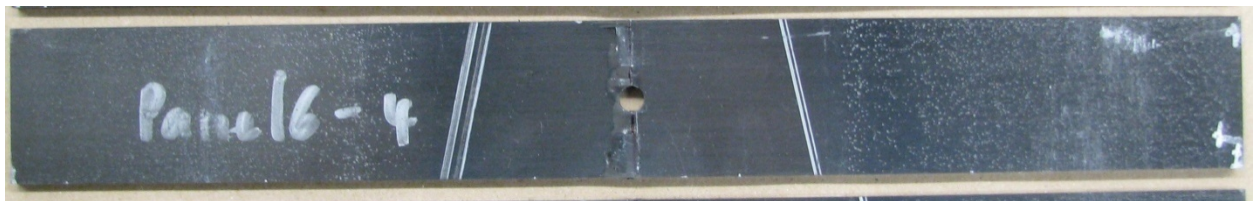
Figure 64. Compressive failure mode for OHC specimen cured at 149°C for 180 min.
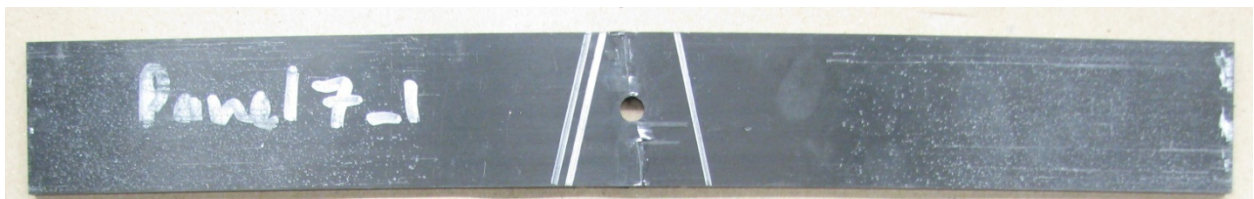
Figure 65. Compressive failure mode for OHC specimen cured at 160°C for 400 min.

Figure 66. Compressive failure mode for OHC specimen cured at 149°C for 400 min.
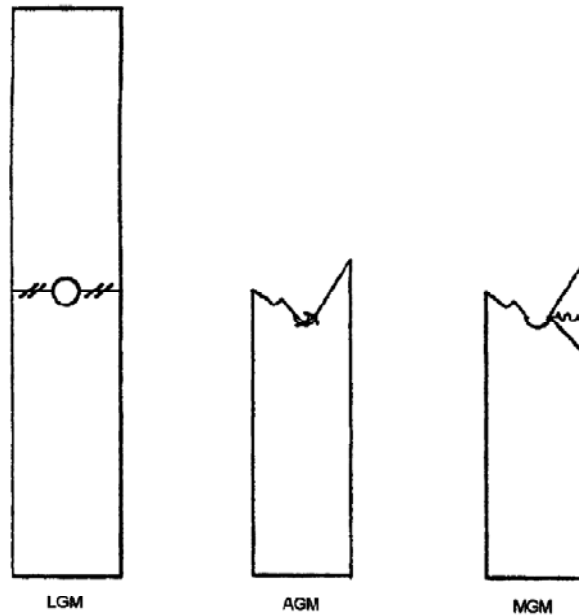
Figure 67. Typical failure modes in OHC test according to ASTM D6484 [88].

4.1.3.4. Void Content

Figure 68 and Table 23 show the average void volume content for different cure cycles. The void content test was performed according to ASTM D3171 [97] using sulfuric acid for removing the resin. The level of void content in the panels was so low that the C-Scan of the cured panels performed at Hawker Beechcraft showed zero percent void content. The negligible void content of the cured panels indicates that cure pressure was applied in the proper pressure window, and therefore, the variations in the material properties were only due to the difference in the state of cure. Tables 24 to 26 and Figures 69 to 71 show the fiber volume content, resin volume content, and density of cured prepregs for different cure cycles, respectively. The resin density of 1.31 g/cm^3 and fiber density of 1.79 g/cm^3 were used for void content calculation.
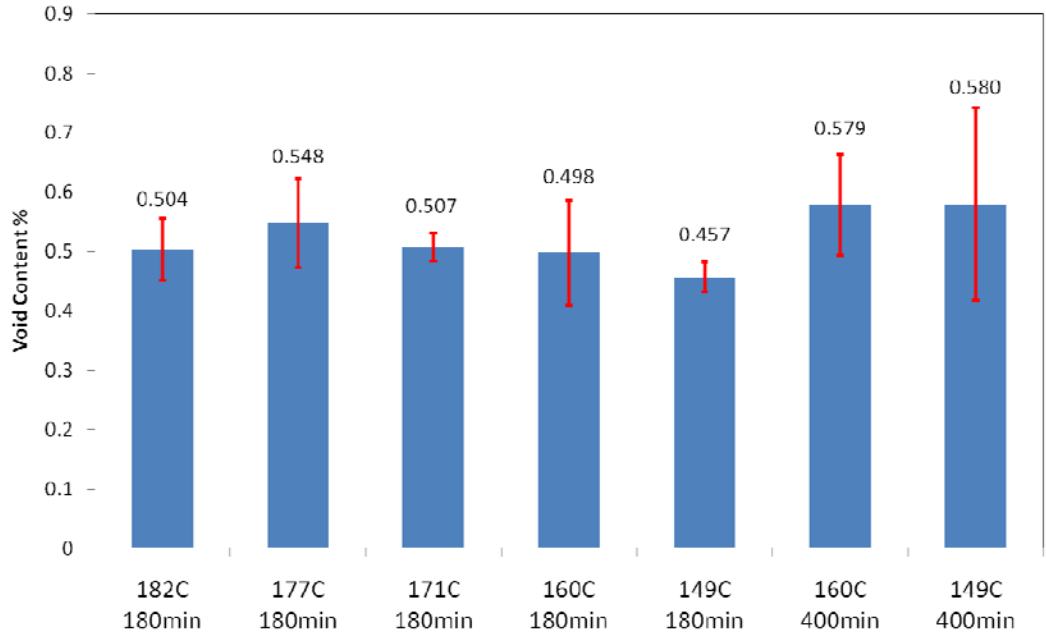
Figure 68. Average void volume content for one-stage cure cycles.

TABLE 23

AVERAGE VOID VOLUME CONTENT FOR ONE-STAGE CURE CYCLES

Cure Cycle	Void Content (%)	Standard Deviation (%)	Coefficient of Variation (CV)
182°C 180 min	0.504	0.052	10.36
177°C 180 min	0.548	0.075	13.65
171°C 180 min	0.507	0.024	4.82
160°C 180 min	0.498	0.089	17.78
149°C 180 min	0.457	0.024	5.33
160°C 400 min	0.579	0.086	14.78
149°C 400 min	0.580	0.161	27.85

TABLE 24

AVERAGE FIBER VOLUME CONTENT FOR ONE-STAGE CURE CYCLES

Cure Cycle	Fiber Content (%)	Standard Deviation (%)	Coefficient of Variation (CV)
182°C 180 min	58.10	0.23	0.40
177°C 180 min	57.56	0.36	0.63
171°C 180 min	57.65	0.47	0.81
160°C 180 min	58.17	0.56	0.97
149°C 180 min	58.67	0.50	0.85
160°C 400 min	58.73	0.71	1.21
149°C 400 min	57.90	0.38	0.65

TABLE 25

AVERAGE RESIN VOLUME CONTENT FOR ONE-STAGE CURE CYCLES

Cure Cycle	Resin Content (%)	Standard Deviation (%)	Coefficient of Variation (CV)
182°C 180 min	41.40	0.21	0.51
177°C 180 min	41.89	0.30	0.70
171°C 180 min	41.84	0.49	1.17
160°C 180 min	41.33	0.52	1.25
149°C 180 min	40.88	0.52	1.27
160°C 400 min	40.69	0.64	1.57
149°C 400 min	41.52	0.24	0.59

TABLE 26

AVERAGE DENSITY OF CURED PREPREG FOR ONE-STAGE CURE CYCLES

Cure Cycle	Density (g/cm^3)	Standard Deviation (g/cm^3)	Coefficient of Variation (CV)
182°C 180 min	1.582	0.00157	0.10
177°C 180 min	1.579	0.00265	0.17
171°C 180 min	1.580	0.00194	0.12
160°C 180 min	1.583	0.00352	0.22
149°C 180 min	1.586	0.00207	0.13
160°C 400 min	1.584	0.00444	0.28
149°C 400 min	1.580	0.00383	0.24
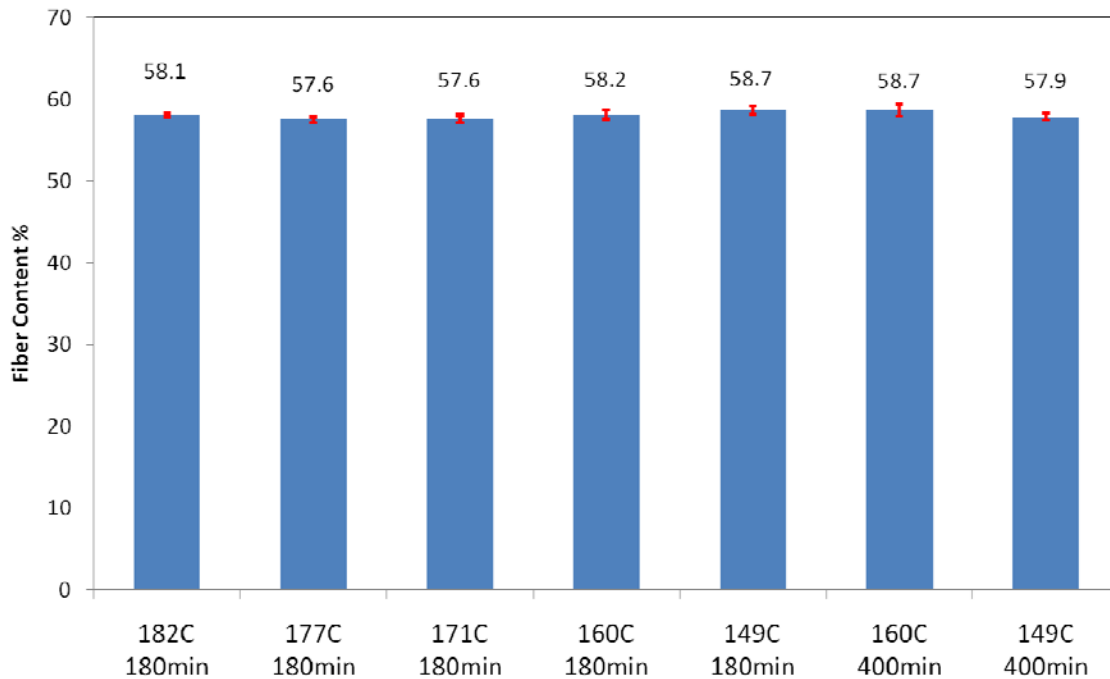
Figure 69. Average fiber volume content for one-stage cure cycles.
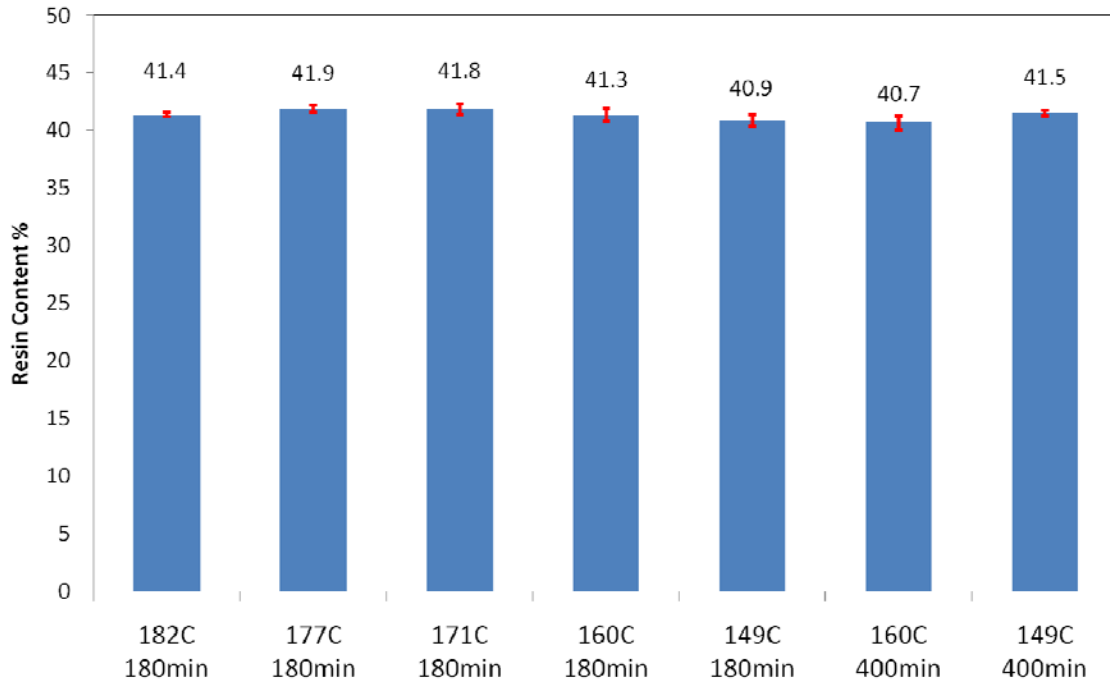
Figure 70. Average resin volume content for one-stage cure cycles.
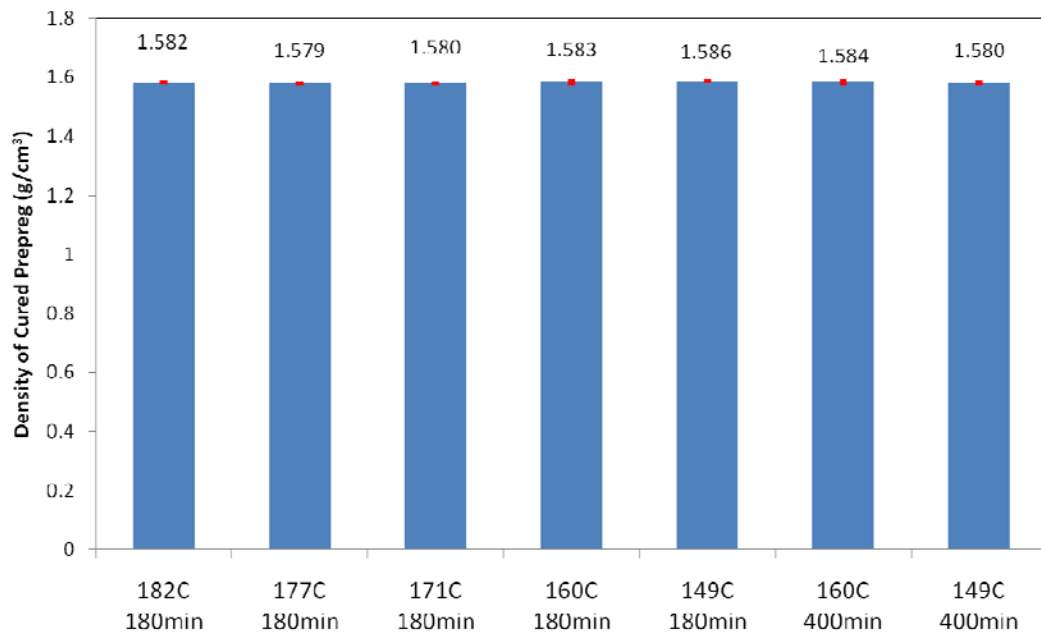
Figure 71. Average density of cured prepreg for one-stage cure cycles.

4.2.   Two-Stage Cure Cycles

As can be seen in Table 9, cure cycles 1 and 3 and cure cycles 2 and 4 were different in the ramp-up rate. As such, the testing results for these cure cycles showed the effect of the ramp-up rate in the material properties. Also, cure cycles 1 and 2 and cure cycles 3 and 4 were different in the first dwell time. Therefore, the testing results for these cure cycles showed the effect of the first dwell time in the material properties.

4.2.1.   Rheometry Results

The viscoelastic properties of the prepreg, including G', G", tanδ, and complex viscosity, were measured for different two-stage cure cycles using the parallel-plate shear rheometer. Similar to one-stage cure cycles, since the complex viscosity was the main viscoelastic property used for describing the state of the material, only the graph for the complex viscosity during the cure and post-cure T_g test was used.

4.2.1.1. Complex Viscosity

Figure 72 shows complex viscosity during cure and post-cure T_g test for different two-stage cure cycles. The complex viscosity graph shows the state of the material throughout the two-stage cure cycles and post-cure cycles. In addition, important material-state transitions during cure such as gelation and vitrification are visible in this complex viscosity graph. Also, other crucial material-state regions, such as the low-viscosity region and pressure-window region, can be found using the complex viscosity data. As such, the complex viscosity seems to be an appropriate option for monitoring the state of the material during cure. As can be seen in Figure 72, the plateau value indicating completion of cure was achieved for all two-stage cure cycles. The complex viscosity reached its plateau in the second stage of the cure for all cure cycles. It is also noticeable that faster ramp rates and higher first-stage dwell temperatures

82

shifted the complex viscosity curves more toward the isothermal cure at 177°C. Moreover, Figure 72 shows that the complex viscosity graphs during the two-stage cure cycles shifted slightly (marked by circles on the graphs), which was due to the transition from the ramp to the isothermal step. The values of the complex viscosity at these slight shifts are 4.34×10^6 Pa.S, 1.88×10^6 Pa.S, 3.85×10^6 Pa.S, and 1.11×10^6 Pa.S for cure cycles 1, 2, 3, and 4, respectively.
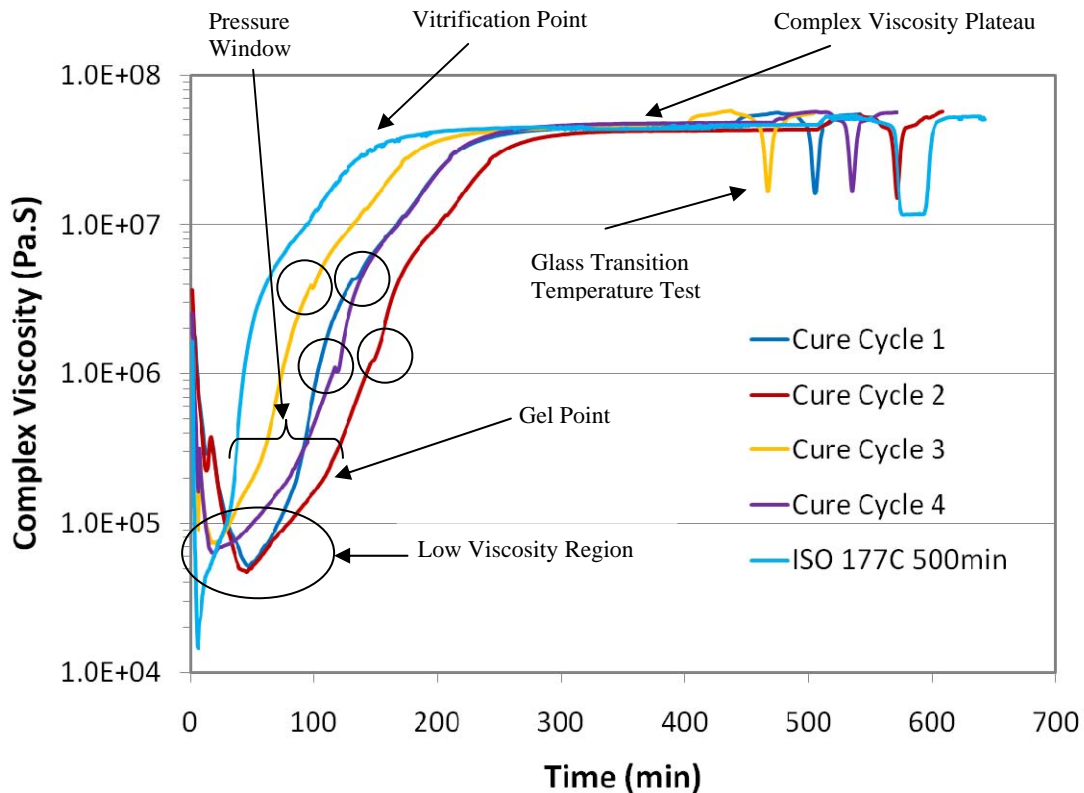
Figure 72. Complex viscosity during cure and post-cure T$_g$ test for two-stage cure cycles and isothermal cure at 177°C.

The magnitude of complex viscosity for two-stage cure cycles cannot be compared to that of the one-stage cure cycles since the thickness and ply orientation of the rheometer samples used for two-stage cure cycles were different than those of the rheometer samples used for one-stage cure cycles. The samples for two-stage cure cycles were prepared using 27 plies in lieu of 28 plies used for one-stage cure cycles and the orientation of the plies for two-stage cure cycles was 0/90 rather than 0/90/90/0 used for one-stage cure cycles.

4.2.1.2. Gel Time

Similar to the one-stage cure cycles, the gel time for two-stage cure cycles was defined as the time at which the tangent of the slope of the complex viscosity graph tends to infinity. For the two-stage cure cycles that were studied, gelation occurred at the beginning of the first isothermal stage and coincided with the complex viscosity value equal to 2×10^5 Pa.S. As mentioned previously, the magnitude of complex viscosity at the gel point depends on several factors, such as properties of the material, thickness of the sample, and orientation of the sample plies. As such, it was expected that reducing the thickness of the sample by reducing the number of sample plies and changing the orientation of the plies would change the magnitude of the complex viscosity at the gel point. As Figure 73 illustrates, the gel time for different two-stage cure cycles increased as the first dwell temperature and ramp-up rate decreased. As such, the sample cured at 177°C had the lowest gel time.
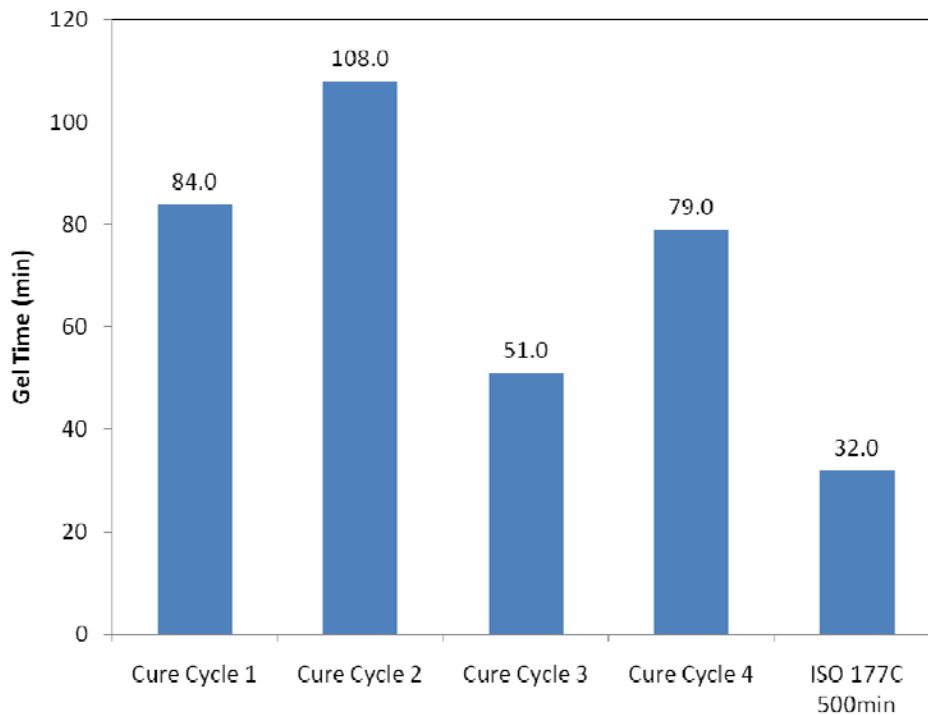
Figure 73. Gel time for two-stage cure cycles and isothermal cure at 177°C.

4.2.1.3. Glass Transition Temperature (T_g)

Figure 74 shows the glass transition temperature for different two-stage cure cycles. As indicated, T_g for all cure cycles is very close to 186^oC, the ultimate glass transition temperature for 977-2 UD, obtained using the parallel-plate rheometer. This indicated that samples were close to the fully cure state. The final degree of cure for the two-stage cure cycles also proved that samples were highly cured. T_g for all specimens was determined using G' data according to SACMA SRM18R-94 [93].
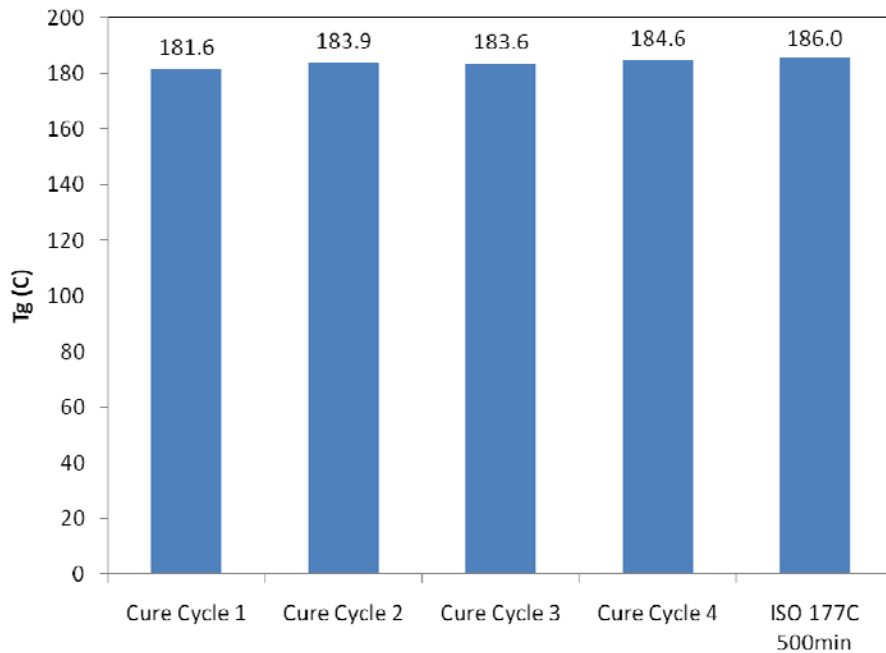
Figure 74. Glass transition temperature for two-stage cure cycles
and isothermal cure at 177^oC.

4.2.1.4. Minimum Complex Viscosity Time

The time at which the complex viscosity of the prepreg sample reached its minimum value for different one-stage cure cycles is shown in Figure 75. The minimum complex viscosity for all cure cycles occurred during the ramp-up stage. As shown, the minimum complex time for

85

cycles with faster ramp-up rate was shorter. Minimum complex viscosity time was used to obtain the pressure window.
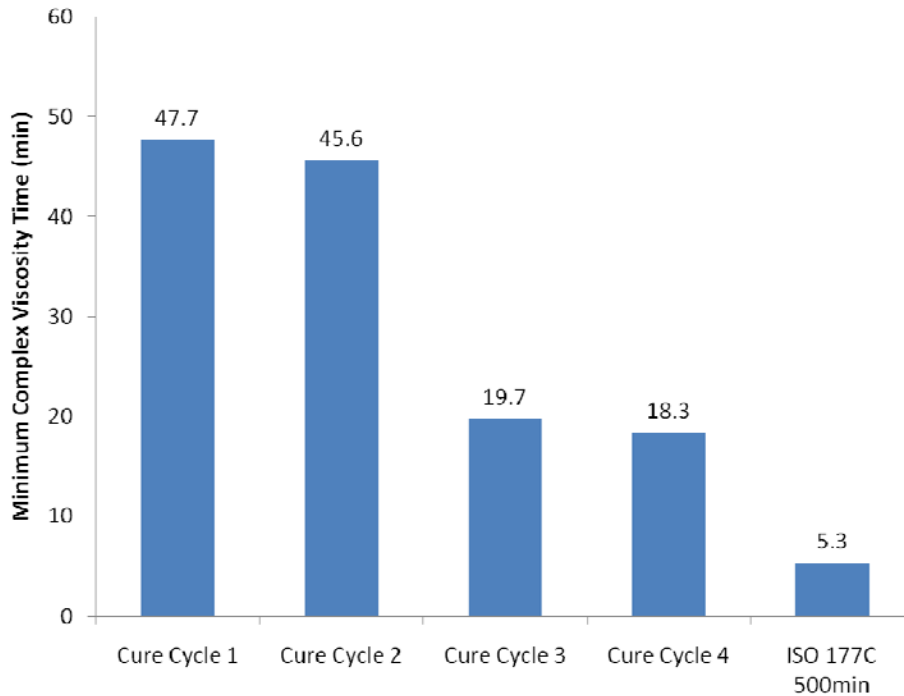
Figure 75. Minimum complex viscosity time for two-stage cure cycles and isothermal cure at 177°C.

4.2.1.5. Pressure Window Time

Figure 76 shows the pressure window time for different two-stage cure cycles. The pressure window time signifies the time span during which the pressurization has a considerable effect on the composite laminates cured in the autoclave. It is defined as the gel time minus the minimum complex viscosity time. Since the minimum complex viscosity time for all of the two-stage cure cycles was not the same, both the gel time and minimum complex viscosity time affected the pressure window time. Cure cycles 2 and 4 had the longest pressure window. Both of these cycles had the lowest first dwell temperature (149°C).
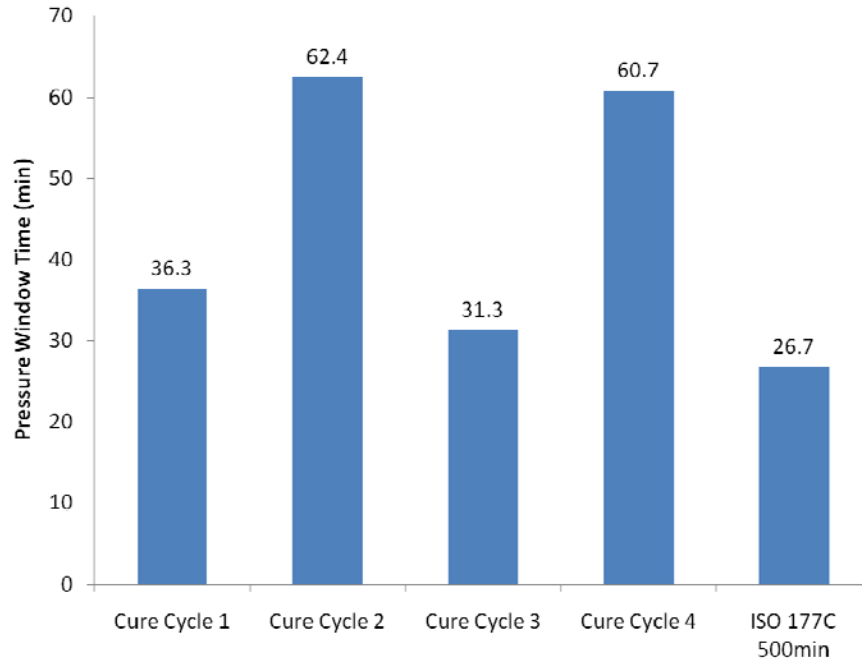
Figure 76. Pressure window time for two-stage cure cycles and isothermal cure at 177°C.

4.2.2. Differential Scanning Calorimetry Results

The heat flow of the prepreg samples during cure was measured for different two-stage cure cycles using the DSC. The measured heat flow was then used to obtain the degree of cure for each cure cycle after the heat-flow baselines for the first and second ramp-up and isothermal heat flows were defined properly.

4.2.2.1. Degree of Cure

The degree of cure during cure for different two-stage cure cycles is shown in Figure 77. The DOC increased rapidly in the first ramp-up and isothermal step, and slowed down to approach the plateau value in the second isothermal step. The rapid increase in the DOC indicates a high cross-linking reaction rate. As such, the curing reactions were kinetics-controlled during the first ramp-up and isothermal step. As the DOC approached its plateau value, the cross-linking reaction rate became significantly slow. The curing reactions in the second

87

isothermal step were diffusion-controlled. Similar to the complex viscosity graphs, DOC graphs during the two-stage cure cycles shifted slightly, which was due to the transition from the ramp-up to isothermal step. This shift was signified as a sudden drop in the time rate of the degree of cure, as shown in Figure 78. It was observed that as for the complex viscosity graphs, faster ramp rates and higher first-stage dwell temperatures shifted the DOC curves more toward the isothermal cure at 177°C.
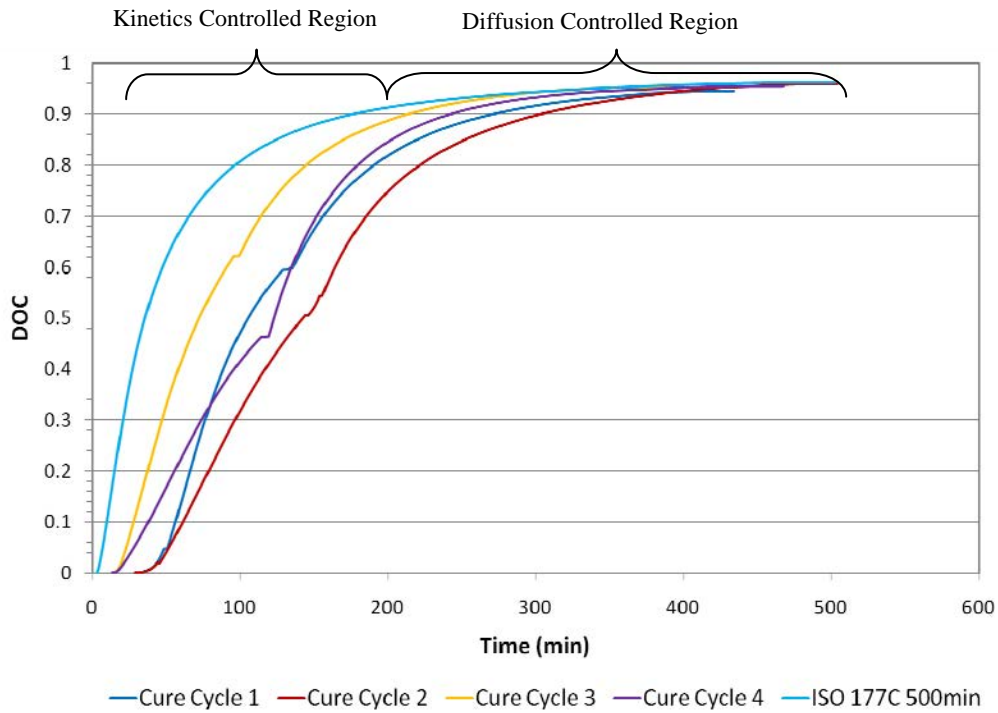
Figure 77. Degree of cure during cure for two-stage cure cycles and isothermal cure at 177°C.
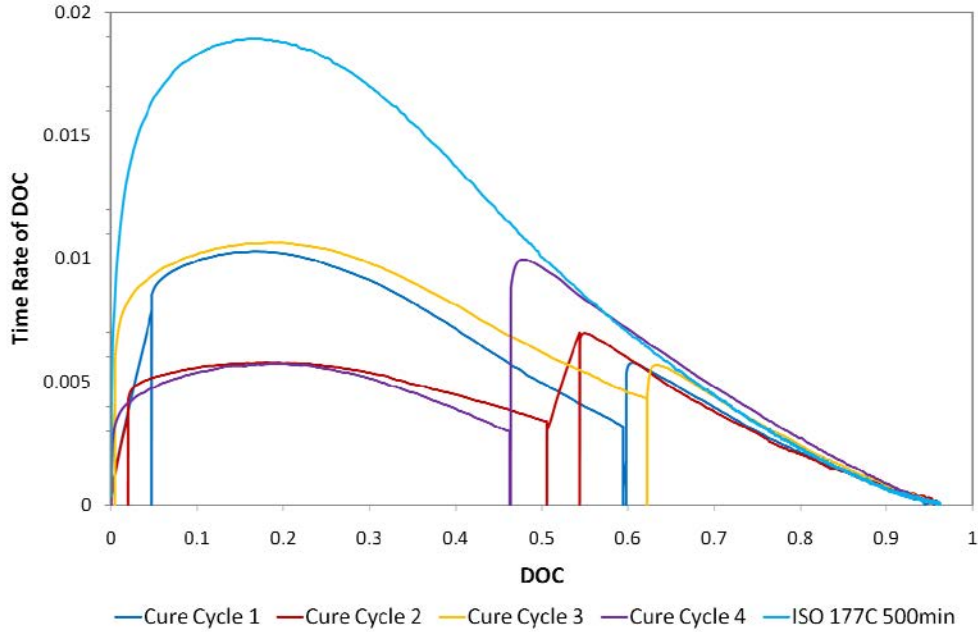
Figure 78. Time rate of degree of cure vs. degree of cure for two-stage cure cycles and isothermal cure at 177°C.

Table 27 contains different heats of reaction and final DOC for two-stage cure cycles. Although the ultimate heat of reaction, H_U, was not the same for different two-stage cure cycles due to variations in prepreg sample weights and also variations in the fiber and resin volume fraction, the residual heat of reaction for different two-stage cycles was not significantly different, indicating that the degree of cure for different cycles was very close. This observation was verified by the final degree of cure data (Figure 79). As Figure 79 shows, the degree of cure for all cure cycles was equal to or greater than 0.95, which in turn indicates that the samples were almost fully cured.

TABLE 27

HEAT OF REACTION AND FINAL DEGREE OF CURE
FOR TWO-STAGE CURE CYCLES

Cure Cycle Number	H_T (J/g)	H_{res} (J/g)	H_U (J/g)	α_{max}
1	142.01	8.24	150.25	0.95
2	143.50	5.90	149.41	0.96
3	144.34	7.13	151.47	0.95
4	126.64	5.94	132.58	0.96
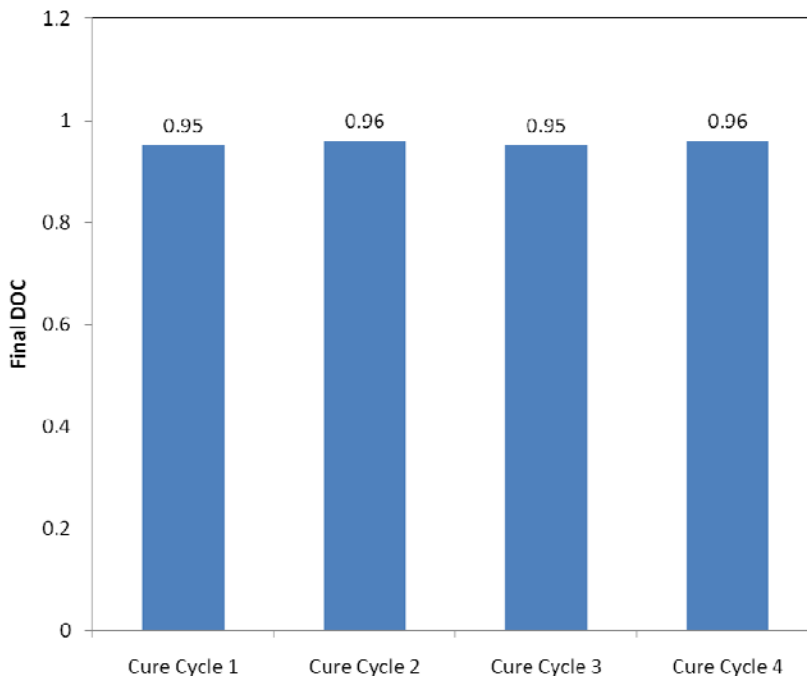
Figure 79. Final degree of cure for two-stage cure cycles.

4.2.2.1.1. Heat-Flow Baseline

The two-stage cure cycles consisted of two ramp-up steps and two isothermal steps. To find the total heat of reaction, the heat-flow integration for each of these steps had to be done separately using the appropriate heat-flow baseline. To obtain the baseline for the first ramp-up and isothermal steps, the same procedure as described for one-stage cure cycles was followed. To obtain the second ramp-up heat-flow baseline, a dynamic scanning was performed on a 977-2 UD sample immediately after the end of the first curing stage. The baseline of the dynamic scanning was a straight line (baseline number 2 in Table 3), which was used to calculate the DOC for the second ramp-up step. To find the baseline for the second isothermal step, the sample was kept at the second isothermal cure temperature immediately after the end of the second ramp-up step until the heat flow approached the plateau value (Figure 80). The heat flow plateau obtained was then used as the baseline for the second isothermal step.
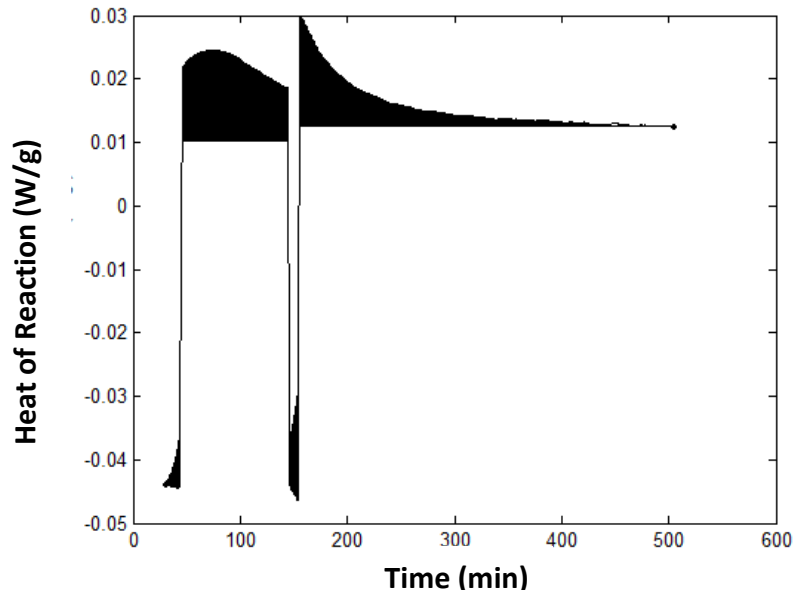
Figure 80. Heat-flow baseline for two-stage cure cycle.

4.3. Modeling and Correlation Results

Complex viscosity, which was the main viscoelastic property studied in this dissertation for monitoring the material state, was modeled for one-stage and two-stage cure cycles using the Kenny viscosity model, as defined by equation (35). The Kenny model was selected since it can precisely model the complex viscosity of 977-2 UD from the start of the cure until the gel time.

Since the Kenny model requires two variables, i.e., degree of cure and cure temperature, for viscosity modeling, the degree of cure was modeled first to determine the degree of cure at any time during the cure. The degree of cure data for one-stage and two-stage cure cycles was modeled using the Springer-Loos model. The Springer-Loos model was selected since it can precisely model the degree of cure of 977-2 UD for the entire cure cycle. The model in the form of equation (19) is suitable for isothermal cure kinetics modeling. If the temperature changes during cure, however, equations (16) and (17) should be substituted into equation (19) to account for changes in the cure temperature.

91

The correlation between final complex viscosity and mechanical properties, i.e., SBS strength, CLC strength, CLC modulus, CLC Poisson's ratio, OHC strength, and OHC modulus, for the samples cured at different one-stage cure cycles was studied. Moreover, the correlation between final complex viscosity and other material state properties, i.e., glass transition temperature, degree of cure, and gel time, and also the correlation between other material-state properties and mechanical properties for the samples cured at different one-stage cure cycles was investigated.

4.3.1. Degree of Cure Modeling

The following procedure was followed to fit the Springer-Loos model to DOC data using the least squares fit method with the Excel solver:

1. Three data columns were created using the proper cure time, DOC, and cure temperature.

2. A forth column was created to predict the DOC using the Springer-Loos model. The first cell of this column was zero and the DOC at cell n+1 was found using the following equation:

$$\alpha_{n+1} = \left(\frac{\Delta\alpha}{\Delta t}\right)_n \Delta t + \alpha_n \tag{63}$$

where α_{n+1} is the DOC at cell n+1, α_n is the DOC at cell n, Δt is the time step, and $(\Delta\alpha/\Delta t)_n$ is found using the following equation:

$$\left(\frac{\Delta\alpha}{\Delta t}\right)_n = \left[A_1\exp(-\frac{\Delta E_1}{RT_n}) + A_2\exp(-\frac{\Delta E_2}{RT_n})\alpha_n\right](1-\alpha_n)(B_1-\alpha_n) \tag{64}$$

where α_n is the DOC at cell n; T_n is the temperature at cell n; A_1, A_2, ΔE_1, ΔE_2, and B_1 are the model parameters; and R is the universal gas constant.

3. The fifth column was created by obtaining the square of the difference between DOC data and the DOC model.

4. The sum of the fifth column cells was found.

5. The sum of the fifth column cells was minimized by changing the model parameters using the Excel solver.

The initial values of the model parameters were found to be important in the convergence of the solution.

4.3.1.1. Springer-Loos Modeling Results

The Springer-Loos model, as defined in equation (64), was used for modeling:

$$\frac{d\alpha}{dt} = \left[A_1 \exp(-\frac{\Delta E_1}{RT}) + A_2 \exp(-\frac{\Delta E_2}{RT})\alpha \right](1-\alpha)(B_1 - \alpha) \tag{65}$$

where α is the degree of cure; $d\alpha/dt$ is the rate of the degree of cure (min^{-1}); and A_1 and A_2 are the first and second exponential constants (min^{-1}), respectively; B_1 is a constant; ΔE_1 and ΔE_2 are the first and second activation energies, respectively (J/mol); T is the temperature (K); and R is the universal gas constant (J/(K.mol)).

4.3.1.2. One-Stage Cure Cycles

Figure 81 shows the time rate of degree of cure vs. degree of cure for selected one-stage cure cycles. Here, the experimental data is plotted along with the model. Figure 82 shows the degree of cure modeling results for selected one-stage cure cycles. As illustrated in both figures, the Springer-Loos model closely followed the behavior of the material and agreed well with the experimental data. Table 28 contains the parameters of the Springer-Loos model for one-stage cure cycles.

93
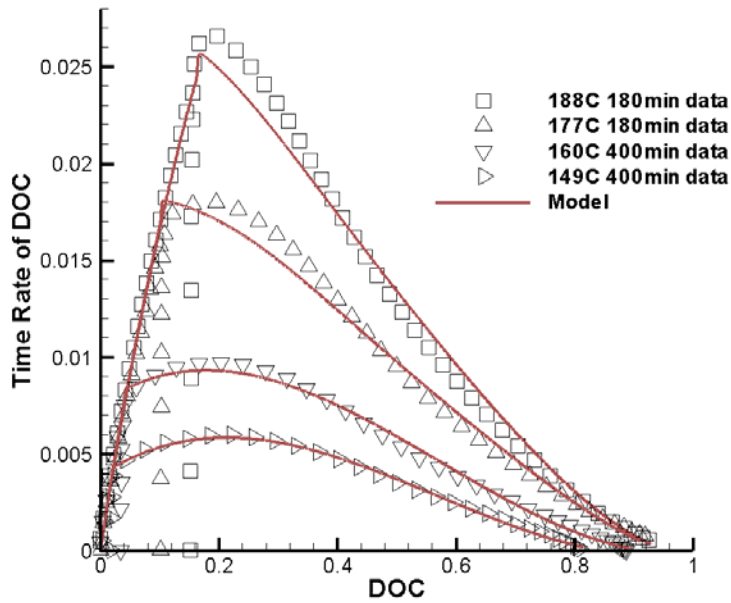
Figure 81. Comparison of experimental data with Springer-Loos model for rate of degree of cure for selected one-stage cure cycles.
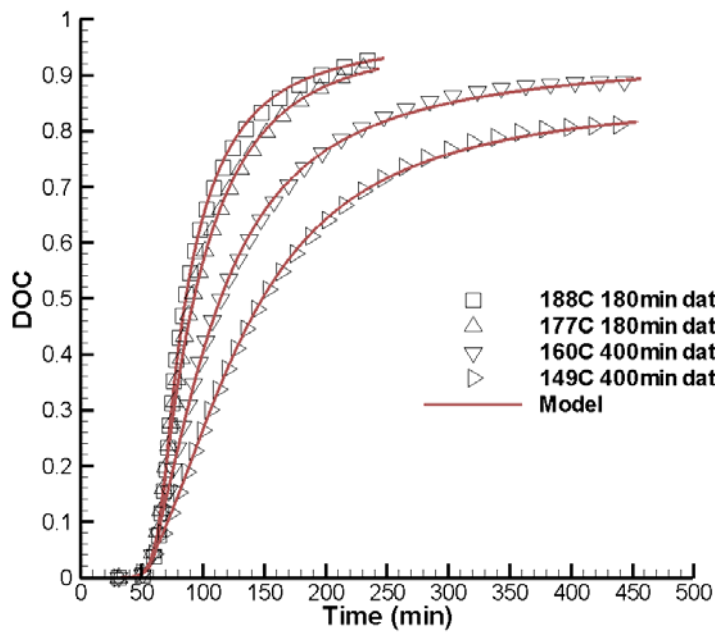
Figure 82. Comparison of experimental data with Springer-Loos model for degree of cure for selected one-stage cure cycles.

TABLE 28

PARAMETERS OF SPRINGER-LOOS MODEL FOR
ONE-STAGE CURE CYCLES

Isothermal Cure Temperature (°C)	A_1 (min^{-1})	A_2 (min^{-1})	B_1	ΔE_1 (J/mol)	ΔE_2 (J/mol)
188	3.14×10^9	7.71×10^2	1.00	9.75×10^4	3.69×10^4
182	5.65×10^9	1.03×10^3	1.03	9.96×10^4	3.78×10^4
177	5.41×10^9	1.09×10^3	1.05	9.89×10^4	3.84×10^4
171	7.90×10^9	1.54×10^3	0.94	1.00×10^5	3.85×10^4
160	9.36×10^9	1.78×10^4	0.93	1.00×10^5	4.69×10^4
149	1.47×10^{10}	2.10×10^3	0.85	1.01×10^5	3.88×10^4

4.3.1.3. Two-Stage Cure Cycles

Table 29 contains the parameters of the Springer-Loos model for two-stage cure cycles. Figure 83 shows the time rate of degree of cure vs. degree of cure for two-stage cure cycles. Here, the experimental data is plotted along with the model. Figure 84 shows the degree of cure modeling results for selected two-stage cure cycles. As both figures show, the Springer-Loos model closely followed the behavior of the material and agreed well with the experimental data.

TABLE 29

PARAMETERS OF SPRINGER-LOOS MODEL FOR TWO-
STAGE CURE CYCLES

Cure Cycle	A_1 (min^{-1})	A_2 (min^{-1})	B_1	ΔE_1 (J/mol)	ΔE_2 (J/mol)
1	3.33×10^6	3.79×10	1.04	7.13×10^4	2.71×10^4
2	1.82×10^6	2.48×10	1.07	6.96×10^4	2.55×10^4
3	6.34×10^7	2.11×10^{-1}	1.05	8.25×10^4	6.76×10^3
4	5.96×10^8	0.192×10	1.15	9.03×10^4	1.72×10^4
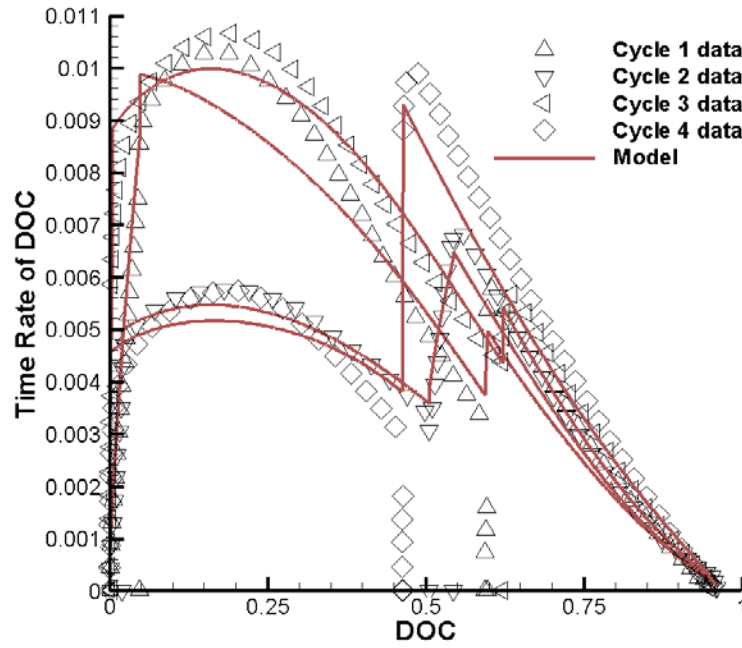
Figure 83. Comparison of experimental data with Springer-Loos model for rate of degree of cure for two-stage cure.
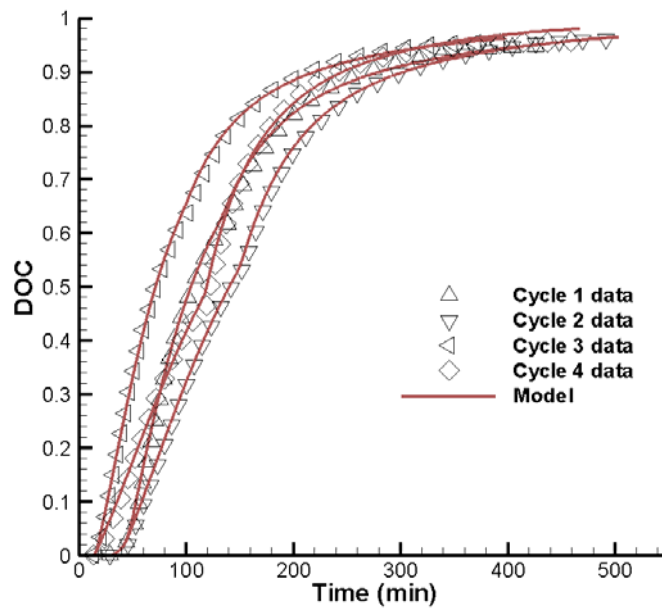
Figure 84. Comparison of experimental data with Springer-Loos model for DOC for two-stage cure cycles.

4.3.2. Complex Viscosity Modeling

The following procedure was followed to fit the Kenny viscosity model to the complex viscosity data using the least squares fit method with the Excel solver:

1. Three data columns were created using the proper cure time, complex viscosity, and cure temperature.

2. The forth column was created to predict the complex viscosity using the Kenny viscosity model. The nth cell of this column was found using the below equation:

$$\ln \eta_n^* = \ln A_\mu + \frac{E_\mu}{RT_n} + (A + B\alpha)\ln\left(\frac{\alpha_g}{\alpha_g - \alpha_n}\right) \qquad (66)$$

where $\ln\eta_n^*$ is the natural log of the complex viscosity at the nth cell; α_n is the DOC at the cell n; T_n is the temperature at the nth cell; A_μ, E_μ, A and B are the model parameters; R is the universal gas constant; and α_g is the degree of cure at gel point.

3. The fifth column was created by obtaining the square of the difference between the complex viscosity data and the complex viscosity model.

4. The sum of the fifth column cells was found.

5. The sum of the fifth column cells was minimized by changing the model parameters using the Excel solver.

The initial values of the viscosity model parameters, as for those of the DOC model, were found to be important in the convergence of the solution.

4.3.2.1. Kenny Modeling Results

The Kenny viscosity model, as defined below, was used for modeling:

$$\ln \eta^* = \ln A_\mu + \frac{E_\mu}{RT} + (A + B\alpha)\ln\left(\frac{\alpha_g}{\alpha_g - \alpha}\right) \qquad (67)$$

where η^* is the complex viscosity (Pa.S); A_μ is a constant (Pa.S); α is the degree of cure; A and B are the first and second exponential constants, respectively; E_μ is the activation energy (KJ/mol); T is the absolute temperature; and R is the universal gas constant (J/(K.mol)).

4.3.2.2. One-Stage Cure Cycles

Figure 85 shows the natural log of complex viscosity for selected one-stage cure cycles. Here, the experimental data is plotted along with the model. As illustrated Figure 85, the Kenny viscosity model closely followed the behavior of the material and agreed well with the experimental data. Table 30 contains the parameters of the Kenny viscosity model for one-stage cure cycles.
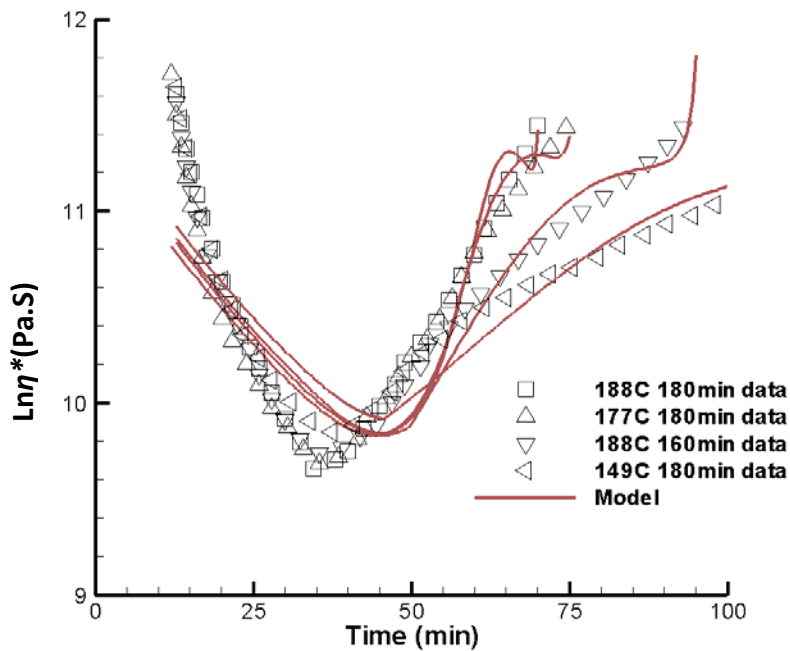
Figure 85. Comparison of experimental with Kenny model for complex viscosity for selected one-stage cure cycles.

TABLE 30

PARAMETERS OF KENNY MODELFOR ONE-STAGE CURE CYCLES

Isothermal Cure Temperature (°C)	A_μ (Pa.S)	E_μ (KJ/mol)	A	B	α_g
188	281.3	14.37	4.29	-9.32	0.42
182	78.70	17.52	4.59	-9.14	0.44
177	274.35	14.23	4.02	-8.27	0.43
171	85.20	18.11	4.12	-8.96	0.41
160	264.24	14.47	3.26	-6.50	0.44
149	322.51	14.16	2.70	-5.24	0.44

4.3.2.3. Two-Stage Cure Cycles

Figure 86 shows the natural log of complex viscosity for two-stage cure cycles. Here, the experimental data is plotted along with the model. As Figure 86 shows, the Kenny viscosity model closely followed the behavior of the material and agreed well with the experimental data. Table 31 contains the parameters of the Kenny viscosity model for two-stage cure cycles.
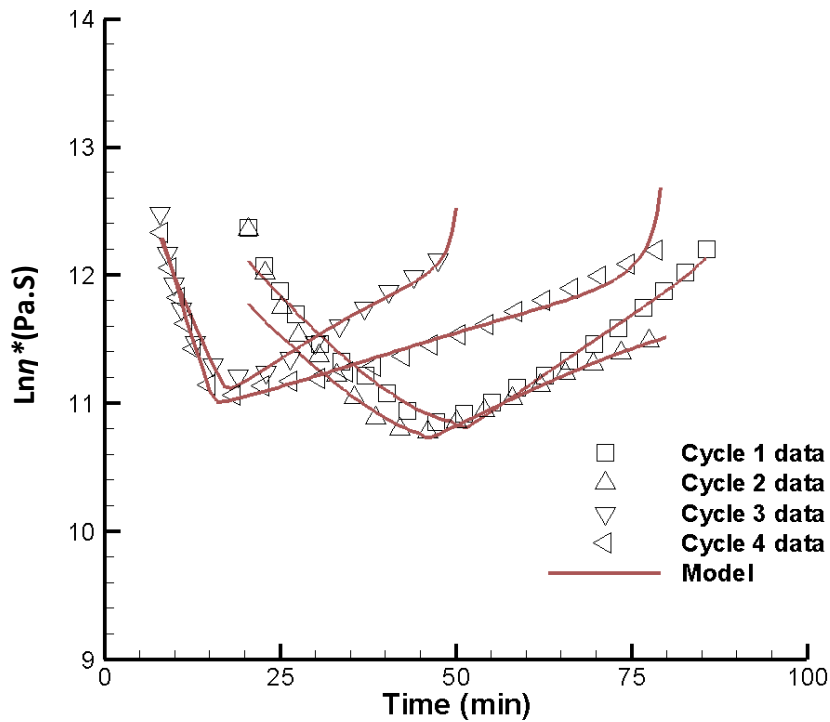
Figure 86. Comparison of experimental with Kenny model for complex viscosity for two-stage cure cycles.

99

TABLE 31

PARAMETERS OF KENNY MODEL FOR TWO-STAGE CURE CYCLES

Cure Cycle	A_μ (Pa.S)	E_μ (KJ/mol)	A	B	α_g
1	80.91	22.58	1.79	-2.59	0.44
2	131.77	20.17	2.01	-4.76	0.35
3	252.50	20.17	1.32	-3.05	0.33
4	29.18	26.78	1.21	-2.67	0.33

4.3.3.   Correlation

The following procedure was followed to investigate the correlation among different material properties for one-stage cure cycles [65]:

1. Two different cases were studied:

   a. When the cure cycles are only different in dwell temperature. This included all cure cycles, except cure cycles 7 and 8.

   b. When the cure cycles are only different in dwell time. This included cure cycles 5 and 7 and also cure cycles 6 and 8.

2. Final complex viscosity, glass transition temperature, gel time, and degree of cure for each cure cycle were normalized using the maximum value of the corresponding property for all cure cycles.

3. The average values of the mechanical properties for each cure cycle were normalized using the maximum average value of the corresponding property for all cure cycles.

4. The graphs for different normalized properties were overlaid to observe the possible similarities in trends.

4.3.3.1. Cure Cycles with Different Dwell Temperatures

Normalized properties obtained for cure cycles 2 to 6 were used for investigating correlation. It is important to note that for the studied cure cycles, the mechanical properties,

except SBS strength, showed no statistical difference. As such, no acceptable correlation between mechanical properties, except SBS strength, and other material properties was found.

4.3.3.1.1. Correlation between Final Complex Viscosity and Other Material State Properties

Figure 87 shows normalized final complex viscosity, T_g, gel time, and DOC for one-stage cure cycles 2 to 6. As can be seen, T_g and DOC gradually decreased with decreasing dwell temperature. This is in contrast to final complex viscosity, which dropped 20 percent only at 149^oC and did not show a considerable change for other dwell temperatures. Gel time values followed nearly the opposite trend from T_g and DOC data. This was expected since gel time increases as the dwell temperature decreases.
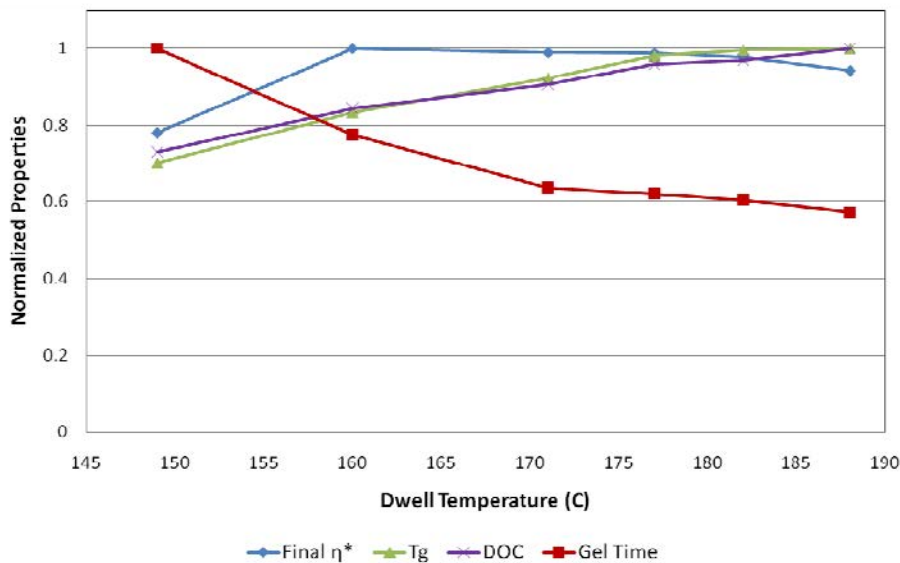
Figure 87. Normalized viscoelastic properties and degree of cure
for one-stage cure cycles 2 to 6.

4.3.3.1.2. Correlation between Mechanical Properties and Other Material Properties

Normalized data for mechanical properties and other material properties for cure cycles 2 to 6 are shown in Figures 88 to 90. For all cured panels, the average mechanical properties except SBS strength were not significantly different and, therefore, could not be used for any correlation. The results showed the average SBS strength of the specimens cured at 149°C for

180 minutes was 10 percent less than that of specimens cured at 160˚C for 180 minutes. As Figure 88 shows, final complex viscosity had a similar trend for these two cure temperatures and, as such, is a good candidate for correlation with SBS strength. Moreover, the average SBS strength of specimens cured at 160˚C to 182˚C for 180 minutes did not show a considerable difference. This was also similar to the final complex viscosity trend for these cure cycles.
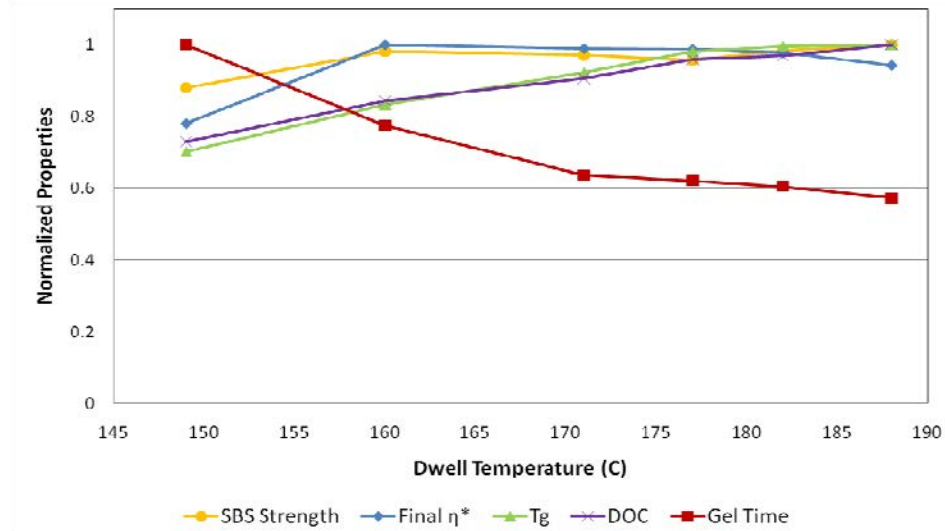
Figure 88. Normalized SBS strength, viscoelastic properties, and degree of cure for one-stage cure cycles 2 to 6.
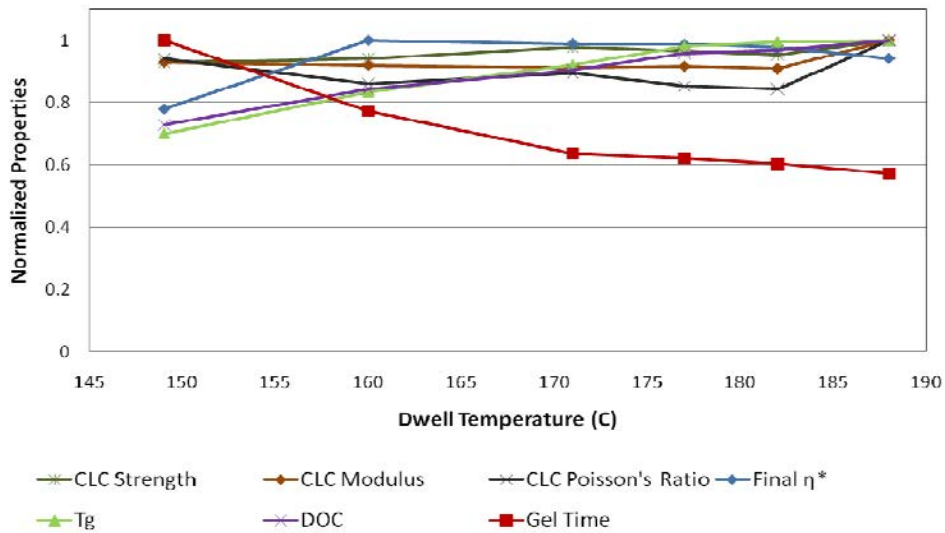
Figure 89. Normalized CLC and viscoelastic properties and degree of cure for one-stage cure cycles 2 to 6.
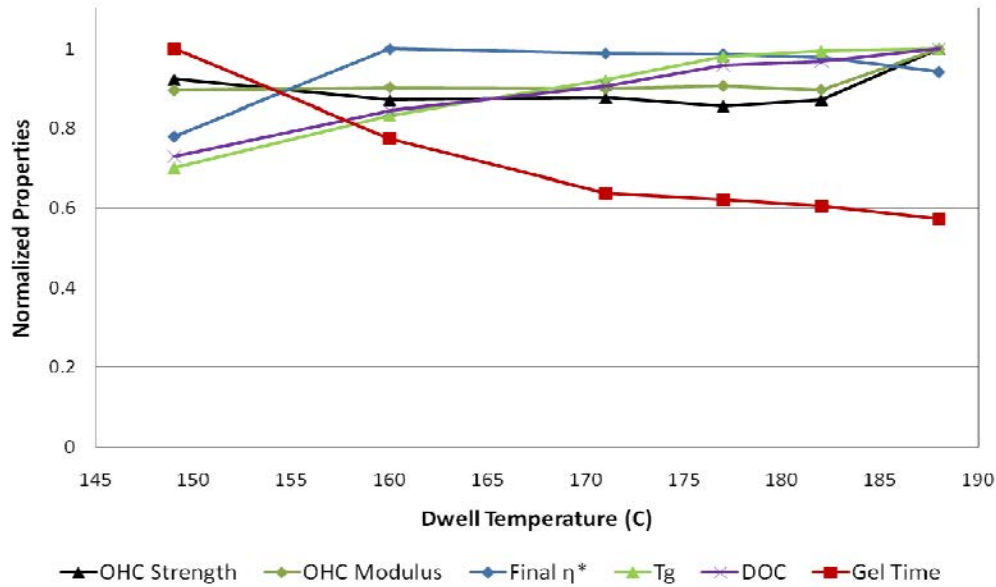
Figure 90. Normalized OHC and viscoelastic properties and degree
of cure for one-stage cure cycles 2 to 6.

4.3.3.2. Cure Cycles with Different Dwell Times

The normalized properties obtained for cure cycles 5 to 8 were used for investigating the

correlation. It is important to note that for the studied cure cycles, all mechanical properties

except SBS strength, of the samples cured at 149°C showed no statistical difference. As such, no

acceptable correlation between the mechanical properties, except SBS strength, and other

material properties was found.

4.3.3.2.1. Correlation between Mechanical Properties and Other Material Properties

Figures 91 and 92 show the normalized SBS strength, CLC strength, and OHC strength,

along with other material-state properties for specimens cured at dwell temperatures of 160°C

and 149°C, respectively. As Figure 91 shows, increasing the dwell time from 180 to 400 minutes,

did not have a significant effect on the mechanical properties of specimens cured at 160°C.

However, T_g and DOC of specimens cured at 160°C were improved by increasing the dwell time.

For specimens cured at 149°C, SBS strength was the only mechanical property that considerably

improved when the dwell time was increased from 180 to 400 minutes (Figure 92). The final

complex viscosity, T_g, and DOC of specimens cured at 149°C were also improved by increasing the dwell time from 180 to 400 minutes.
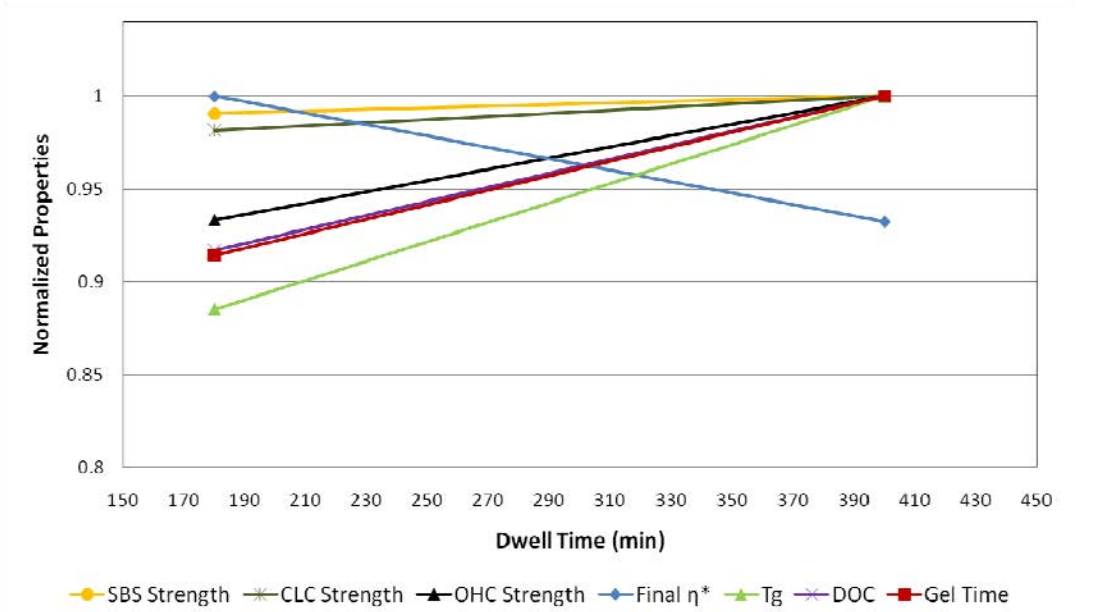
Figure 91. Normalized mechanical and viscoelastic properties and degree of cure for one-stage cure cycles 5 and 7.
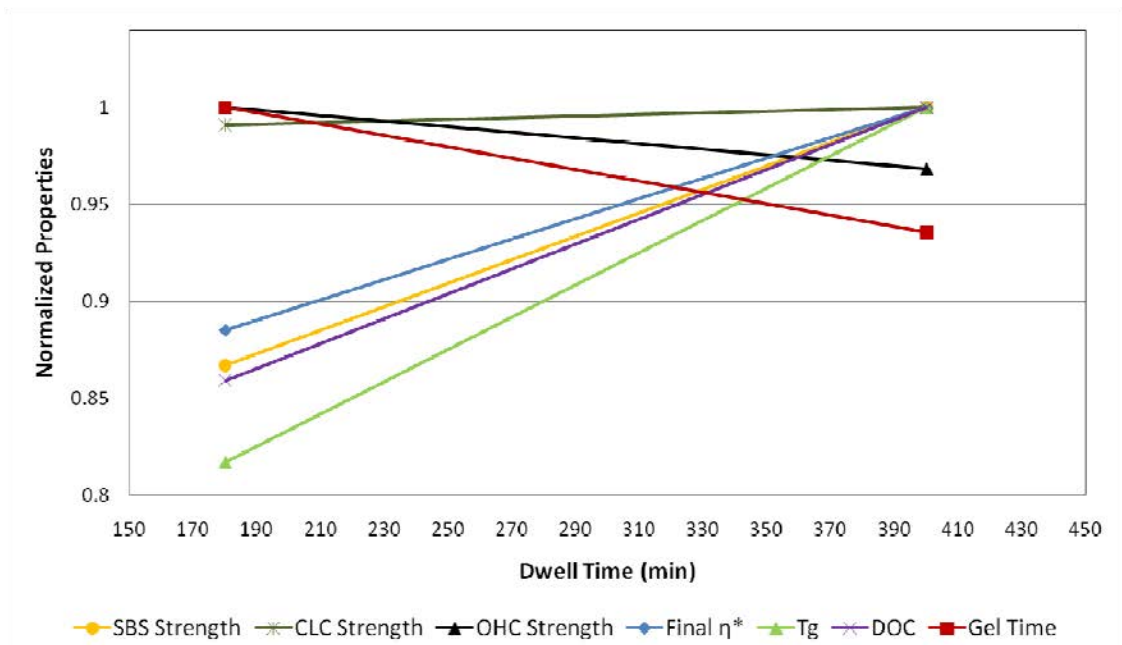
Figure 92. Normalized mechanical and viscoelastic properties and degree of cure for one-stage cure cycles 6 and 8.

104

CHAPTER 5

CONCLUSIONS

5.1.   Conclusions

Thermal, rheological, and mechanical properties of a polymer composite cured at different one-stage and two-stage cure cycles were studied in this dissertation. A commercial carbon fiber prepreg, Cycom 977-2 UD, was used. This curing-toughened epoxy resin prepreg is formulated for autoclave or press molding. An encapsulated sample rheometer was used to obtain the viscoelastic properties of the prepreg including complex viscosity, gel time, and minimum viscosity time, as well as glass transition temperature, and pressure window time for one-stage and two-stage cure cycles. A differential scanning calorimeter was used to obtain the degree of cure for one-stage and two-stage cure cycles. To obtain the mechanical properties of 977-2 UD material at room temperature, open-hole compression, combined loading compression, and short beam shear tests were performed on specimens cut from seven panels cured at different one-stage cure cycles. All of the cured panels had a glass-like finish, and the void content of all panels was about 0.5 percent. The negligible void content of the cured panels indicated that the cure pressure was applied in the proper pressure window, and therefore, the variations in the material properties were only due to the difference in the state of cure.

The one-stage cure cycles were designed to study the effect of dwell temperature variations on the properties of 977-2 UD material for dwell temperatures both above and below the manufacturer's recommended cure temperature (177°C), while the dwell time was kept constant at 180 minutes, the manufacturer's recommended cure time. Since the specimens cured at 160°C and 149°C for 180 minutes were not fully cured and, therefore, their properties were expected to drop, it was important to know if increasing the dwell time could help improve the

material properties for these dwell temperatures. As such, additional specimens were cured at 160$^{\text{o}}$C and 149$^{\text{o}}$C with a long-enough dwell time to ensure that no further curing could occur at these dwell temperatures. Since the degree of cure for both dwell temperatures reached a plateau value after 400 minutes, the new dwell time was selected to be 400 minutes.

The two-stage cure cycles were designed to study the effect of heat-up rate and first dwell temperature on the properties of 977-2 UD. While the selected heat-up rate for cure cycles 1 and 2 was 2.8 C/min which is a common heat-up rate for curing 977-2 UD in the autoclave, the heat-up rate for cure cycles 3 and 4 was 8.3 C/min, which is close to the fastest possible heat-up rate for many autoclaves. The first dwell temperature for the two-stage cure cycles for the 977-2 resin system is usually between 120$^{\text{o}}$C and 165$^{\text{o}}$C. As such, the first dwell temperature for all studied cure cycles was either 149$^{\text{o}}$C or 163$^{\text{o}}$C. The first dwell time for two-stage cure cycles for the 977-2 resin system is usually between 60 and 100 minutes. Therefore, the first dwell time for all cure cycles was either 80 or 100 minutes. The first dwell time for the cure cycles with a lower first dwell temperature (cure cycles 2 and 4) was longer in order to give the material more time to cure. The second dwell temperature for all studied cure cycles was set at 177$^{\text{o}}$C to ensure that the samples were fully cured.

Results of the studied one-stage cure cycles indicated that the final viscoelastic and mechanical properties did not vary significantly over the relatively wide range of dwell temperatures (from 160˚C to 182˚C for specimens cured for 180 minutes). This suggests that materials that might otherwise be rejected due to cure temperature variations could still attain acceptable mechanical properties, even if they were cured at temperatures lower than the vendor's specifications. The results also supported the notion that there was a correlation between the viscoelastic properties and the mechanical properties of the specimens cured at the

one-stage cure cycles studied. The least-cured specimens (those cured at 149°C for 180 minutes) attained a final DOC of 0.7, their SBS strengths being significantly less than those of the other specimens with DOC ranging from 0.81 to 0.96. The final complex viscosities of those specimens cured with a one-stage cure cycle in the encapsulated sample rheometer showed a similar drop-off trend for the least-cured specimens. As such, the SBS strength showed a good correlation with the complex viscosity. The SBS strength had a weaker correlation with the T_g and DOC for the same cure cycles. The T_g had a strong correlation with DOC for all one-stage cure cycles. The gel time did not correlate with the other material properties.

The drop-off in SBS strength of the least-cured specimens was accompanied by a change in the failure mode during the SBS tests. The failure mode for all SBS specimens, except those cured at 149˚C for 180 minutes, was compression-interlaminar shear. The failure mode for SBS specimens cured at 149˚C for 180 minutes was interlaminar shear. The CLC strength for all specimens cured at one-stage cure cycles did not vary significantly. The failure mode for all CLC specimens was brooming in the middle of the gage section. Neither the modulus nor the Poisson's ratio of the CLC specimens cured at one-stage cure cycles varied significantly. The OHC strength and modulus were not influenced by the one-stage cure cycles. The failure mode for all OHC specimens was laminate-compressive failure laterally across the center of the hole.

Increasing the dwell time from 180 to 400 minutes had no significant effect on the mechanical properties of specimens cured at 160˚C. However, the T_g and DOC of the specimens cured at 160˚C were improved by increasing the dwell time. For the specimens cured at 149˚C, the SBS strength was the only mechanical property that improved when the dwell time was increased from 180 to 400 minutes. The final complex viscosity, T_g, and DOC of the specimens cured at 149˚C were also improved by increasing the dwell time from 180 to 400 minutes.

Test results for specimens with a two-stage cure cycle indicated that faster ramp rates and higher first-stage dwell temperatures caused a shift of the complex viscosity and the DOC curves toward those of the isothermal cure at 177°C. This was indicative of faster curing. Moreover, the complex viscosity and DOC graphs had a slight downwards shift at the time of transition from the ramp to the isothermal step. The DOC for all two-stage cure cycles was greater than 0.95, which indicated that the samples were almost fully cured.

It was necessary to define the heat-flow baseline to obtain the degree of cure data for one-stage and two-stage cure cycles. The DOC for the entire cure cycle for both one-stage and two-stage cure cycles was modeled with the Springer-Loos cure kinetics model. The complex viscosity up to the gel time was modeled using the Kenny viscosity model for both one-stage and two-stage cure cycles. The values of DOC and complex viscosity predicted with these two models agreed well with the values measured during testing.

Results presented in this dissertation suggest that the ESR can be used as an ex-situ cure-monitoring instrument to mimic autoclave/oven curing and, hence, eliminate the need for multiple measurement instruments. The cure time-temperature data, provided by thermocouples attached to the composite part in the autoclave/oven, is the only input to the rheometer for cure monitoring. Complex viscosity measured with the ESR was shown to be the best viscoelastic property for monitoring the state of the material during cure for the following reasons: (a) it could be precisely measured throughout the cure and post-cure cycles using the rheometer, (b) it was capable of detecting changes in the material state during cure, (c) it could be adequately modeled by existing viscosity models, and (d) it could be correlated to the mechanical properties of the composite material.

Utilizing the ESR as the main ex-situ cure-monitoring instrument makes it possible to offer a new approach to curing composite materials. In this new approach, called Material State Management, the acceptance of the cured composite material is based on the viscoelastic properties of the material, as measured by the ESR during cure and post-cure monitoring. Moreover, the viscoelastic properties of the material measured during the cure cycle can be used to create improved cure specifications. In the MSM approach, cure process confidence limits can be prescribed, based on the viscoelastic properties of the material using the material-state database and models.

The MSM approach to curing addresses shortcomings of the current time-temperature approach to curing. For example, the MSM approach lowers the risk during curing by offering larger cure confidence limits and eliminates the need for extensive coupon testing to certify the cured parts. Moreover, important changes in the material state during cure will be observable, and the actual final mechanical properties of the material will be predictable once the viscoelastic properties of the material are known. Also, it would be possible in the new approach to correlate the key variables during cure. For example, complex viscosity can be related to the cure temperature and degree of cure.

5.2.   Recommendations for Further Studies

The MSM approach to curing composite materials presented in this dissertation can be enhanced by the following: (a) creating a comprehensive material state database and corresponding models, and (b) establishing a strong correlation between viscoelastic properties, such as the complex viscosity and mechanical properties of the resulting composite materials.

The following steps are recommended to create a comprehensive material-state database and model:

1. Investigate the relationship of viscoelastic properties and material properties of a variety of composite materials.

2. For each subject material, obtain the viscoelastic properties, DOC, and important material-state transitions during cure and post-cure cycles.

3. Use this data to develop the following models:

    a. Material-state models (such as complex viscosity and DOC) for predicting the behavior of the material throughout the cure cycle.

    b. Material-state transition models (such as gel time, vitrification time, and minimum viscosity time models) for predicting the important material-state transitions throughout the cure cycle.

    c. Glass transition temperature model for predicting the post-cure behavior of the material.

4. Use the above-mentioned data and models to develop a cure map, such as a TTT diagram, for each of the subject materials.

The following should be done to establish a strong correlation between the viscoelastic properties and mechanical properties of the subject material:

1. Obtain the material properties for a broader range of the DOC. This would require testing specimens cured at a broader range of dwell time and temperature.

2. Study the different mechanical properties of the material (such as tensile strength, shear strength, flexural strength, impact strength, tear strength, and fracture toughness).

3. Perform fatigue testing in addition to static testing to obtain more mechanical properties.

4. Obtain hot/wet and hot/dry mechanical properties in addition to the room temperature/dry mechanical properties.

REFERENCES

LIST OF REFERENCES

[1]   Campbell F. C., *Manufacturing Processes for Advanced Composites*, 1st ed., Elsevier Science, 2004.

[2]   Chung D., *Carbon Fiber Composites*, Butterworth-Heinemann, 1994.

[3]   Menczel, J. D., and Prime R. B., *Thermal Analysis of Polymers Fundamentals and Applications*. Hoboken, New Jersey, John Wiley & Sons, 2009.

[4]   Dykeman D., *"Minimizing Uncertainty in Cure Modeling for Composites Manufacturing,"* Ph.D. Dissertation, Materials Engineering, The University of British Columbia, 2008.

[5]   Odian G., *Principles of Polymerization*, 4th ed., Wiley-Interscience, 2004.

[6]   Wu C., Zuo J., and Chu B., *"Molecular Weight Distribution of a Branched Epoxy Polymer: 1,4-butanediol Diglycidyl Ether with cis-1,2-cyclohexanexanedicarboxylic anhydride,"* *Macromolecules,* Vol. 22, No. 2, 1989, pp. 633-39.

[7]   Reading, M., and Hourston, D., *Modulated Temperature Differential Scanning Calorimetry: Theoretical and Practical Applications in Polymer Characterisation*, 1st ed., Springer, 2006.

[8]   Sperling L. H., *Introduction to Physical Polymer Science*, 4th ed., Wiley-Interscience, 2005.

[9]   Ramis, X., and Salla, J. M., *"Time-Temperature Transformation (TTT) Cure Diagram of an Unsaturated Polyester Resin,"* *Journal of Polymer Science, Part B: Polymer Physics,* Vol. 35, No. 2, 1997, pp. 371-88.

[10]   Berenberg, B. "Improving Autoclave Performance." *High Performance Composites*. URL: http://www.compositesworld.com/articles/improving-autoclave-performance, posted March 1, 2003 (accessed October 15, 2008).

[11]   Dave, R. S., and Loos, A. C., *Processing of Composites*, 1st ed., Hanser Gardner Publications, 1999.

[12]   Sharif Kashani, P., *"An Ex-situ Material State Monitoring of Curing Based on Viscoelastic Properties in Polymer Composites,"* Master's Thesis, Mechanical Engineering, Wichita State University, 2007.

[13]   White, S. R., and Kim, Y. K., *"Effects of Staged Curing on Mechanical Properties of Thermosetting Matrix Composites,"* in *Proceedings of the American Society for Composites*, Lancaster, PA, 1992, pp. 69-79.

LIST OF REFERENCES (continued)

[14] Gernaat, C., Alavi-Soltani, S., Guzman, M., Rodriguez, A., Minaie, B., and Welch J., *"*Correlation between Viscoelastic and Mechanical Properties for an Out-of-Autoclave Polymer Composite,*"* presented at SAMPE Fall Technical Conference, Wichita, 2009.

[15] Lee, W., Loos, A. C., and Springer, G. S., *"*Heat of Reaction, Degree of Cure, and Viscosity of Hercules 3501-6 Resin,*" Journal of Composite Materials,* Vol. 16, No. 6, 1982, pp. 510-20.

[16] Pillai, V., Beris, A. N., and Dhurjati, P., *"*Intelligent Curing of Thick Composites Using a Knowledge-Based System,*" Journal of Composite Materials,* Vol. 31, No. 1, 1997, pp. 22-51.

[17] Mulligan, D., *"*Cure Monitoring for Composites and Adhesives,*" Rapra Review Reports* 2003.

[18] Maistros, G. M., and Partridge, I. K., *"*Monitoring Autoclave Cure in Commercial Carbon Fibre/Epoxy Composites,*" Composites Part B: Engineering,* Vol. 29, No. 3, 1998, pp. 245-50.

[19] Fomitchov, P. A., Kim, Y. K., Kromine, A. K., and Krishnaswamy, S., *"*Laser Ultrasonic Array System for Real-Time Cure Monitoring of Polymer-Matrix Composites,*" Journal of Composite Materials,* Vol. 36, No. 15, 2002, pp. 1889-901.

[20] Whitney, T. M., and Green, R. E., Jr., *"*Cure Monitoring of Carbon Epoxy Composites: An Application of Resonant Ultrasound Spectroscopy,*" Ultrasonics*, Vol. 34, No. 2-5, 1996, pp. 347-53.

[21] Woo, E. M., and Seferis, J. C., *"*Acoustic Cure Monitoring of Epoxy Matrices and Composites,*" in *Annual Technical Conference - Society of Plastics Engineers*, Boston, MA, 1986, pp. 375-79.

[22] Harrold, R. T., and Sanjana, Z. N., *"*Acoustic Waveguide Monitoring of the Cure and Structural Integrity of Composite Materials,*" Polymer Engineering and Science,* Vol. 26, No. 5, 1985, pp. 367-72.

[23] May, R. G., and Claus, R. O., *"*In-Situ Fiber Optic Sensor for Composite Cure Monitoring through Characterization of Resin Viscoelasticity, *" in *Proceedings of SPIE - The International Society for Optical Engineering*, Scottsdale, AZ, 1996, pp. 24-34.

[24] Dragasius, E. and Bansevicius, R., *"*Piezoelectric Sensors for Cure Monitoring of Thermosets,*" in *Vibroengineering 6th International Conference Proceedings*, Kaunas, Lithuania, 2006, pp. 215-19.

LIST OF REFERENCES (continued)

[25]   Oshima, N., Inoue, K., Motogi, S., and Fukuda T., *"*Constructing of Cure Monitoring System with Piezoelectric Ceramics for Composite Laminate,*"* in *Proceedings of the SPIE - The International Society for Optical Engineering*, 2003, pp. 41-48.

[26]   Lee, D. G., and Kim, H. G., *"*Non-Isothermal In Situ Dielectric Cure Monitoring for Thermosetting Matrix Composites,*" Journal of Composite Materials,* Vol. 38, No. 12, 2004, pp. 977-93.

[27]   Choi, J. H., Kim, I. Y., and Lee, D. G., *"*Development of the Simple Dielectric Sensor for the Cure Monitoring of the High Temperature Composites,*" Journal of Materials Processing Technology,* Vol. 132, 2003, pp. 168-76.

[28]   George, G. A., Cash, G. A., and Rintoul, L., *"*Cure Monitoring of Aerospace Epoxy Resins and Prepregs by Fourier Transform Infrared Emission Spectroscopy,*" Polymer International,* Vol. 41, No. 2, 1996, pp. 169-82.

[29]   Hong, K. C., Vess ,T. M., Lyon, R. E., Chike, K. E., Aust, J. F., and Myrick M. L., *"*Remote Cure Monitoring of Polymeric Resins by Laser Raman Spectroscopy,*"* in *Proceedings of International SAMPE Symposium and Exhibition*, Anaheim, CA, 1993, pp. 427-35.

[30]   Monni, J., Niemela, P., Alvila, L., and Pakkanen, T. T., *"*Online Monitoring of Synthesis and Curing of Phenol-Formaldehyde Resol Resins by Raman Spectroscopy,*" Polymer,* Vol. 49, No. 18, 2008, pp. 3865-74.

[31]   Paik, H., and Sung, N., *"*Fiberoptic Intrinsic Fluorescence for In-Situ Cure Monitoring of Amine Cured Epoxy and Composites,*" Polymer Engineering and Science,* Vol. 34, No. 12, 1994, pp. 1025-32.

[32]   Vatanparast, R., Li, S., Hakala, K., and Lemmetyinen H., *"*Thermal Cure Monitoring of Phenolic Resole Resins Based on In Situ Fluorescence Technique,*" Journal of Applied Polymer Science,* Vol. 83, No. 8, 2002, pp. 1773-80.

[33]   Chen, J. Y., Hoa, S. V., Jen, C. K., Viens, M., and Monchalin, J. P., *"*Ultrasonic Evaluation of Graphite/Epoxy Composites with Different Curing Conditions,*" Polymer Composites,* Vol. 19, No. Compendex, 1998, pp. 225-32.

[34]   Dusi, M. R., Lee, W., Ciriscioli ,P. R., and Springer, G. S., *"*Cure Kinetics and Viscosity of Fiberite 976 Resin,*" Journal of Composite Materials,* Vol. 21, No. 3, 1987, pp. 243-61.

[35]   Manley, T. R., and Scurr, G., *"*Use of Thermal Analysis to Study the Degree of Cure of Epoxy Resins,*"* in *Thermal Analysis, Proceedings of the Seventh International Conference*, Kingston, Ontario, Canada, 1982, pp. 1380-85.

[36] Turk, M. J., Ansari, A. S., Alston, W. B., Gahn, G. S., Frimer, A. A., and Scheiman, D. A., *"Evaluation of the Thermal Oxidative Stability of Polyimides via TGA Techniques," Journal of Polymer Science, Part A: Polymer Chemistry,* Vol. 37, No. Compendex, 1999, pp. 3943-56.

[37] Gillham, J. K., *"Torsional Braid Analysis (TBA): A Technique for Characterizing the Cure and Properties of Thermosetting Systems,"* in *Proceedings of the ACS Division of Polymeric Materials: Science and Engineering - Fall Meeting, September 26, 1988 - September 30, 1988*, Los Angeles, CA, 1988, pp. 851-58.

[38] Gotro, J., and Yandrasits, M., *"Cure Monitoring Using Dielectric and Dynamic Mechanical Analysis,"* in *ANTEC 87 Conference Proceedings - Society of Plastics Engineers 45th Annual Technical Conference & Exhibit.*, Los Angeles, CA, 1987, pp. 1039-42.

[39] Johnson, S. A., and Roberts, N. K., *"Chemical Behavior of Graphite/Polyimide Composite Material During Cure Utilizing Dielectric and Gas Chromatographic Analysis,"* in *Proceedings of 19th International SAMPE Technical Conference. Vol.19, The Nation's Future Material Needs*, Covina, CA, 1987, pp. 241-52.

[40] Cheung, A. T., and Yijin, X., *"Gases Evolved During Cure and Solder Reflow of Encapsulants and Underfills,"* in *Proceedings of 51st Electronic Components and Technology Conference*, Piscataway, NJ, 2001, pp. 1315-20.

[41] Bosze, E. J., Alawar, A., Bertschger, O., Tsai, Y. I., and Nutt, S. R., *"High-Temperature Strength and Storage Modulus in Unidirectional Hybrid Composites," Composites Science and Technology,* Vol. 66, No. 13, 2006, pp. 1963-69.

[42] TAInstruments. (2008). *Differential Scanning Calorimetry (DSC) Basic Theory & Applications Training*. URL: ftp://ftp.tainstruments.com/pub/training/DSC_Training-2008-1.pdf, 2008 (accessed October 15, 2008).

[43] Yousefi, A., Lafleur, P. G., and Gauvin, R., *"Kinetic Studies of Thermoset Cure Reactions:A Review," Polymer Composites,* Vol. 18, No. 2, 1997, pp. 157-68.

[44] Liang, G., and Chandrashekhara, K., *"Cure Kinetics and Rheology Characterization of Soy-Based Epoxy Resin System," Journal of Applied Polymer Science,* Vol. 102, No. 4, 2006, pp. 3168-80.

[45] Barrett, K. E. J., *"Determination of Rates of Thermal Decomposition of Polymerization Initiators with a Differential Scanning Calorimeter," Journal of Applied Polymer Science,* Vol. 11, No. 9, 1967, pp. 1617-26.

[46] Kamal, M. R., *"Thermoset Characterization for Moldability Analysis," Polymer Engineering and Science,* Vol. 14, No. 3, 1974, pp. 231-39.

[47] Chern, C. S., and Poehlein, G. W., *"*Kinetic Model for Curing Reactions of Epoxides with Amines,*" Polymer Engineering and Science,* Vol. 27, No. 11, 1987, pp. 788-95.

[48] Sun, L. F., *"*Thermal Rheological Analysis of Cure Process of Epoxy Prepreg,*"* Ph.D. Dissertation, Chemical Engineering, Louisiana State University, 2002.

[49] Cole, K. C., *"*New Approach to Modeling the Cure Kinetics of Epoxy Amine Thermosetting Resins. 1. Mathematical Development,*" Macromolecules,* Vol. 24, No. 11, 1991, pp. 3093-97.

[50] Hubert, P., Johnston, A., Poursartip, A., and Nelson, K., *"*Cure Kinetics and Viscosity Models for Hexcel 8552 Epoxy Resin,*"* in *Proceedings of International SAMPE Symposium and Exhibition*, Long Beach, CA, 2001.

[51] Brinson, H. F., and Brinson, L. C., *Polymer Engineering Science and Viscoelasticity: An Introduction*, 1st ed., Springer, 2007.

[52] Menard, K. P., *Dynamic Mechanical Analysis: A Practical Introduction*, 2nd ed., CRC Press, 2008.

[53] Morrison, F. A., *Understanding Rheology*, illustrated ed., Oxford University Press, 2001.

[54] Dias da Silva, V., *Mechanics and Strength of Materials*, 1st ed., Springer, 2005.

[55] TAInstruments. "(2008). *Rheology Theory and Applications Course*. URL: ftp://ftp.tainstruments.com/pub/training/Rheology_Training-2008-1.pdf, 2008 (cited 15 October 15 2008).

[56] Ampudia, J., Larrauri, E., Gil, E. M., Rodriguez, M., and Leon, L. M., *"*Thermal Scanning Rheometric Analysis of Curing Kinetic of an Epoxy Resin. I. An Anhydride as Curing Agent,*" Journal of Applied Polymer Science,* Vol. 71, No. Compendex, 1999, pp. 1239-45.

[57] Kenny, J. M., Apicella, A., and Nicolais, L., *"*Model for the Thermal and Chemorheological Behavior of Thermosets: I Processing of Epoxy-Based Composites,*" Polymer Engineering and Science,* Vol. 29, No. 15, 1989, pp. 973-83.

[58] Rieger, J., *"*The Glass Transition Temperature Tg of Polymers-Comparison of the Values from Differential Thermal Analysis (DTA, DSC) and Dynamic Mechanical Measurements (Torsion Pendulum),*" Polymer Testing,* Vol. 20, No. 2, 2001, pp. 199-204.

[59] Williams, J. G., and Delatycki, O., *"*Glass Transition Temperature for Epoxy-Diamine Networks,*" Journal of Polymer Science, Part A-2 (Polymer Physics),* Vol. 10, No. 7, 1972, pp. 1297-304.

[60]   Bicerano, J., *Prediction of Polymer Properties*, 3rd ed., CRC Press, 2002.

[61]   Baker, A., Dutton, S., and Kelly, D., *Composite Materials for Aircraft Structures*, 2nd ed., AIAA, 2004.

[62]   DiBenedetto, A. T., *"*Prediction of the Glass Transition Temperature of Polymers: A Model Based on the Principle of Corresponding States,*"* *Journal of Polymer Science, Part B (Polymer Physics),* Vol. 25, No. 9, 1987, pp. 1949-69.

[63]   Gordin, S. D., Eslami, A. M., and Price, H. L., *"*Gel Time and Temperature for Two Thermosetting Resins,*"* in *ASEE Annual Conference Proceedings*, Salt Lake City, UT, 2004, pp. 6077-86.

[64]   Lee, S. Y., and Springer, G. S., *"*Effects of Cure on the Mechanical Properties of Composites,*"* *Journal of Composite Materials,* Vol. 22, No. 1, 1988, pp. 15-29.

[65]   Gernaat, C. R., *"*Correlation between Rheological and Mechanical Properties in a Low-Temperature Cure Prepreg Composite,*"* Master's Thesis, Mechanical Engineering, Wichita State University, 2008.

[66]   Dai, Gil L., Hak, Sung K., and Sang, Wook P., *"*Smart Cure Cycle with Cooling and Reheating for Co-Cure Bonded Seel/Carbon Epoxy Composite Hybrid Structures for Reducing Thermal Residual Stress,*"* *Composites Part A (Applied Science and Manufacturing),* Vol. 37, No. 10, 2006, pp. 1708-21.

[67]   White, S. R., and Hahn, H. T., *"*Cure Cycle Optimization for The Reduction of Processing-Induced Residual Stresses in Composite Materials,*"* *Journal of Composite Materials,* Vol. 27, No. 14, 1993, pp. 1352-78.

[68]   Ling, L., Bo-Ming, Z., Dian-Fu, W., and Zhan-Jun, W., *"*Effects of Cure Cycles on Void Content and Mechanical Properties of Composite Laminates,*"* *Composite Structures,* Vol. 73, No. 3, 2006, pp. 303-09.

[69]   Liu L., Zhang B., Wu Z., and Wang D., *"*Effects of cure pressure induced voids on the mechanical strength of carbon/epoxy laminates,*"* *Journal of Materials Science and Technology,* Vol. 21, No. 1, 2005, pp. 87-91.

[70]   Twardowski, T. E., Lin, S. E., and Geil, P. H., *"*Curing in Thick Composite Laminates - Experiment and Simulation,*"* *Journal of Composite Materials,* Vol. 27, No. 3, 1993, pp. 216-50.

[71]   White, S. R., and Kim, Y. K., *"*Staged Curing of Composite Materials,*"* *Composites Part A: Applied Science and Manufacturing,* Vol. 27, No. 3, 1996, pp. 219-27.

[72]   Gardiner, G., "Automating and Optimizing Autoclave Cure." *High Performance Composites*.   URL: http://www.compositesworld.com/articles/automating-and-optimizing-autoclave-cure, July 2008 (accessed October 15, 2009).

[73]   Thomas, L., *Use* o*f Multiple Heating Rate DSC a*nd *Modulated Temperature DSC t*o *Detect a*n*d Analyze Temperature-Time-Dependent Transitions* i*n Materials.* URL: http://www.tainstruments.com/pdf/literature/TA291.pdf, 2001 (accessed October 15, 2008).

[74]   White, S. R., and Hahn, H. T., *"*Process Modeling of Composite Materials: Residual Stress Development During Cure. Part II. Experimental Validation,*" Journal of Composite Materials,* Vol. 26, No. 16, 1992, pp. 2423-53.

[75]   Hargis, M., Grady, B., Aktas, L., Bomireddy, K., Howsman, S., Altan, M., Rose, T., and Rose, H., *"*Calorimetric and Rheological Measurements of Three Commercial Thermosetting Prepreg Epoxies,*" Journal of Composite Materials,* Vol. 40, No. 10, 2006, pp. 873-97.

[76]   Höhne, G., Hemminger, W., and Flammersheim, H., *Differential Scanning Calorimetry* Springer-Verlag, Heidelberg, 2003.

[77]   Danley, R., and Caulfield, P., *DSC Baseline Improvements Obtained by a New Heat Flow Measurement   Technique.   *URL: http://www.tainstruments.com/library_download.aspx?file=TA268.pdf, 2003 (accessed October 15, 2009).

[78]   Kissinger, H. E., *"*Reaction Kinetics in Differential Thermal Analysis,*" Analytical Chemistry,* Vol. 29, No. 11, 1957, pp. 1702–06.

[79]   Hemminger, W. F., and Sarge, S. M., *"*Baseline Construction and Its Influence on the Measurement of Heat with Differential Scanning Calorimeters,*" Journal of Thermal Analysis,* Vol. 37, No. 7, 1991, pp. 1455-77.

[80]   Scott, M. G., and Ramachandrarao, P., *"*Kinetics of Crystallization of an Fe-P-C Glass,*" Materials Science and Engineering,* Vol. 29, No. 2, 1977, pp. 137-44.

[81]   Kumar, A., and Gupta, R., *Fundamentals of Polymer Engineering*, 2nd ed., CRC Press, 2003.

[82]   Ferry, J., *Viscoelastic Properties of Polymers*, 3rd ed., Wiley, 1980.

[83]   Riande, E., Diaz-Calleja, R., Prolongo, M., Masegosa, R., and Salom, C., *Polymer Viscoelasticity: Stress and Strain in Practice*, 1st ed., CRC Press, 1999.

[84]   Macosko, Ch. W., *Rheology: Principles, Measurements, and Applications*, 1st ed., Wiley-VCH, 1994.

[85]   Shenoy, A.V., *Rheology of Filled Polymer Systems*, 1st ed., Springer, 1999.

[86]   Cox, W. P., and Merz, E. H., *"Correlation of Dynamic and Steady Flow Viscosities," Journal of Polymer Science Part a-Polymer Chemistry,* Vol. 28, No. 118, 1958, pp. 619-22.

[87]   Lee, S., *Handbook of Composite Reinforcements*, Wiley-VCH, 1992.

[88]   American Society for Testing and Materials, *"*Standard Test Method for Short-Beam Strength of Polymer Matrix Composite Materials and Their Laminates,*"* in *ASTM Standard: D 2344/D 2344M – 00*.

[89]   Adams, D., "Current compression Test Methods," in *High Performance Composites*. URL: http://www.compositesworld.com/articles/current-compression-test-methods, May 2005 (accessed October 15, 2008).

[90]   American Society for Testing and Materials, *"*Standard Test Method for Compressive Properties of Rigid Plastics,*"* in *ASTM Standard: D 695 – 02a*.

[91]   American Society for Testing and Materials, *"*Standard Test Method for Open-Hole Compressive Strength of Polymer Matrix Composite Laminates,*"* in *ASTM Standard: D 6484/D 6484M – 04*.

[92]   Cytec. *Cycom 977-2 Toughened Epoxy Resin*. URL: http://www.cytec.com/engineered-materials/products/Datasheets/CYCOM%20977-2.pdf (accessed October 15, 2008).

[93]   Suppliers of Advanced Composite Materials Association, *"*SACMA Recommended Method for Glass Transition Temperature (Tg) Determination by DMA of Oriented Fiber-Resin Composites,*"* in *SRM 18R-94*.

[94]   Guo, Z., Liu, L., Zhang, B., and Du, S., *"*Critical Void Content for Thermoset Composite Laminates,*" Journal of Composite Materials,* Vol. 43, No. Compendex, 2009, pp. 1775-90.

[95]   American Society for Testing and Materials, *"*Standard Test Method for Compressive Properties of Polymer Matrix Composite Materials with Unsupported Gage Section by Shear Loading,*"* in *ASTM Standard: D 3410/D 3410M – 03*.

[96]   Bullions, T.A., *"*Manufacture of and Environmental Effects on Carbon Fiber-Reinforced PhenylEthynyl-Terminated Poly(EtherImide),*"* Ph.D. Dissertation, Materials Engineering Science, Virginia Polytechnic Institute and State University, 2000.

[97]   American Society for Testing and Materials, *"*Standard Test Methods for Constituent Content of Composite Materials,*"* in *ASTM Standard: D 3171 – 99*.